Heat Transfer in Light Activated Dental Resin Composites

A THESIS
SUBMITTED TO THE FACULTY OF THE GRADUATE SCHOOL
OF THE UNIVERSITY OF MINNESOTA
BY

Shilpa Mohapatra

IN PARTIAL FUFILLMENT OF THE REQUIREMENTS
FOR THE DEGREE OF
MASTER OF SCIENCE

Francis A. Kulacki
Department of Mechanical Engineering
University of Minnesota
and
Alex Fok
Department of Restorative Sciences
University of Minnesota

December 2013

Acknowledgements

I owe many thanks to great many people who helped and supported me during the writing of this master thesis.

I thank, Professor F.A.Kulacki, my advisor for being a constant motivator and a true guide. He supported me all along the thesis by going through my documents and making necessary corrections, as and when needed.

I express my gratitude towards Professor Alex Fok, my co-advisor, who helped me with multiple ideas during my thesis. I thank Professor Susan C. Mantell for reviewing my thesis for the defense.

My deepest thanks are for my husband, Mr. Sanjeev Kumar Mishra, and my parents whose alimony inspired me to drive this thesis towards the path of glory and success.

I would also thank my Institution and all my faculty members without whom this project would have been a distant reality. I also extend my heartfelt thanks to all my well wishers.

Dedication

To my parents, in-laws and Sanjeev Kumar Mishra

Abstract

The objective of this research is to design a satisfactory analytical and experimental model so as to determine the heat generated during the process of polymerization in the light-activated composite dental resin materials in the process of restoration of cavities in teeth.

When the curing light is subjected at the top surface of the composite resin, the overall temperature at the pulp-dentine junction increases. This temperature rise is due to the generation of heat within the composite resin. The energy released by the light activation unit along with the exothermic polymerization reaction, which occurs within the monomer molecules of the resin compound, increases the temperature at the pulp-dentin junction.

With the increase of the temperature beyond a certain scale (~ 20 ^{o}F),the condition of the nerves and blood vessel at the pulp-dentin junction deteriorates in 60% of cases studied, and the pulp fails to recover from the intra-pulpal temperature increase. A major conclusion is that the restorative resin compound which produces the minimum temperature rise over the time-period of curing, ~ 40 s is the best composite to use for dental restoration purpose.

In this paper the temperature rise due to polymerization for the three composite dental resins such as, 3M™ ESPE™ Z100™ Restorative, Filtek™ LS Low Shrink Posterior Restorative System, and 3M^{TM} ESPE^{TM} Filtek Bulk Fill Flowable Restorative (assumed to be made up off 100% resins) are measured.

The depth of curing of the restorative resin is equally important as the generation of heat. If the resin is not fully cured, i.e., incomplete polymerization occurs then it can adversely affect the mechanical properties, environmental resistance, wear behavior and biocompatibility with the pulpal tissue of these restorative materials. So, the knowledge of the heat generation and curing depth are essential in determining the effectiveness of a resin from the restoration point of view.

To determine the two parameters; the heat generation due to polymerization of the resins and the curing depth, a detailed literature review is done on some relating topics in Chapter 1, so as to create a foundation for the thesis problem. Analysis and experiments have been conducted. The temperature rise versus time and temperature rise versus the

curing depth are measured using thermal infrared techniques. Experimental results are compared to an one-dimensional heat conduction model for which the solutions is obtained using the general integral transform method. The comparison between measurement and prediction is good from the trend and shape of the plots point of view but did not agree well on the basis of the values of temperature, time and specimen depth.

As the curing depth of the three resins are well beyond 5-6 mm (practical filling depth) , so all of them could be used for the dental restorative purpose. But the results showed the heat generation due to polymerization is highest for 3M™ ESPE™ Filtek Bulk Fill Flowable Restorative and lowest for 3M™ ESPE™ Z100™ Restorative. Thus this makes 3M™ ESPE™ Z100™ Restorative the most suitable restorative resin out of the three for dental filling purpose.

Table of Contents

List of Tables

Page

List of Figures

Page

Nomenclature

A	area [m^2]
A'	frequency coefficient of reaction rate [1/s]
b	depth of the plane [m]
B	dimensionless activation energy
C	specific heat [J/Kg K]
C_A, C_{A0}	concentration of functional groups [mol/m^3]
$d(r)$	shape distribution function
E_a	reaction rate activation energy [J/mol]
$F(t)$	time dependent incident fluence of the laser pulse [J/m^2]
$f(r)$	spatial dependence of the azimuthally symmetric laser irradiance
h	convective heat transfer coefficient [W/m^2K]
h'	half slab thickness [m]
$h(t)$	temporal dependence of the laser irradiance
H_R	heat of reaction [J/mol]
I	intensity distribution of the light [mol/m^2s]
I_a	intensity of the absorbed light [mol/m^3s]
I_m	maximum incident irradiance [W/m^2]
$J(r,t)$	thermal energy crossing unit area per unit time [J/m^2s]
K	temperature dependent rate constant [1/s]
K_0	pre-exponential factor [1/s]
k_p	polymerization rate constant [$m^3/mols^2$]
k_t	termination rate constant [$m^3/mols^2$]
k	thermal conductivity [W/m K]
k'	dimensionless reaction rate
l, L	length of the specimen [m]
M	monomer concentration [mol/m^3]
M_0	initial concentration of monomer [mol/m^3]

n	order of reaction
Q	temporally and spatially varying laser power input [W/m^2]
q'''	heat generation term [W/m^3]
$q'''_{is}(t)$	partial heat of reaction developed during a DSC experiment [J/Kg]
q'''_{tot}	maximum heat of reaction [J/Kg]
R	universal gas constant [J/Kg K]
R'	surface reflectivity
S	concentration of the photo-initiator [mol/m^3]
t	time taken [s]
t'	dimensionless time based on conduction
t^*	dimensionless time based on polymerization rate
T	temperature in degree [K]
T_i, T_0	initial temperature [K]
T_a, T_{amb}	ambient temperature[K]
T^*	adiabatic temperature rise
T'	dimensionless temperature based on initial temperature
$\Delta T'_{ad}$	dimensionless adiabatic temperature rise
ΔT	temperature difference between the first and second exposure of curing light
T_s	temperatures at the mold wall [K]
T_u	temperatures at the polymer [K]
T_w, T_b	base temperature
V	Volume in [m^3]
x	Axial distance [m]
y'	dimensionless y-axis

Greek

α	thermal diffusivity [m^2/s]

$\alpha^{'}$	maximum degree of reaction
ρ	density of the resin [Kg/m^3]
ψ	penetration depth [m]
ε	molar absorptivity constant for the photo-initiator[m^2/mol]
ϕ	quantum yield for initiation
τ	time constant
η	dimensionless length
θ	relative temperature difference [K]
ρC	heat capacity per unit volume [J/m^3K]
μ_a	absorption coefficient [1/m]
$\Theta(t)$	light exposition in time
φ	absorption profile of light

Subscript

amb	ambient condition
ad	adiabatic condition
i,0	initial condition
b	base temperature

Chapter 1

Introduction

Tooth decay is quite a common problem. The tooth decay or otherwise known as dental caries is a process which results in the formation of the cavity in the tooth. This happens when the bacteria in our mouth produces acids after feeding on the sugars present in the food. As the tooth enamel and dentin region are mostly made up off minerals thus these are susceptible to decay in the acidic medium. If this problem is not treated at right time, it can cause severe pain, infection and finally tooth loss.

The damaged tooth can be restored by varieties of processes, such as fillings, crowns, bridges, implants, dentures etc. Out of all these types, filling is the most well-known restoration process. During the process of filling a hole is drilled in the enamel to dentin region of the tooth and it is filled with restorative resins which is then cured with the help of the curing light. There are several kinds of restorative materials, including amalgam, porcelain, glass ionomer cement, composite resin and resin modified glass-ionomer cement. Among these, the dental composite resins are widely used for their superior quality, reliability and aesthetic values.

However the major set-backs in the field of restoration are heat generation due to curing light and the polymerization of the resin. This generated heat raises the temperature of the entire tooth and causes an undesirable result at the pulp-dentin junction where it results in damaging the pulpal vessel [20]. It is evident that the intact dental pulp responds to measured increases in applied heat in a fairly constant and predictable manner. This is the main concern in the field of dental restoration.

There are multiple reasons for this temperature rise. Some of them are: the output intensity of the light activation unit, quality of light filter, irradiation time, material composition of the resin, residual dentin thickness, cavity dimension etc.

All these above mentioned reasons causing temperature rise is barely under our control. Practically thinking, a dentist or the dental hospital cannot afford multiple laser-lights for multiple resins all the times. It's really hard to do. But it's easy to try multiple resins with a single intensity of laser light and decide which one suits our intention the best. In order to reach to the conclusion which resin outdoes others, we can plot graphs

between the temperature rise (due to curing light and polymerization of resin) against the time. The resin material generating least possible temperature rise and having greater depth of cure in a certain time frame is really convenient to use.

In this thesis, three dental composite resins, 3M™ ESPE™ Z100™ Restorative, Filtek™ LS Low Shrink Posterior Restorative System, and 3M™ ESPE™ Filtek Bulk Fill Flowable Restorative, are considered to determine which among these resins is the most suitable to use for the dental restorative purpose in terms of least heat generation during the process of polymerization and maximum specimen depth.

Three generations are represented by these three composites, 3M™ ESPE™ Filtek Bulk Fill Flowable Restorative being the most recent and 3M™ ESPE™ Z100™ Restorative being the oldest one.

When the light is subjected on the resin during the process of restoration photo polymerization occurs that results in the hardening of the composite resin. This method involves the basic steps of converting a monomer molecule into a polymer chain with the help of the photo-initiator and the filler content present in the resin.

A photo-initiator is the molecule which generates a reactant species by absorbing light from the source, as a result initiates the process of polymerization [24]. The reactant species interacts with the monomer molecule to produce an activated monomer. The polymer chain is formed when the reactive monomer combines with another monomer. The process of polymerization ends when one reactive monomer meets another activated monomer.

Sometimes the exposure duration are insufficient to produce the reactant species and the radicals get trapped in the glassy polymeric matrix [24], this is called radical trapping. The fillers present in the composite resins plays a vital role in releasing these trapped radicals.

So, the monomer concentration , the photo-initiators and the fillers are important factors in the process of polymerization of the composite resins. This type of polymerization mostly occurs in the resins containing the methacrylate group. 3M™ ESPE™ Filtek Bulk Fill Flowable Restorative and 3M™ ESPE™ Z100™ are examples of such resins.

The 3M™ ESPE™ Filtek Bulk Fill Flowable Restorative contains bisGMA ((2,2-bis[4-(2-hydroxy-3-methacryloxypropoxy)phenyl]propane),UDMA(urethane dimethacrylate), bisEMA(6)((2,2-Bis[4-methacryloxypoly-ethoxyphenyl)propane]) and Procrylate resins. The fillers are a combination of zirconia/silica with the particle size range of 0.01 to 3.5 micron and ytterbium triflouride filler particle size from 0.01 to 5.0 micron. On the other hand, the 3M™ ESPE™ Z100™ Restorative is a unique, single filler composites, wherein the filler is 100% silica/zirconia that allows more particle per gram of the composite, making it excellent from the strength and wear resistance point of view.

The Filtek™ LS Low Shrink Posterior Restorative System consists of 0.9% photoinitiator, 76% filler, 23% silorane resin, 0.13% stabilizer and 0.005% pigments. The polymerization process in this resin is based on the new ring-opening silorane chemistry.

In this paper, the three resins are assumed to have 100% resins content, for the simplication in calculation.

As the chemical composition of the three resins are different, they are expected to behave differently when light is projected on them. Thus the heat released as a result of polymerization is also different in each. The composite resin which produces the minimum temperature rise and maximum curing depth over a time frame is considered the best among these three.

Inorder to find the temperature rise and curing depth versus time an experimental method is designed in Chapter 4. This design is validated with the help of the analytical model presented in Chapter 3.

Chapter 2

Literature Review

Numerous dental composite resins have been developed and tested for the restoration of teeth. Thus, there are numerous journal articles about different restorative resins. This literature review focuses on the key elements of the solution to the problem under investigation: the mathematical modeling of the heat source terms, the solution of the one-dimensional transient heat conduction equation containing such terms, and comparison of the results to measured temperatures in systems that can be modeled by this equation. Particular attention will be paid to the formulation of the heat source arising from the temperature-dependent curing of the resin composite filling.

2.1 Analytical Investigations

Analytical solutions to the complete curing problem are limited. Most published solutions either employ finite element methods or combine numerical analysis with experiments.

Bechtel [2] provides analytical and numerical solutions to the heat conduction equation which involves heating of absorbing media with a pulsed laser. Several models of laser irradiance are used by Bechtel to determine the spatial and temporal fields of temperature. The surface and the volume generation terms are discussed in this paper and comparison is made with previously existing models. The second order partial differential heat conduction equation is solved using Green's function in a phase-wise manner. "The non-homogeneous heat conduction equation is solved first with the generation term in it and then that solution is applied to the problem of laser heating of solid semi-infinite targets with an exponential attenuation of the incident laser beam within the absorbing target." In order to solve this particular problem, Bechtel assumes that the incident irradiance is large compared to the power of thermal radiation per unit area, and thermal properties such as absorptivity, thermal conductivity and the thermal diffusivity are independent of the temperature. It is found that if the thermal diffusion depth is greater than the optical attenuation depth, then the surface and volume generation models produced approximately the same results. On the contrary, if the thermal diffusion depth is nearly the same or smaller than the optical attenuation depth, then the

surface generation model produced different results in comparison to the model of volume generation.

Bechtel [2] in his mathematical formulation attempted to solve a second order differential heat transfer equation taking the assumptions mentioned above. The heat transfer equation is,

$$\nabla \cdot J(r,t) + \rho C \frac{\partial T(r,t)}{\partial t} = q'''(r,t), \tag{2.1}$$

where $T(r,t)$ is the temperature , $J(r,t)$ is the thermal energy crossing unit area per unit time, ρ and C are the density and specific heat of the solid, ρC is the heat capacity per unit volume, and q'''(r,t) is the net energy per unit volume per unit time generated within the solid, using two boundary conditions and one initial condition. According to the Fourier's law, $J(r,t)$,

$$J(r,t) = -k\nabla T(r,t) \tag{2.2}$$

Bechtel considered a semi-infinite slab occupying the region $z \geq 0$ in Fig. 1. The slab is irradiated by a laser beam propagating in the z-direction.
According to the paper, the boundary conditions at $z = 0$ and $z \to \infty$ are,

$$\left.\frac{dT(r,t)}{dz}\right|_{z=0} = 0 \text{ and } T(z \to \infty, t) = T_\infty \text{ respectively} \tag{2.3}$$

The source term is modeled mathematically by,

$$q'''(r,t) = I_m(1-R')\mu_a \exp(-\mu_a z) f(r) h(t) \tag{2.4}$$

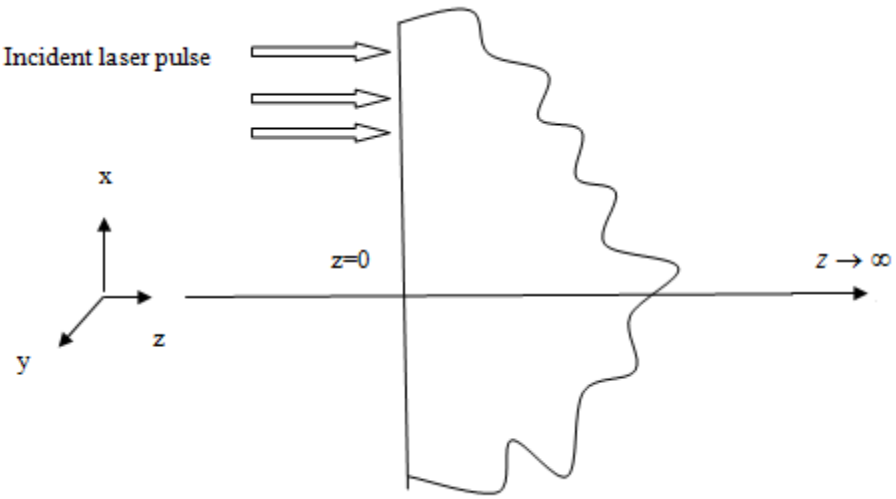

Figure 1.Semi-infinite target and the incident laser pulse [2].

where $R^{'}$ is the surface reflectivity, I_m is the maximum incident irradiance, μ_a is the absorption coefficient, $f(r)$ is the spatial dependence of the azimuthally symmetric laser irradiance, $h(t)$ is the temporal dependence of the laser irradiance and t is the time. Bechtel's solution for the surface temperature rise is simplified to the following expression:

$$\Delta T(0,t) = \frac{I_m(1-R^{'})}{k\mu_a}\{\exp(\alpha\mu_a{}^2 t)erfc(\mu_a(\alpha t)^{1/2} - 1)\} + \frac{2I_m(1-R^{'})}{k}\frac{(\alpha t)^{1/2}}{\pi^{1/2}} \qquad (2.5)$$

Typical results are shown in Figure 2.

where α is the thermal diffusivity of the solid.

The target considered by Bechtel is solid and metallic in nature, so the phenomenon of polymerization does not come into play. The paper mentions only one heat generation term, i.e. the conversion of the incident light to heat. Irrespective of all these criterions, the governing equation with the initial and

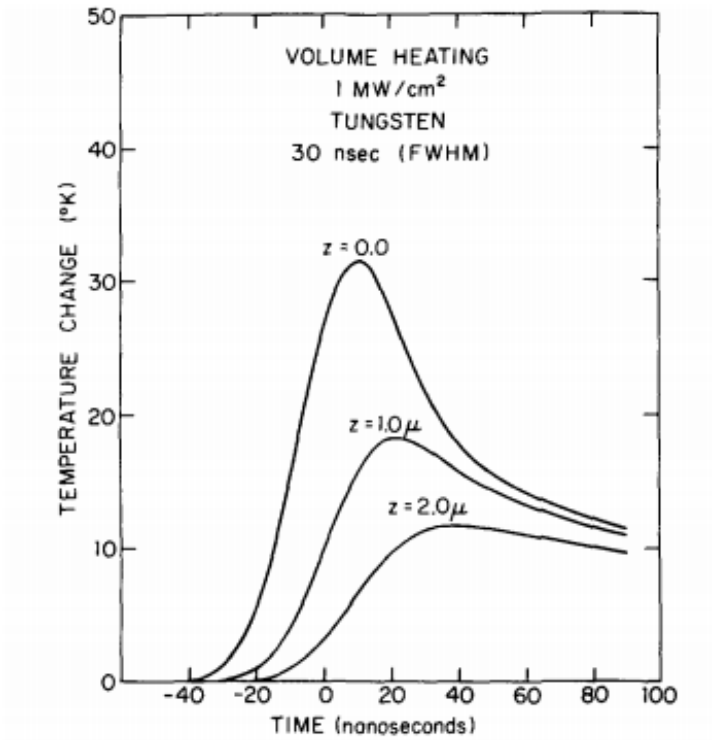

Figure 2. The temperature change produced by a 30-nsec Gaussian laser pulse of wavelength 1.06 μm incident on a tungsten target. The peak incident irradiance is 1MW/ cm^2 [2].

boundary conditions are stated well by Bechtel with valid reasoning.

Broyer et al. [3] developed a model which took into consideration the polymerization or curing process which occurs in molding operations such as casting, thermoset molding or reaction injection molding (RIM). In this case the temperature of the mold is controlled by the circulation of the fluid surrounding the mold wall. Several assumptions are made by the authors in solving the heat conduction problem. These are: convection and mass diffusion are neglected, no flow condition, a homogeneous and well-mixed reaction system, one-dimensional heat conduction, n^{th}-order kinetics, constant thermo physical properties, well-mixed boundary condition, heat of reaction, H_R, is constant and the reactant polymer is in close contact with the mold wall.

Broyer solved a heat conduction problem with time dependent boundary condition by using the "modified separation of variables" technique. The analytical solution to this problem determines the unsteady temperature profile of the mold wall. This analytical result is combined with the non-linear differential equations of heat and mass transfer for the curing of the polymer, which is then solved numerically. This model is tested for the

"fast polymerizing RIM polyurethane in a slab mold". The temperature is measured with thermocouples attached to the slab mold. This process is repeated for various mold wall materials. The result revealed that the temperature profiles of the theory and the numerical simulation are in close agreement with each other.

According to Broyer et al., the generation term/source term in the energy equation is significant because all polymer reaction molding processes are exothermic, and both the reactants and products have low thermal conductivity. The model for the polymer reaction molding process using the one-dimensional heat transfer equation,

$$\rho C \frac{\partial T}{\partial t} = \frac{\partial}{\partial y}(k \ \frac{\partial T}{\partial y}) + H_R R_p \tag{2.6}$$

where $R_p = k_p C_A^{\ n}$ is the polymerization rate , $H_R R_p$ is the heat-generation/source term, H_R is the heat of reaction, k is thermal conductivity, C_A is the concentration of functional groups, n is the order of the reaction and k_p is the polymerization rate constant.

Numerical solutions are obtained for an adiabatic wall, an isothermal wall and a wall with constant heat flux. The temperature versus time results obtained by using the Crank-Nicholson method are shown in Figures 3 - 6.

The dimensionless variables mentioned in the Figures 3 - 6 are $T^{'}$, T^{*}, $\Delta T^{'}_{ad}$, $t^{'}$, B, $k^{'}$ and $y^{'}$, where

$$T^{'} = T / T_i \tag{2.7}$$

$$y^{'} = y / h^{'} \tag{2.8}$$

$$T^{*} = (T - T_i)/(T_{ad} - T_i) \tag{2.9}$$

$$\Delta T^{'}_{ad} = T_{ad} - T_i / T_i \tag{2.10}$$

$$t' = \frac{\alpha t}{h'^2} \tag{2.11}$$

$$B = E_a / RT_i \tag{2.12}$$

$$k' = C_{A0}{}^{n-1} h'^2 A e^{-B} / \alpha \tag{2.13}$$

where A is the Frequency coefficient of reaction rate, B is the dimensionless activation energy, C_{A0} is the concentration of functional groups, E_a is the reaction rate activation energy, h' is the half slab thickness, k' is the dimensionless reaction rate R is the universal gas constant, t' is the dimensionless time based on conduction, t is the time taken, t^* is the dimensionless time based on polymerization rate, T_i is the initial temperature, T^* is the adiabatic temperature rise, T' is the dimensionless temperature based on initial temperature, $\Delta T'_{ad}$ is the dimensionless adiabatic temperature rise and α is the thermal diffusivity .

These dimensionless variables are used to make Eqn. (2.6) and boundary and initial conditions dimensionless and then solved eventually by using different cases as, adiabatic, isothermal and constant wall heat flux condition.

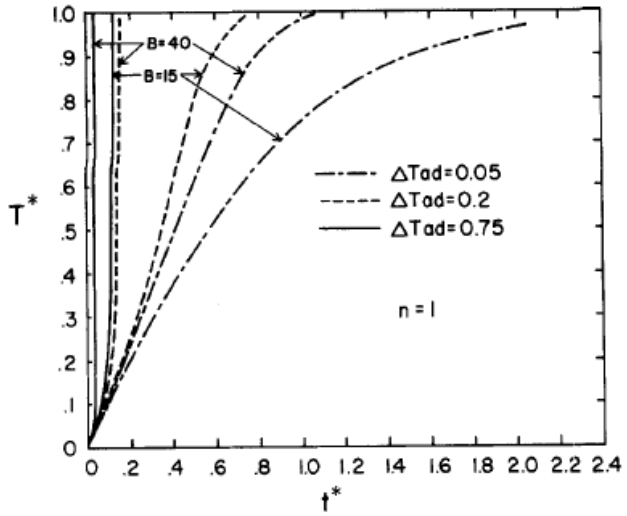

Figure 3. Adiabatic temperature rise for the first order polymerization reaction with a range of generation rates [3].

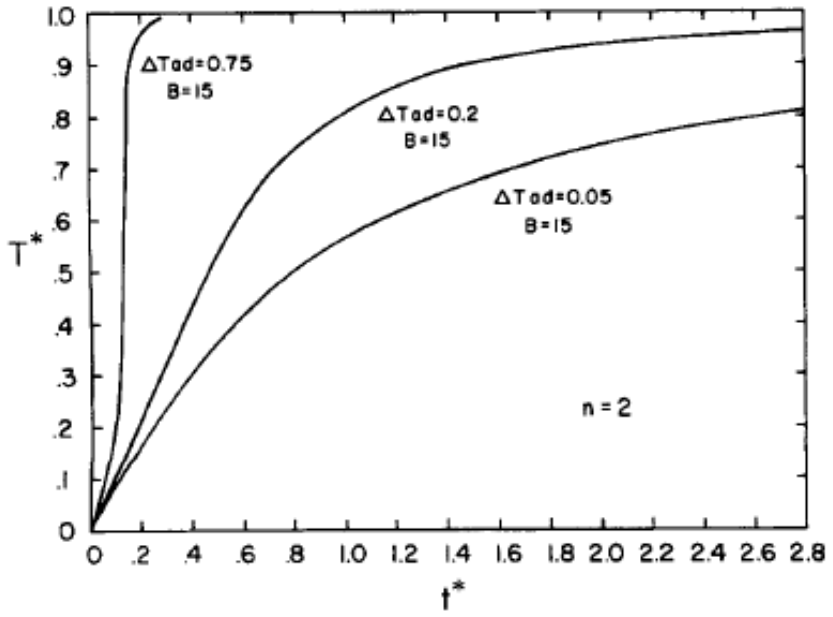

Figure 4. Adiabatic temperature rise for the second order polymerization reaction with a range of generation rates [3].

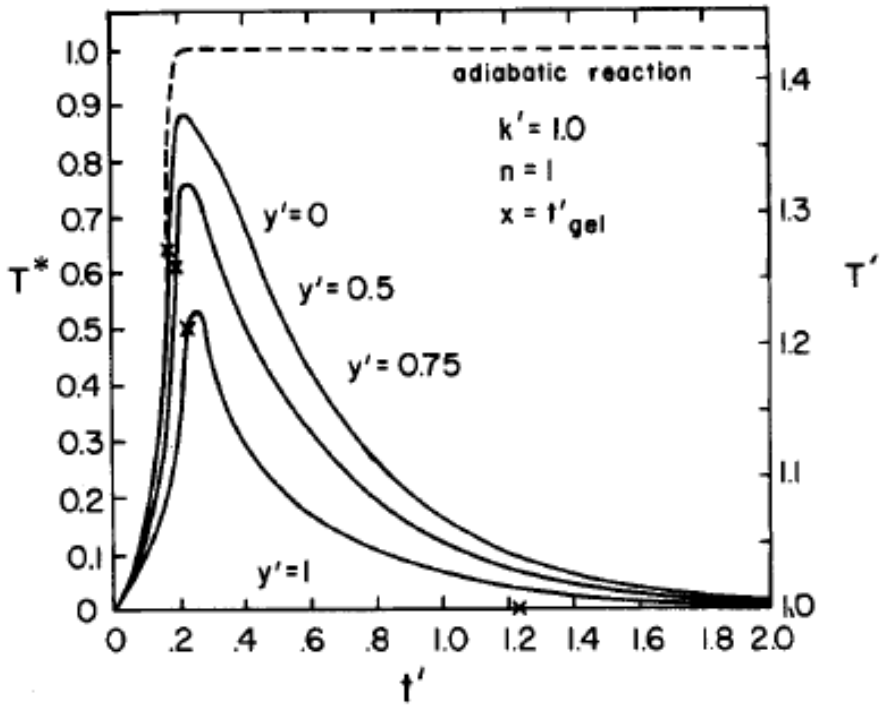

Figure 5. Temperature rise in different cross-sections of the reacting slab for the isothermal condition [3].

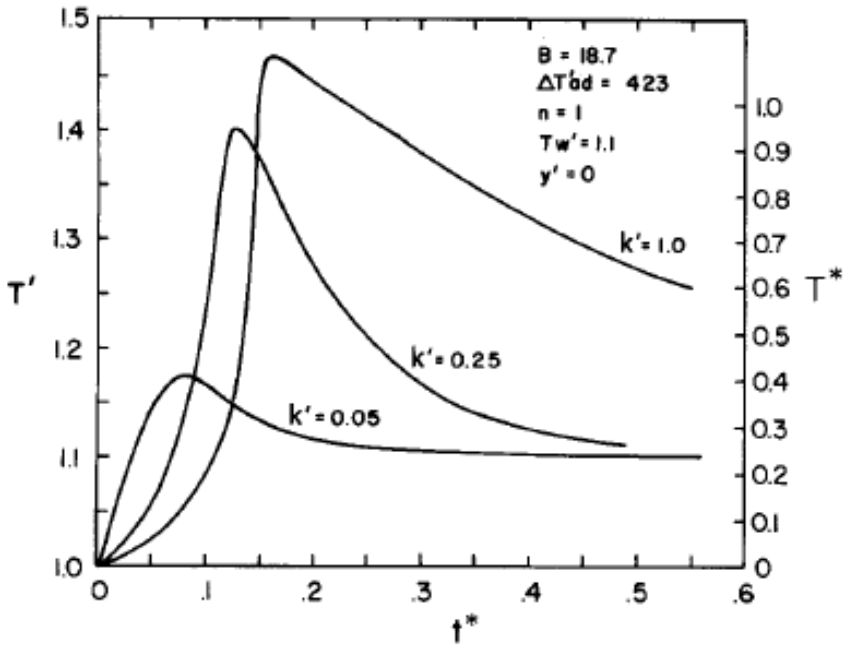

Figure 6. Temperature rise in the reacting slab for different k' values and isothermal walls [3].

The mathematical modeling of the source term in paper [3] helped in understanding the underlying concepts of chemical kinetics and the variables involved in the source terms.

Fok et al. [5] present a lumped analysis of the heat transfer problem of light-cured dental composites during polymerization using temperature measurements made with a thermal infrared (IR) camera. A small volume of composite is used to derive the heat source terms for both the composite and the curing light. The temperature of the composite is measured during curing using an IR camera and measured again after it has been cured with the curing light switched on for the same period of time. The difference in the two temperature profiles provides a measure of the heat source term for the polymerization. Z100, BulkFill and LS are the three composites tested by Fok et al. in [5]. The thermo-physical properties of the resin composites are assumed constant by Fok et al. [5] throughout the experiments. Firstly, the simpler case of heating the cured composite with the curing light is considered. The governing differential equation for temperature for the curing light, only, is assumed to be:

$$\rho CV\frac{dT}{dt} = q_l{}'''V - hA(T - T_0) \tag{2.14}$$

where $q_l{}'''$ is the heating rate per unit volume from the curing light and is assumed to be constant, h is the convective heat transfer coefficient, T_0 is the initial temperature , V and A are volume and area of the sample, respectively.

With the relative temperature difference defined as $\theta = T - T_0$, the solution of Eqn. (2.14) is,

$$\theta = \theta_\infty(1 - e^{-k_1 t}) \tag{2.15}$$

It follows that,

$$\ln(1 - \frac{\theta}{\theta_\infty}) = -k_1 t \tag{2.16}$$

where $\theta_\infty = \frac{k_2}{k_1} q_1{}'''$ and $k_1 = \frac{hA}{\rho CV}$ and $k_2 = \frac{1}{\rho C}$.

Hence, k_1 and h are to be determined from the slope of the graph of $\ln(1 - \frac{\theta}{\theta_\infty})$ versus t (Figure 7), and $q_l{}'''$ can be determined from k_1, k_2 and θ_∞. It is found that the $q_l{}'''$ for Z100 (in blue color) is the lowest in comparison to BulkFill (in green color) and LS (in red color) , Fig. 8 (ii).

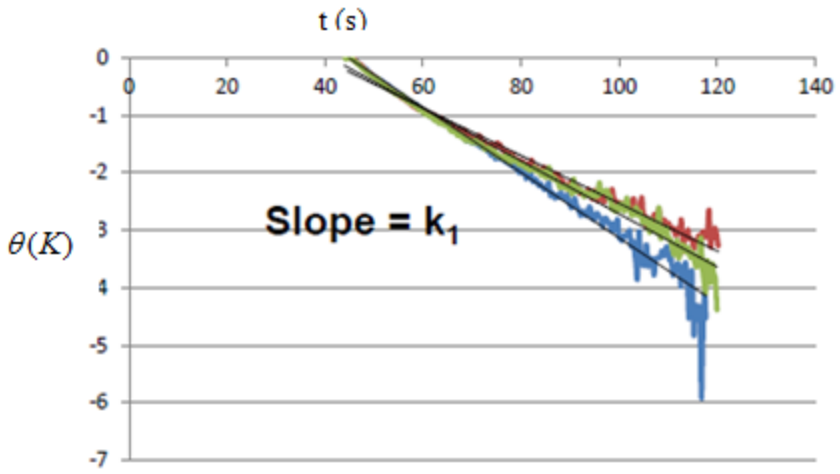

Figure 7.Temperature versus time graph for $\ln(1-\frac{\theta}{\theta_\infty})$ [5].

Fok et al. [5] next consider the case of the heating of the composite while it is being cured. The heat transfer equation requires the addition of a time-dependent source term, q'''_c, due to the finite heat released from the composite as it polymerizes, i.e.

$$q_c''' = q_{co}''' e^{-k_3 t} \tag{2.17}$$

where q'''_{c0} is a constant term.

The governing differential equation thus becomes,

$$\rho CV \frac{dT}{dt} = q'''_l V - hA(T - T_0) + q_c''' e^{-k_3 t} \tag{2.18}$$

The temperature change due to heat released from the material only is determined by subtracting Eqn. (2.15) from the solution of Eqn. (2.18). The value of k_3 is found from the time at which the maximum temperature occurs, which in turn is found by differentiating the solution of Eqn. (2.18) with respect to t and equating the result to zero.

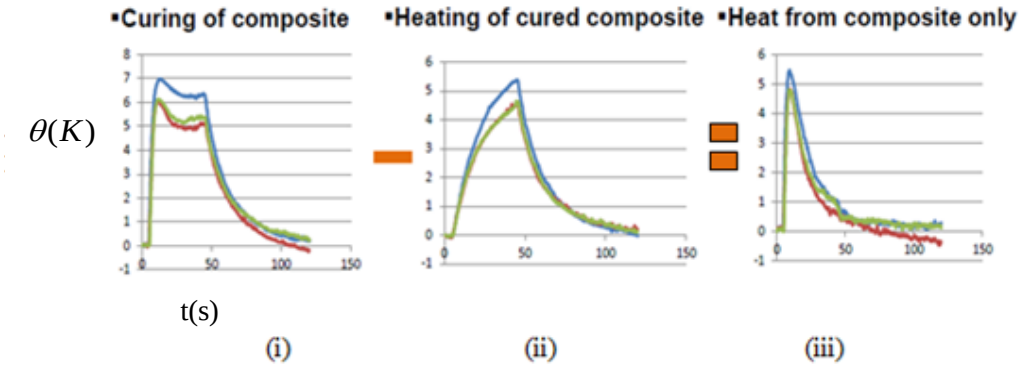

Figure 8. Determination of the heat produced from the curing of dental composites. The heat from the composite only (iii) is calculated by subtracting the heating of the cured composite (ii) from the curing light from the total heat produced during curing of the composite(i) [5].

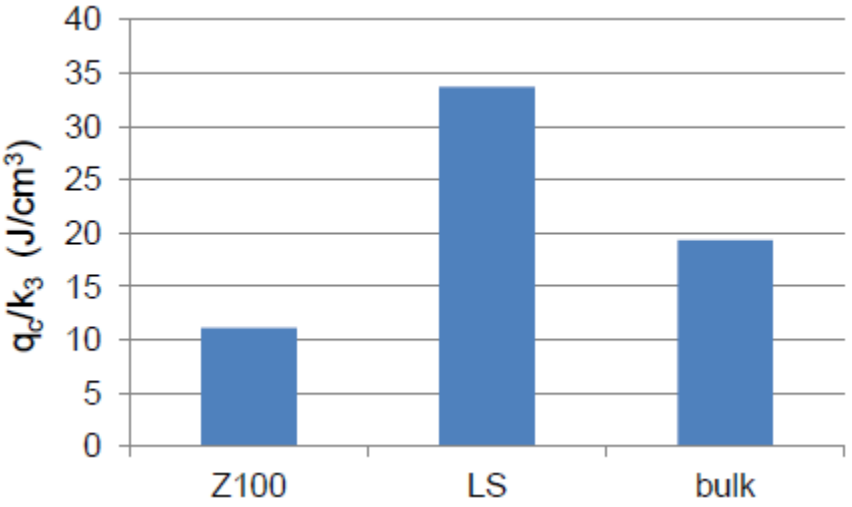

Figure 9. Comparison between the three resins in terms of the total heat produced per unit volume [5].

To determine the temperature rise due to the exothermic polymerization reaction, the temperature rise during the second exposure (occurring at the same time as the temperature peak of the first exposure) is subtracted from the temperature during the 1st exposure as illustrated in Figure 8.

The temperature versus time graphs are plotted for the three composite resins, Z100, LS and BulkFill [28,29,30]. The results suggest that Z100 has the lowest total heat produced per unit volume. The bar graph is shown in Figure 9.

Fok et al. [5] used a lumped model with uniform temperature. In reality, however, the heat source, q_c''', and temperature is a function of time and axial distance.

Olcer [16] suggested analytical solutions to the one dimensional, transient, non-homogeneous heat transfer equation. This paper shows the derivation of the expressions for unsteady temperature in finite regions of arbitrary geometry under conditions of prescribed heat flux on all boundaries and with time-dependent heat sources and arbitrary initial conditions. The mathematical problem considers the time dependent heat source term with any arbitrary initial condition. The one-dimensional heat transfer governing equation is stated below:

$$\nabla^2 T(P,t) + \frac{1}{k} q'''(P,t) = \frac{1}{\alpha} \frac{\partial T(P,t)}{\partial t} \tag{2.19}$$

where k is the thermal conductivity, α is the thermal diffusivity, T is the temperature, t is time and q''' is the heat generation term. And the above equation is solved with the initial condition:

$$T(P,t) = F(P) \qquad P \text{ in } R, t = 0$$

where R is a stationary, homogeneous, isotropic region and P is a point in R, and with the second kind of boundary condition expressed as:

$$k \frac{\partial T(P,t)}{\partial n_i} = f_i(s_i,t), \qquad P \text{ on } S_i,\ t > 0 \tag{2.20}$$

where i = 1,2... , S_i is the i^{th} coordinate surface of R, and n_i is the outward normal of S_i. Thus the governing equation can be solved with the help of the initial and boundary condition and the relation between the temperature and time could be plotted. The paper by Maffezzoli et al. [13] considers the kinetics of the photo-polymerization process which occurs in commercial dental resins.

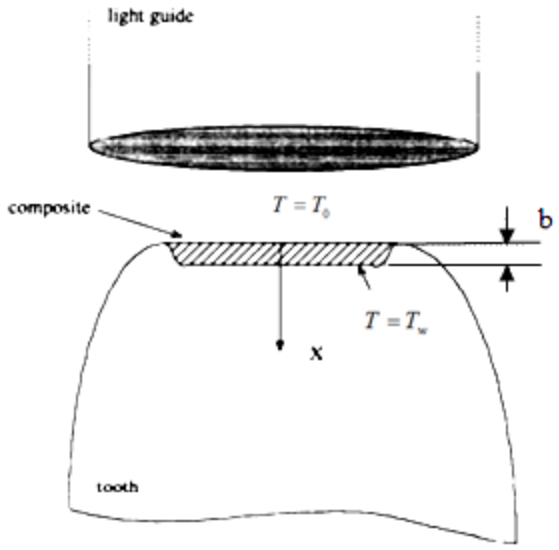

Figure 10. Sketch of the geometry used for simulating curing of dental composite restoration [13].

This process of photo-polymerization is analyzed by using differential scanning calorimetry (DSC). According to this paper, when the light is projected onto the resin surface, it results in a fast and highly anisothermal bulk polymerization reaction. The exothermic nature of the polymerization reaction generates the heat in the resin, as a result increases the temperature of the resin compound. Both isothermal and non-isothermal behavior for a particular resin due to the polymerization reaction is described in the paper. First of all, the isothermal kinetics is analyzed by using the DSC. The DSC measures the glass transition temperature, T_g. The measured glass transition temperature is correlated to the degree of reaction of the polymer resin at various isothermal cure temperatures. The DSC also helps in measuring the rates of the polymerization reaction at different temperatures. This constitutes the isothermal model of Maffezzoli et al. [13]. The isothermal model is then incorporated with the energy balance equation to find the degree of reaction and temperature of cure of the composite for the non-isothermal case. Factors such as the geometry of the system, thermal diffusivity of the composite and the rate of heat generated by curing are taken into account in the kinetic model in order to determine the temperature and the degree of reaction of the composite resin.

According to Maffezzoli et al. [13], the thickness of the restoration of the resin determines the speed of the heat dissipation i.e. if the restoration is thick, the isothermal condition is difficult to attain. The position of the highest temperature in the resin is also dependent on its material composition and polymerization conditions. It varies from one resin to the other. The temperature inside the resin can be calculated by solving the energy balance equation mentioned earlier. The geometry of the plane as shown in Figure 10 is taken into consideration.

The heat conduction is considered to take place only in the transverse direction (x-axis) assuming that the thickness of the geometry is small compared to the other two dimensions. In simple words, if the length of the specimen is greater than its cross-sectional area then the heat could be assumed to flow in the x-direction only. This assumption is made to simplify the problem. The thermal effect when the light is exposed on the resin and the polymerization reaction is neglected in this model. Values for the thermal conductivity, density and specific heat (measured by DSC between $30\,^{0}C$ and $60\,^{0}C$) of the resin are 0.24 W/mK, 1.5 g/cm^3 and 1.26 J/gK, respectively.

The governing equation for the energy balance is:

$$\rho C \frac{\partial T}{\partial t} = k \frac{\partial^2 T}{\partial x^2} + \rho \frac{dq'''}{dt}, \tag{2.21}$$

where $\frac{dq'''}{dt}$ is the rate of heat generation by the chemical reactions,

$$\frac{dq'''}{dt} = q'''_{tot} \frac{d\alpha'}{dt}, \tag{2.22}$$

where the rate of reaction $\frac{d\alpha'}{dt}$ is given by:

$$\frac{d\alpha'}{dt} = K\alpha'^{m}(\alpha'_{m} - \alpha')^{n}, \tag{2.23}$$

where m and n are temperature-independent parameters and K is a temperature-dependent rate constant given by an Arrhenius-type equation,

$$K = K_o \exp(-\frac{E_a}{RT}) \tag{2.24}$$

where K_0 is the pre-exponential factor, R is the gas constant, E_a the activation energy and T is the absolute temperature.

In Eqn. (2.22), $\alpha^{'}$ represents the maximum degree of reaction obtained in isothermal DSC cure experiments,

$$\alpha^{'} = q^{'''}_{is}(t) / q^{'''}_{tot}, \tag{2.25}$$

where $q^{'''}_{is}(t)$ is the partial heat of reaction developed during a DSC experiment and $q^{'''}_{tot}$ represents the maximum heat of reaction.

Equation (2.21) is solved with the following initial and boundary conditions,

$$t = 0,\ \alpha^{'} = 0,\ T = T_0 \tag{2.26}$$

$$t > 0,\ x = 0,\ -k\frac{\partial T}{\partial x} = h(T_a - T) \tag{2.27}$$

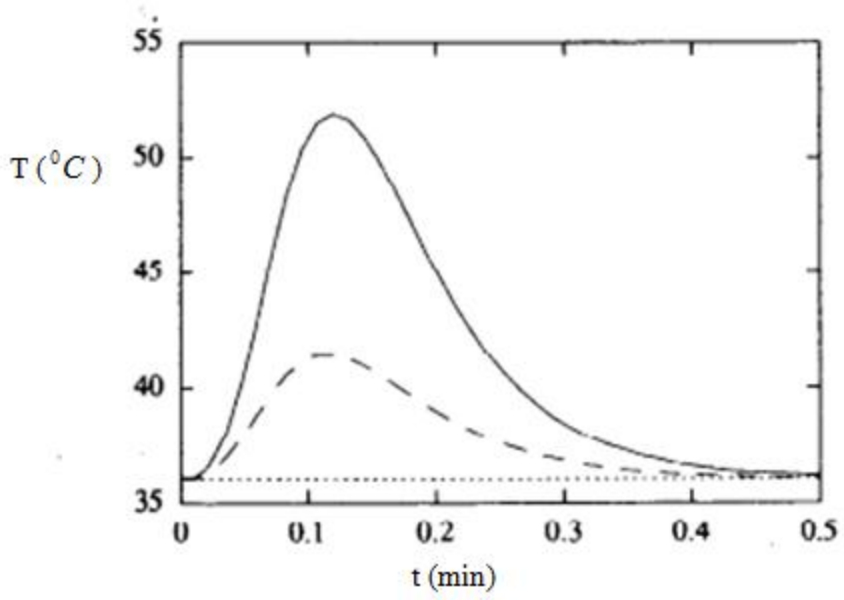

Figure 11. Temperature versus time on the external surface (x = 0 mm and x = 1 mm) and at the center of the composite (x=0.5 mm) [13].

$$t > 0,\ x = b, T = T_w, \tag{2.28}$$

where T_a is the ambient temperature and T is the temperature.

The governing equations are solved using the implicit finite difference method. The temperature versus time plot for the mathematical model is shown in Figure 11. The figure shows the temperature change at two points: one at the external surface and the other at the central position of the resin restoration.

This model is very beneficial in understanding the heat energy generation during both isothermal and non-isothermal curing. As most of the curing processes are non-isothermal in nature due to the finite restoration thickness, the analysis given in this paper for the non-isothermal case of heat transfer can serve as a strong basis for the kind of photo-polymerization problems considered in this thesis.

The problem considered by Lee et al. [10] is quite similar to that analyzed by Broyer et al. [3] cited earlier. In this case, Lee et al. [10] presented a theoretical model for the polymer reaction molding operations. Basic forming processes such as casting, lamination, thermoset molding, or reaction injection molding (RIM) come under the polymer reaction molding category. Homogeneous nature of the medium, a well-mixed

system at time = 0, no flow, one-dimensional heat conduction, negligible molecular diffusion, nth order kinetics, constant thermal properties and negligible convection and mass diffusion are some of the assumptions that are made before solving the problem. The heat conduction equation with time-dependent boundary conditions is solved using the modified separation of variables technique. The analytical solution to this problem determines the unsteady mold wall temperature profile. The solution is then combined with the non-linear differential equations of the heat and mass transfer for curing polymers, which are then solved numerically. The procedure of solving the mathematical model is very similar to that described in the paper by Broyer et al. [3].

According to Lee et al. [10], in most of the polymer reaction molding operations sharp temperature gradient exists inside the mold cavity during reaction and curing process.

Since the molded part is very thin, Lee et al. [10] performed a one-dimensional heat transfer analysis for this type of heat transfer through a thickness problem. The heat of the reaction, H_R, is taken to be constant. After considering all these assumptions, the basic equation of the system framed for the polymer phase is:

$$\rho\, C \frac{\partial T}{\partial t} = k\, \frac{\partial^2 T}{\partial y^2} + H_R A e^{-\frac{E_a}{RT_u}} C_A{}^n, \tag{2.29}$$

where $-\frac{\partial C_A}{\partial t} = A^{-\frac{E_a}{RT}} C_A{}^n$. Initial and boundary conditions are,

$$T_u = T_{uo} \text{ and } C_A = C_{Ao},\ t = 0, \text{ for all } 0 \le y \le d \tag{2.30}$$

$$\frac{\partial T_u}{\partial y} = 0\ , \qquad y = 0, \text{ for } t > 0 \tag{2.31}$$

$$T_u = T_s \qquad y = d \text{ , for } t > 0 \tag{2.32}$$

where T_u and T_s are the temperatures in the polymer and at the mold wall, respectively.

Equation (2.29) is made dimensionless and solved with the help of the modified separation of variables technique, and the result is later incorporated with the non-linear differential equations of heat and mass transfer. Measurement of the temperature profiles in the polymer slab and mold wall compared well to the model's prediction.

The model by Lee et al. stated the basic concepts for setting up a polymerization reaction mathematical model, but is limited to the extent that the problem is solved numerically at the end, rather than a complete analytical classical solution.

The temperature rise at the pulp-dentin junction due to the polymerization of the resin composite restoration is considered by Jakubinek et al. [8]. When the curing light is projected at the top of the resin during the restoration process some of the light gets absorbed into the material and converted into heat. Some activates the polymerization process which generates more heat. This model is solved numerically by Jakubinek et al. [8] to simulate the temperature rise during the filling process. The variables or the factors, such as, intensity of the curing light, curing time and the enthalpy of polymerization of the resin composite are found out to be the most important parameters from the numerical result.

The paper by Jakubinek et al. [8] mainly concentrated on modeling the source or the heat generation term. The assumptions that are made to make the problem simple and easy to solve are:

(i) the light intensity decreases according to

$$I = I_0 e^{-z/\psi} \tag{2.33}$$

where I_0 is the intensity at the surface, and z is the depth into a material with 1/e penetration depth, ψ , and is converted entirely into heat. It can be estimated as a per unit volume heat source by slicing out the geometry, shown in red line in Fig. 12,

into thinner sections, and (ii) the heat produced in the polymerization of the composite is released uniformly over both its volume and over time during which the composite is exposed to the light. In order to support this assumption the heat source which is there in the n^{th} layer of the resin , Figure 12, due to the curing light, Q_{Ln}, is determined by subtracting the intensity of the light that is entering from the intensity of the light that is leaving the thin section of the geometry, divided by the thickness of the slice, d,

$$q'''_{L,n} = \begin{cases} \frac{I_0}{d}(e^{-(n-1)d/\psi} - e^{-(nd/\psi)}) \text{, for } 0 \le t \le t_L \text{ or 0, otherwise} \end{cases} \quad (2.34)$$

over the volume of the composite. For finding the temperature distributions, Jakubinek numerically simulated a two-dimensional, axi-symmetric tooth model using the software COMSOL^{TM} 3.3a by taking into account the above mentioned assumptions.

To validate the numerical simulations, an in-vitro experiment is conducted. In the experiment, a real molar tooth extracted from a person is used. The molar is submerged in a cement-enamel junction in a 37 ^{o}C water bath. This experiment depicted the real life scenario of a human tooth. As the pulp region of the real tooth has blood vessels in it, Jakubinek circulated water through the pulp chamber at a rate of 4mL/h using a peristaltic pump. A thermocouple is inserted into the pulp region so as to measure the temperature rise near the pulp-horn during the process of curing due to light. The photograph of the experimental set-up (a) and the corresponding 2D finite element model (b) is shown in Figure 12.

As per the journal, two experiments are needed to determine the heat generation due to polymerization. In the first exposure, the curing light causes the resin to polymerize. The temperature rise in the first exposure is caused due to the heat generated by the curing process as well as due to the absorbed heat energy from the light activation unit. While the second exposure, which is done immediately, suggests the temperature rise only due to the absorption of the heat energy by the resin.

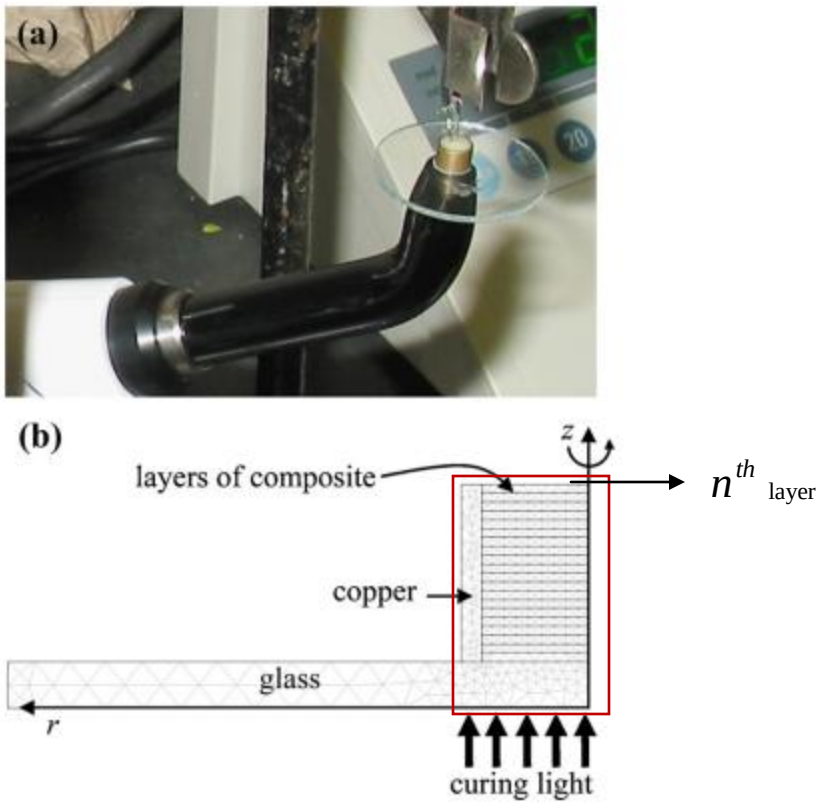

Figure 12. (a) Experimental set up. (b) Corresponding two-dimensional axisymmetric finite element model [8].

Thus the difference between the two experiments gives the temperature rise due to polymerization reaction only. The numerical model provided a good approximation to the experimentally observed temperature increase. The predicted temperature in comparison to measurements is displayed in Figure 13.

This papers is of great importance because of the motive of research and the design of the experimental set-up. The experimental set-up is simple and easy to design. The graphs posted in this paper can be compared later to prove the validity of the ongoing research work and experimental set-up.

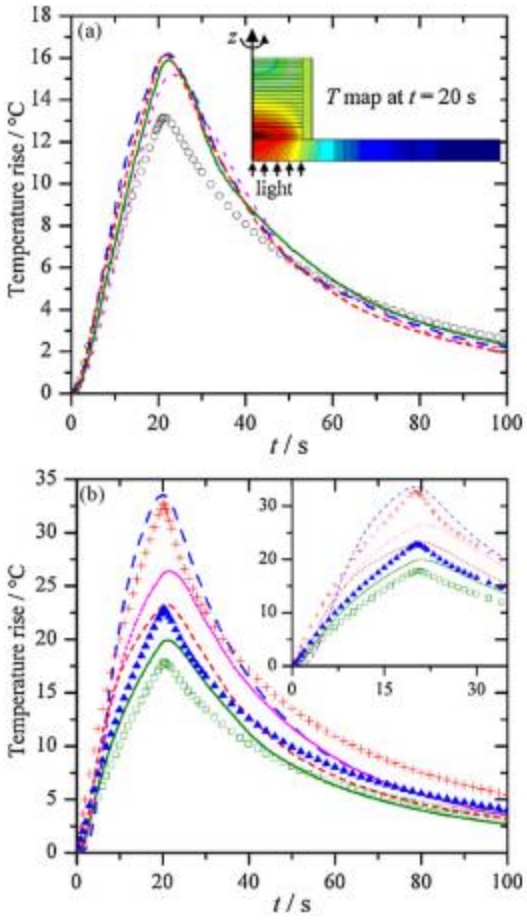

Figure13. FEM results at the center node for ΔH_{polym}=0, 10J/g (□) , 20J/g (Δ) and 40J/g (+), in comparison to the experimental data for (a) pre-cured composites, temperature profile at t = 20 s and (b) composite curing light curing, region from 0 to 30 s [8].

Lin et al. [11] presents the current understanding on heat transfer in human tooth by reviewing both experimental study and mathematical modeling. This paper has comparative study of various models which is quite helpful in understanding the basic concepts of heat transfer in tooth. It also provided reference to multiple papers which are quite helpful from the research point of view. It analyzed a model for the laser interaction with tooth hard tissue, where it stated about the one-dimensional heat conduction equation based on the Fourier conduction law and energy conservation equation.

To analyze the heating of tooth hard tissue by laser, Zuerlein et al. [26,27] proposed a one-dimensional heat conduction equation,

$$\frac{\partial T(z,t)}{\partial t} = \frac{k}{\rho C}\frac{\partial^2 T(z,t)}{\partial z^2} + \frac{q'''(z,t)}{\rho C} \tag{2.35}$$

where the source term $Q(z,t)$ is the temporally and spatially varying laser power input:

$$q'''(z,t) = Q(z,t) = (1-R')F(t)\mu_a e^{-\mu_a z}, \tag{2.36}$$

where z (m) is the depth from tooth front surface, R' is the reflectance of laser beam of a specific wavelength on a specific tissue surface, μ_a is the absorption coefficient, $F(t)$ (J/m^2) is the time dependent incident fluence of the laser pulse (assuming that absorption is consistent with the Beer-Lambert law). When a specific type of laser ,e.g. CO2 Erbium[1]:YSGC and Erbium: YAG lasers is used, the important optical properties are the reflectivity and absorptivity, while scattering is negligible in highly absorbing materials (e.g., tooth) [6,26]. Combination of Eqns. (2.35) and (2.36) leads to,

$$\frac{\partial T(z,t)}{\partial t} = \frac{k}{\rho C}\frac{\partial^2 T(z,t)}{\partial z^2} + \frac{(1-R')F(t)\mu_a e^{-\mu_a z}}{\rho C} \tag{2.37}$$

By solving Eqn. (2.37) numerically, the tooth temperature is found out as a function of both position and time.

Various assumptions are made inorder to simplify the three dimensional tooth problem to an one-dimensional mathematical model. The front and the back surfaces of the tooth sample is assumed to be insulated and the absorption depth is assumed to be much smaller than the diameter of the laser light. Considering the assumptions, the heat conduction problem can be solved in the axial direction only.

In Lin's [11] model the heat generation term by the curing light is taken as a function of both position and time, which is of great use from the on-going research point of view. This work not only helped in understanding the source term due to the curing light, but also identifies the key variables associated with the heat generation term.

[1] Solid state laser where in the laser medium is doped.

Along with determining the temperature rise of a resin as the function of position and time, estimating the accurate curing depth of the resin is also important. If the depth of cure of the resin is not proper then it can cause some undesirable effects in the tooth. So knowing the curing depth of the individual resins is important from its dental application point of view. A paper by Chen et al. [4] suggests a method for evaluating the curing depth accurately. The journal suggests a pilot study of the simple photon migration model to determine the curing depth of the resin. The primary purpose of this model is to calculate the total amount of radiant exposure, i.e. the product irradiance with time, for the dental resin. The irradiance is described as the total amount of electromagnetic radiation per unit area incident on a surface. The calculated radiant exposure is then related to the depth of cure of that particular resin using the polymer kinetics model [20].

The Monte-Carlo method of numerical simulation is used to calculate the amount of photon that is migrated into the composite resin. As a result it helps in predicting the radiant exposure distribution. The correlation between the radiant exposure distribution with either the degree of conversion or the hardness helps in determining the light curing efficiency for a light activated composite system.

In the experiment, Chen [4] used a composite cylinder of 21 mm by diameter and 15 mm deep made up off Z100, Shade A2. The composite cylinder is then cured with a tungsten-halogen lamp emitting 600 mW/cm^2 which is placed 1mm above the composite cylinder for a time period of 60 seconds.

To evaluate the curing extent distribution the measurement of the degree of conversion and the hardness is done for every 2×1 mm grids along the longitudinal cross section. The most common way to determine the degree of conversion of the light activation composites is by using the Fourier Transform Infrared spectroscopic analysis (FTIR). The calculated radiant exposure (H) distribution along the cross section is related to the distribution of curing extent, $\frac{DC}{DC_{\max}}$, and fit with two polymer curing kinetics models: the exponential model

$$DC = DC_{\max}[1 - \exp((\ln 0.5)H / H_{DC}^{50\%})] \tag{2.38}$$

and Racz's [20] model,

$$DC = DC_{\max} / [1 + ((H / H_{dc})^{50\%})^{-2}], \tag{2.39}$$

where $H_{DC}^{50\%}$ is a fitting parameter representing the threshold for 50% of the maximum curing level.

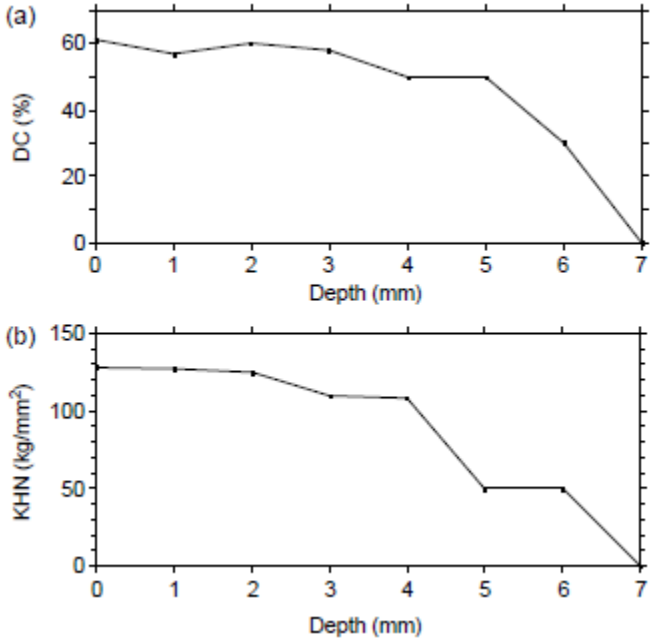

Figure 14. (a) The DC versus depth along the central position (x=0 mm)
(b) KHN versus depth along the central position[4].

On knowing the optical properties, the geometry of the composite, the spectrum and the geometry of the light source is known then the Monte-Carlo model can simulate the value for the depth of cure accurately as shown in Figure 14.

A real life scenario is considered by Motawea et al. [15] who used a three-dimensional transient thermo-elastic finite element model to calculate the temperature changes and the thermal stress distribution in the crowned mandibular first molar teeth. The motive of this research is to find out the effect of the crown materials and cement types on thermal stress distribution of human tooth (first molar). An numerical finite element method is used to solve the three dimensional crowned mandibular problem.

Resin, glass ionomer, and zinc phosphate cements are evaluated through the numerical simulation method. The temperature changes due to the intake of the hot liquid along with the thermal stress distribution due to this temperature changes are simulated. The temperature changes and the stress distribution is plotted and the results are analyzed. All these steps helped Motawea et al. [15] decide which among the cement crowned materials and the cement types is most suitable to use.

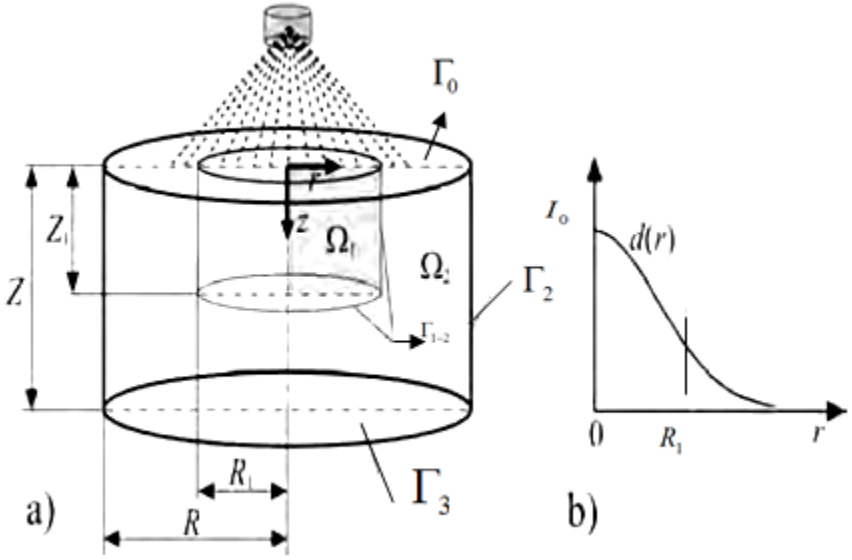

Figure 15. (a) Experimental set up. (b) Intensity distribution at Z = 0. [23].

The study of the heat source term involving the entire chemical kinetics of the photosensitive resin composite when it is subjected to curing light is found in a very limited number of papers. The paper by Siedlecki et al. [23] is one of them.

When the photosensitive resin composites are exposed to the curing light, the photoinitiator molecules present in it gets activated. The intra-molecular cleavage occurs in the activated photo-initiator molecules to release free radicals that eventually initiates the polymerization reaction. The source term by Siedlecki et al. [23] takes all the steps of polymerization; initiation, propagation and termination, into account. The equations framed in the paper [23] for the axially-symmetrical domain is solved numerically.

A cylindrical two dimensional domain is considered. The monomer/polymer mass is placed inside the porcelain form shaped as a cylinder with Radius R_1 and height Z_1. The entire set-up for the problem is shown in Figure 15.

Siedlecki solved a two dimensional equation:

$$C_m \rho_m \frac{\partial T_m}{\partial t} = k_m \nabla^2 T_m + q_m''', \tag{2.40}$$

where index m $= \{1, 2\}$ identifies the monomer/polymer and the form of sub-domain, respectively. The q_m''', heat source function, for m = 1, can be written as:

$$q_1''' = \Delta H_R \times R_p \tag{2.41}$$

Equation (2.40) is solved using the initial and boundary conditions at the contact surface between the monomer/polymer and form and the external surface of both the sub-domains,

$$T_m\Big|_{t=0} = T_i \tag{2.42}$$

$$-k_1 \frac{\partial T_1}{\partial n} = -k_2 \frac{\partial T_2}{\partial n} \tag{2.43}$$

$$T_1 = T_2 \tag{2.44}$$

$$-k_m \frac{\partial T_m}{\partial n} = -h(T_{amb} - T_m) \tag{2.45}$$

$$\frac{\partial T_m}{\partial n} = 0 \tag{2.46}$$

$$\frac{\partial T_m}{\partial r}\Big|_{r=0} = 0 \tag{2.47}$$

where $\frac{\partial}{\partial n}$ is a normal derivative , T_{amb} is the ambient temperature, ΔH_R is the heat of the

polymerization reaction, R_p is the polymerization rate, T_i is the initial temperature. Equation. (2.43) and Eqn. (2.44) states the composite layer boundary condition, where T_1, k_1 and T_2, k_2 are the absolute temperature and the thermal conductivity of the restoration and the porcelain cylinder , respectively. The R_p term in the Eqn. (2.41) is given as:

$$R_p = k_p M \sqrt{\frac{\phi I_a}{k_t}} \tag{2.48}$$

where ϕ is the quantum yield for initiation, k_p and k_t are the propagation and termination rate constants, respectively and M is the temporary monomer concentration. And the I_a (r,z,t), which is the intensity of the absorbed light into the polymer/monomer mass is:

$$I_a = \varepsilon S I\,, \tag{2.49}$$

and

$$I = I_0 d(r)\Theta(t)\exp(-\varepsilon S z)\,, \tag{2.50}$$

where I_0 is the intensity of the beam, $d(r)$ is the shape distribution function, $\Theta(t)$ is the light exposition in time, ε is the molar absorptivity constant for the photo initiator and S = S(r,z,t) is the temporary concentration point of the domain.

In this paper Siedlecki used the thermophysical parameters of the monomer/polymer: C_1=1700J/kg ^0C, ρ_1=1150 kg/m^3, k_1= 0.2 W/(m ^0C), ΔH_p = 166 kJ/mol, $\frac{k_p}{k_t^{0.5}}$=0.26 $(m^3/mols)^{1/2}$, ε = 20 m^2/mol, ϕ = 0.1, and thermophysical parameters of porcelain: C_2=2300 J/kg ^0C, ρ_2=840 kg/m^3, k_2= 1.3 W/m ^0C. The initial concentration of the monomer and photo-initiator are M_{init} = 3 kmol/m^3 and S_{init} = 0.15 kmol/m^3 and the initial temperature and the heat transfer coefficient are T_{amb} = 20 ^0C and h=10 W/$m^{2\,0}C$. The Eqn. (2.40) is solved numerically using the initial and

boundary conditions along with the above mentioned thermophysical values. The temperature versus time plot as a result of the numerical solution is shown in the Figure 16.

The source (heat generation) term suggested in [23] took into consideration all the chemical processes taking place inside the resin when it is subjected to the curing light. The paper has a strong mathematical base which is of great importance for both the ongoing and future thesis projects.

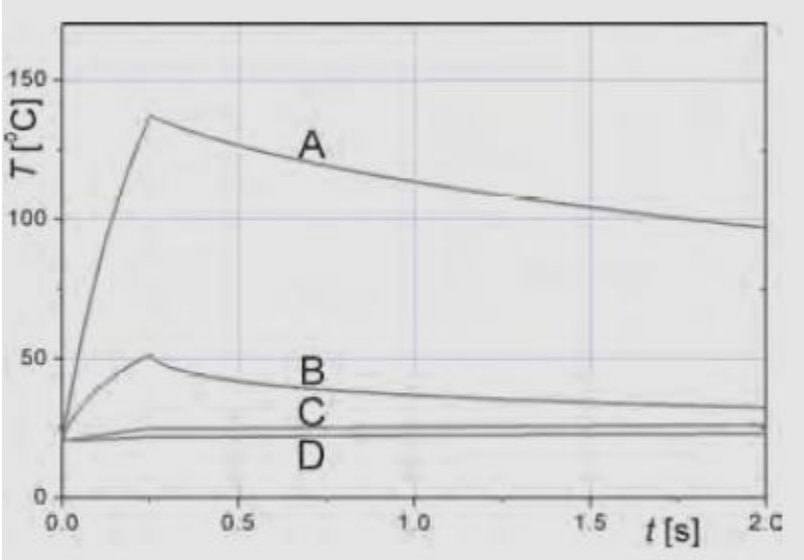

Figure 16.Temperature versus time at selected points in the monomer/polymer mass [23].

Balland et al. [1] got the probable absorption profile of light by taking into consideration the diffusion effects, depth of cure and exposure time as:

$$\varphi = \left[\frac{1}{\left(\frac{\tau}{t}\right)^{1/2} \log\left\{ \frac{1}{1-[1-\exp(-\sqrt{t/\tau})]\exp[-\vartheta(t)]x^{\upsilon(\tau)}} \right\}} \right]^{-2/a'} \tag{2.51}$$

where τ is the time constant, $a^{'}$=-1.26, x is the depth, $\upsilon = 1.34t^{0.07}$ and $\vartheta = 0.97t^{-0.44}$. The plot between the absorption profile and the depth for different period of time is shown in the Figure 17.

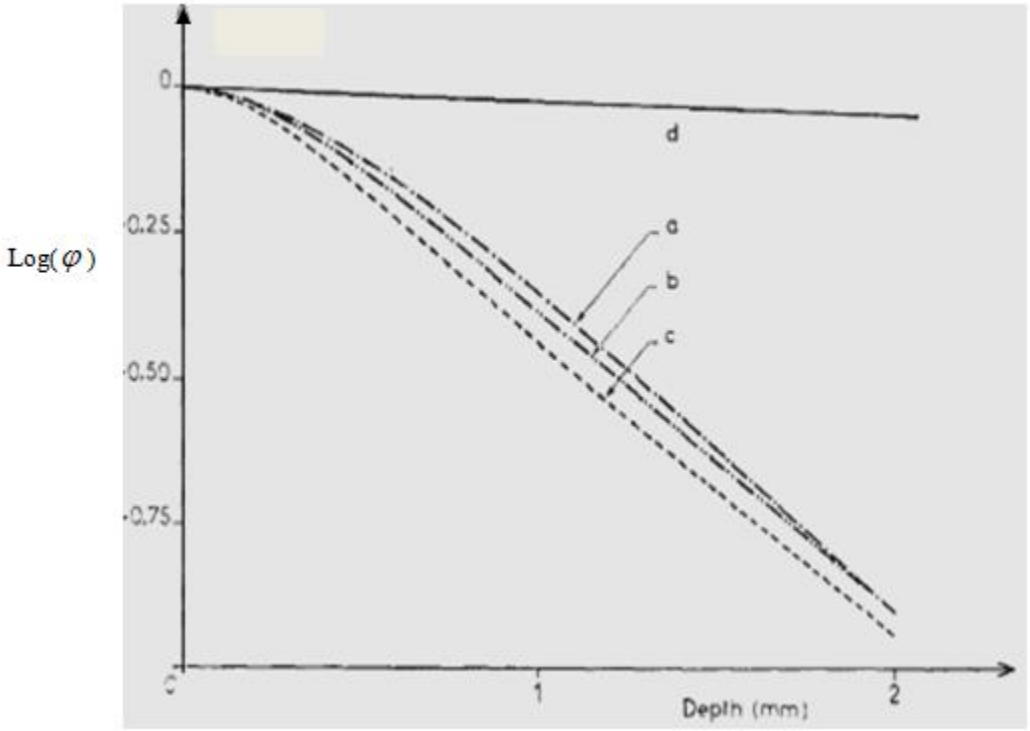

Figure 17. Absorption profile versus depth for different exposure times. (a)22 s, (b)66 s (c) 110 s, and (d) uncharged resin. [1].

Perry et al. [18] suggested a mathematical model for the photo polymerization reaction for a stationary laser. Perry suggested a very intuitive analytical model for the photo-polymerization process taking into consideration all the steps from the projection of the curing light on the polymer resin till the termination polymerization reaction occurring inside the resin as a result of the polymerization reaction. In this article, the absorption of light, the conversion of the photoinitiator and the conversion of the monomer are modeled. Two cases are considered for the monomer conversion.

The first case is the termination which occurs due to the radical combination. This model is solved both analytical and numerically by using the Joshi and Shultz model [22] and Beer-Lambert's law respectively. The second case states about the process of termination

which occurs as a result of the radical trapping. This second model is solved using an analytical model. Both the analytical model of the first and second cases are compared and both are nearly the same. Some graphs comparing depth of cure and the percentage conversion of monomer concentration to polymer chain, and the critical depth (maximum

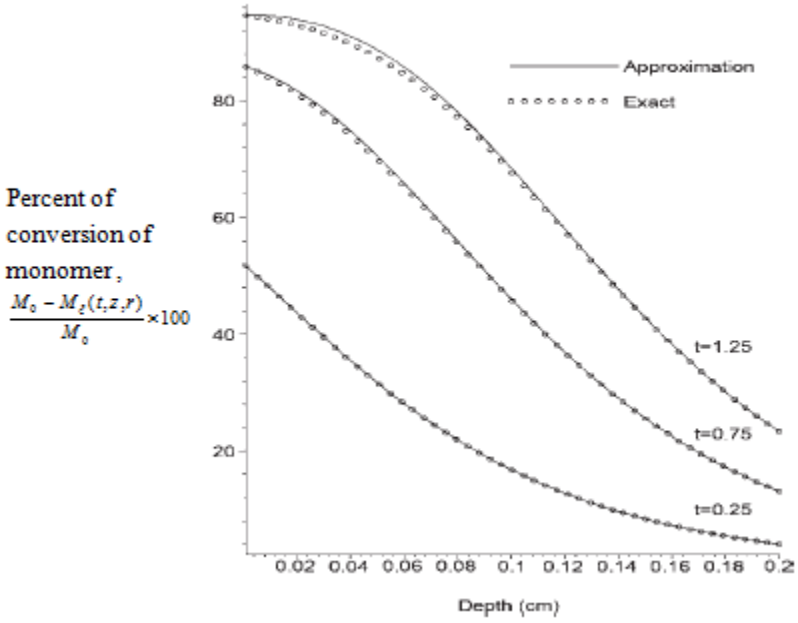

Figure 18. Comparison between the analytical and exact approximation for the percent conversion of monomer and depth of cure of the resin at r=0 and $\frac{k_p}{k_t^{1/2}} = 260\,(cm^3 s^{-1} mol^{-1})^{1/2}$ [18].

cure depth for some optical value of photoinitiator concentration) versus photoinitiator concentration are shown in Figures 18 - 19.

The percentage of monomer concentration to polymer chain can be expressed as,

$$\frac{M_0 - M_\xi(t,z,r)}{M_0} \times 100 \tag{2.52}$$

where M_0 is the initial concentration of the monomer, ξ =EX, RC, M_{EX} is the monomer concentration of the exact solution and M_{RC} is the monomer when termination is by radical combination.

This model [18] not only modeled a detailed mathematical approach for photo polymerization but also plotted multiple graphs for future reference.

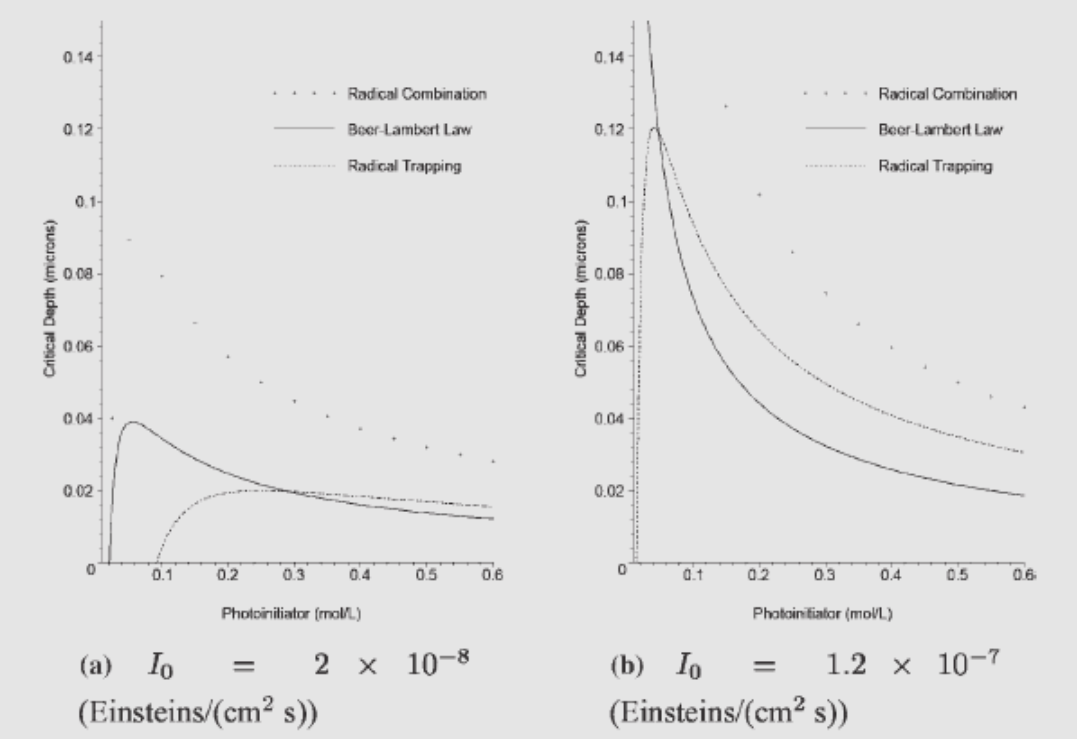

Figure 19. Comparison of the critical depth as a function of photoinitiator for different initial intensity and different terminal kinetics [18].

2.2 Experimental Investigations

Kleverlaan et al. [9] estimated the curing efficiency and the heat generation of two high-intensity halogen lamps, the Australis 10 HIP (1100 mWcm^{-2}) in curing three resin composites (InTen-S, Tetric Ceram, and Filtek Z250). By measuring the Vicker's hardness and the depth of cure of the resin curing efficiency of the composite could be evaluated.

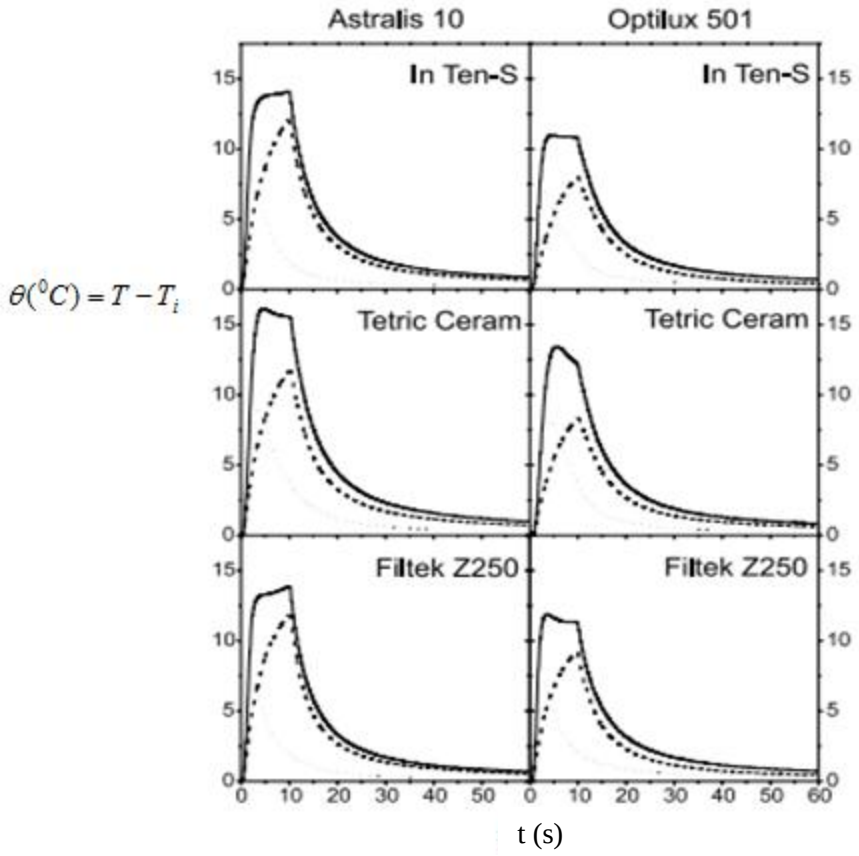

Figure 20. Temperature rise during curing (solid line) and during subsequent irradiation (dashed line) in InTen-S, Tetric Ceram and Filtek Z250 cured with the Astralis 10 (10 s HIP) and Optilux 501 (10 s Boost). The exotherm of the polymerization reaction (dotted line) is obtained by subtraction of the last two curves. The lines represent the average of three experiments [9].

The temperature curves for InTen-S, Tetra Ceram and Filtek Z250 cured with the Astralis 10 (HIP) and Optilux 501 (Boost) during polymerization and after subsequent irradiation is shown in Figure 20. The temperature curve for the exotherm of the polymerization reaction is obtained by subtraction of the two experimental curves [12,14,21].

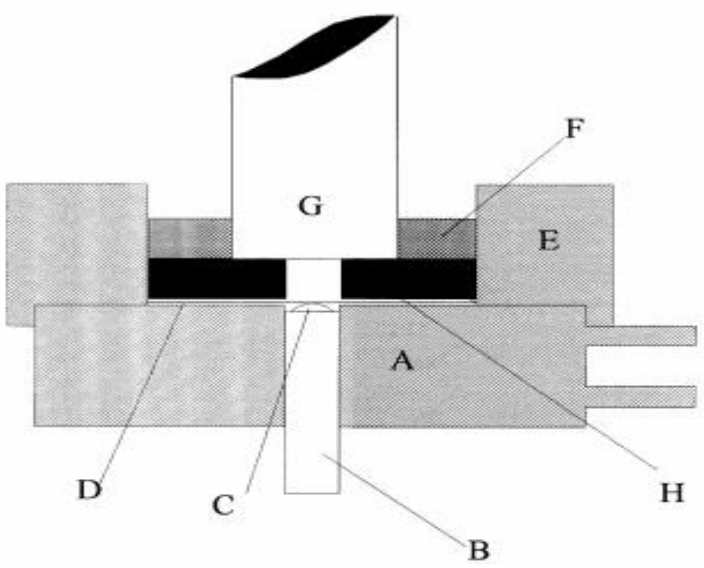

Figure 21. Line diagram of apparatus used to measure temperature rise. A, water jacket; B, thermistor mount; C, thermistor tip; D, 4 mm aperture; E, alignment ring; F, light guide alignment ring; G, light guide; H, black nylon spacer ring [21].

As per the plots, it is found out that there is no such difference between the two different lamps for the three resin composites. The rise in temperature during curing is recorded to be between 11.2 ^{o}C and 16.2 ^{o}C. The above results show that the temperature rise due to Optilux 501 is less in all the three cases in comparison Astralis 10.

Shortall et al. [21] measured the temperature rise during polymerization of light-activated resin composites at distances of 0, 2, 4, and 6 mm from the thermistor tip through a 4 mm aperture by using a thermistor. To keep the light guide tip in proper alignment with the sensor surface at each of the preset distances the black nylon spacer rings with an alignment guide is used. This setting also helps in stopping the light reflection from influencing the results. Three readings are taken at each of the four preset distances for the light exposure of 60 s. The water bath surrounding the apparatus is maintained at $37 \pm 0.5\ ^{o}$C. All the readings are taken with the temperature of the water always maintained at $37 \pm 0.5\ ^{o}$C. The line diagram of the apparatus used to measure temperature rise is shown in Figure 21.

Lloyd et al. [12] measured the temperature rise that occurs during the setting of the visible light-cured composites with the help of a modified differential thermal

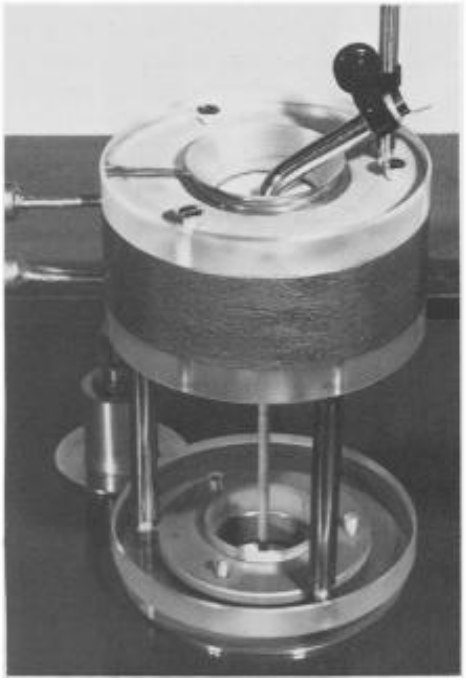

Figure 22. The modified DTA head in place on the instrument with the fiber optic from the light source in position on the sample in its well. The insulated heating jacket surrounds the head - entry and exit water pipes are to the left [12].

analyzer. The modified DTA (Differential thermal analysis) and the techniques used in the experiment are suitable for the measurement of temperature rises together with corresponding times. Figure 22 shows the modified DTA.

In the paper by Masutani et al. [14], the motive is to monitor the temperature rise during the exothermic polymerization reaction of five selected visible light-activated composites resins cured with five activator lights.

A white Teflon cylindrical mold of 8 mm DIA and 4 mm depth is filled with composite resin. To monitor the temperature a chromel-alumel thermocouple is inserted into the center of the specimen. The light is projected for 60 s period for the first time and again and again for five times after the specimen returns to 24 ^{o}C. The relative intensity of the light is measured by the radiometer. Thus the temperature time graphs are plotted this way. To determine the temperature rise due to the exothermic polymerization reaction, the temperature rise during the second exposure is subtracted from the peak temperature during the first exposure. According to the author the resin composite must be placed incrementally and cured with a moderate intensity of light for a longer period

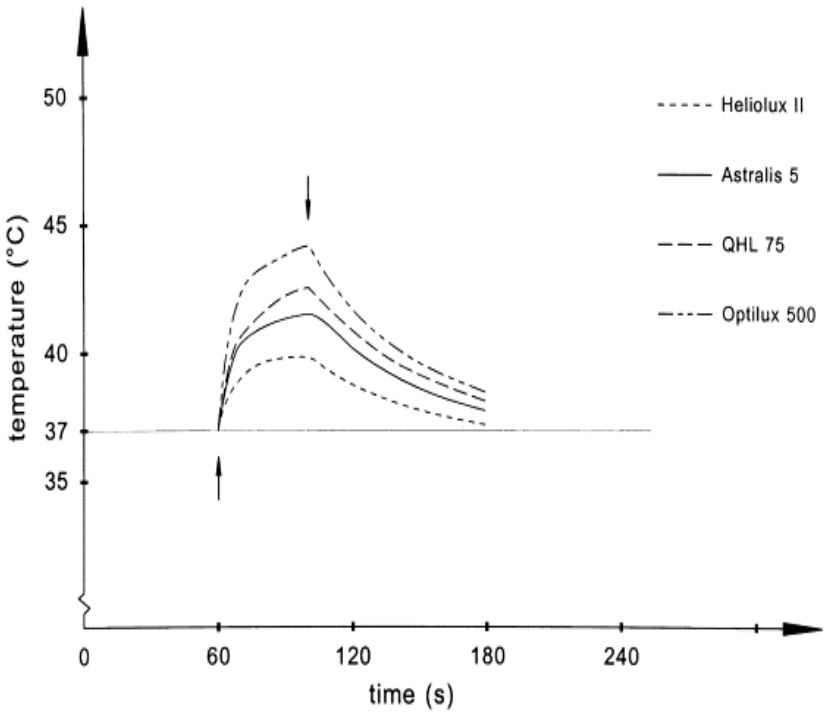

Figure 23. Characteristics of pulp chamber temperature versus time curve using the Heliolux II, Astralis 5, QHL 75 and Optilux 500 curing units. Arrows indicate the beginning and ending of the 40 s irradiation time [7].

of time than using a high intensity of light for a short period of time. It helps in reducing the volume shrinkage to a greater extent.

Hannig et al. [7] prepared a class II cavity in extracted molar teeth, leaving layer 1 mm thick between pulp chamber and proximal cavity wall. A 2mm composite resin layer is applied to the proximal box and light-cured with the selected curing units. Light curing took place for 40s, 5s and 10s for different compounds. Measurement of pulp chamber temperature changes during polymerization is performed with a type K thermocouple positioned at the pulp-dentin junction. Mean values are calculated from 10 measurements with each light-curing unit. The temperature versus time graph for different light activation unit is shown from Figures 23 - 25.

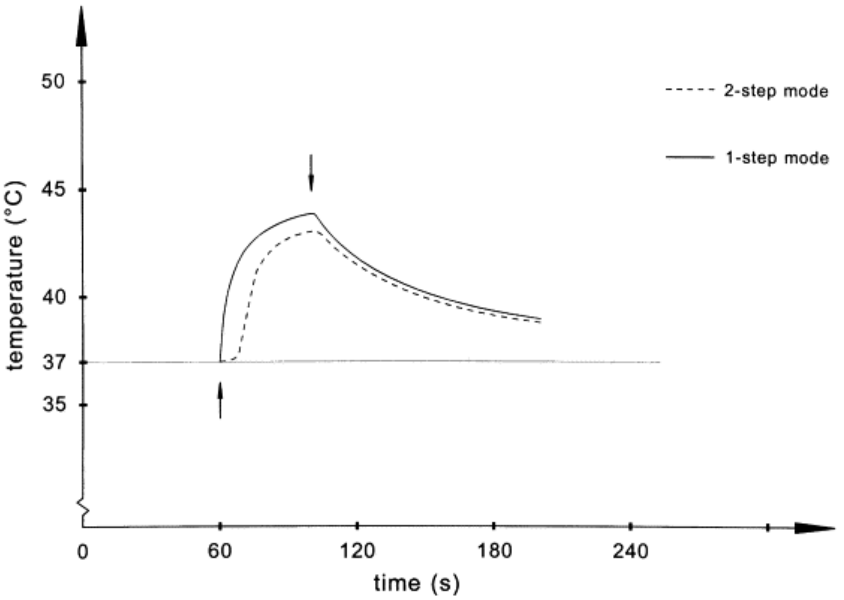

Figure 24. Characteristics of pulp chamber temperature versus time curves using the Elipar Highlight curing unit in the 1-step and 2-step mode. Arrows indicate the beginning and the ending of the 40s irradiation time [7].

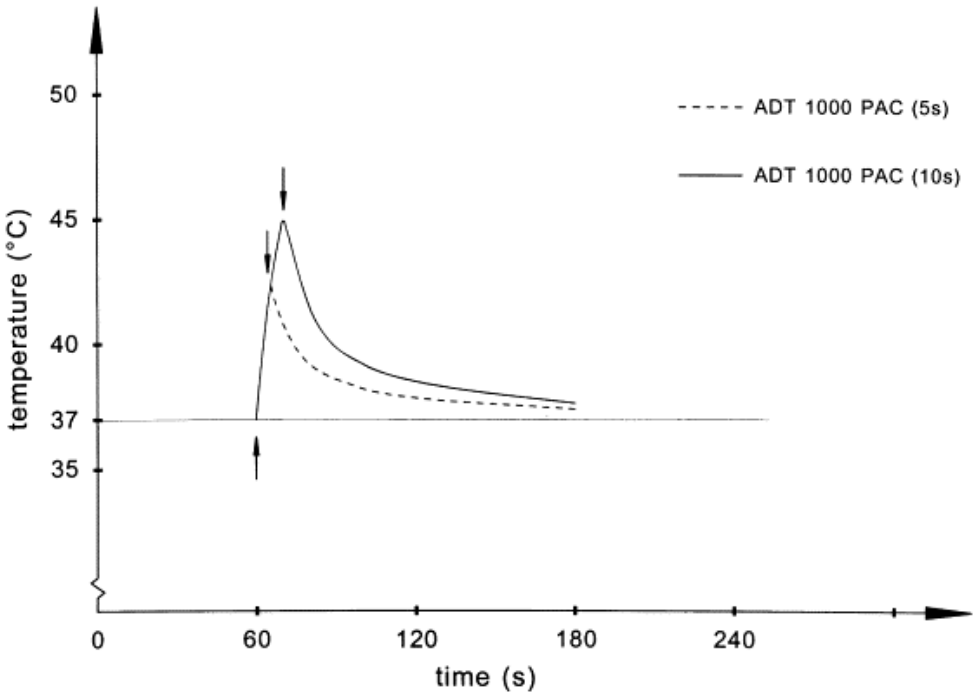

Figure 25. Characteristics of pulp chamber temperature versus time curves caused by irradiation for 5 and 10 s using the ADT 1000 PAC system. Arrows indicate beginning and ending of the 5s/10s irradiation time [7].

Chapter 3

Mathematical Formulation and Analytical Methods

In this chapter, the exact solution to the problem of heating of the restorative resin compound by the curing light is taken into consideration. Before getting deeper into the mathematical formulation, the basic theory of polymerization and heat generation in the restoration process is described.

3.1 Basic theory behind the heat generation in the restorative resins

When the curing light is projected on the surface of the composite resin, the temperature in the resin rises due to heat generation through light activation of polymerization. This heat generation is due to two factors. The first is the absorption of energy from the curing light source which travels through the layers of the composite via heat conduction. The second cause is the polymerization reaction, which occurs due to the absorption photons. Polymerization reaction initiated by photon absorption is termed as photo-polymerization and is exothermic, thus raising the temperature of the composite.

In photo-polymerization, small monomers join together to form a long chain polymers. According to Stansbury [24] the photo-initiator present in the photo-sensitive resins helps in absorbing the light energy and as a result, generates the reactant species that directly or indirectly helps promoting the polymerization reaction. There are three basic steps involved in this reaction: initiation, propagation and the termination.

In the initiation step, the photo-initiator molecules absorb the light and decompose into free radicals, which initiate the polymerization reaction. Initiators, e.g., benzoin methyl ether, decompose into two radicals as a result of intra-molecular α-cleavage due to the photon absorption and both have the power to initiate additional reactions. These free radicals react with the monomer molecules present in the resin to form the initial activated monomers. The activated monomer combines with a non-activated monomer to form the polymer chain. This is the propagation step. Termination of the chain reaction occurs when an activated monomer reacts with another activated monomer. Thus the termination step occurs due to either the combination or the disproportionate concentration of the two activated monomer molecules.

Rabek [19] states describes the mechanism polymerization reaction clearly. The equations for the initiation, propagation and the termination reactions are,

$$\text{Initiation systems} \rightarrow M^{*} \qquad \text{Initiation, } R_i \qquad (3.1)$$

$$M + M^{*} \rightarrow M^{*} \qquad \text{Propagation, } k_p \qquad (3.2)$$

$$M^{*} + M^{*} \rightarrow \text{polymer} \qquad \text{Termination, } k_t \qquad (3.3)$$

where R_i is the initiation rate, k_p is the propagation rate constant, k_t is the termination rate constant, and M^{*} is the activated monomer molecule, respectively. Thus heat generation due to the curing light and polymerization results in the increase of the temperature of the resin with respect to time. The heats of reaction, H_R, for each step combine to produce the overall heat generation within the resin as long a source of light activation is present.

In the following, the initiation rate, propagation rate, monomer concentration, propagation rate constant, termination rate constant etc. involved in the polymerization reaction are taken into consideration in designing the heat generation term for the polymerization reaction.

3.2 Introducing the one-dimensional heat transfer problem

The entire structure of a tooth is shown in Figure 26. When tooth decay occurs, restoration in is done by drilling a hole, or cavity, and filling it with a composite resin to be cured by photo-polymerization. As the tooth is a three-dimensional structure, prediction of heat transfer and temperature versus time is thus a three-dimensional problem. For the sake of simplification, this problem is re-cast as one-dimensional problem without the loss of generality. A small rectangular slice, or segment, of the tooth is taken as the solution domain so that the modeling of the heat generation term can be easily handled mathematically.

Figure 27 shows a physical realization of the solution domain as a Teflon block with a 2 mm × 4 mm channel (the slice) machined in it. The restorative resin is to fill the channel in the experiments conducted in this investigation and is long enough (22 mm) so that light activation ceases before polymerization extends the full length of the domain.

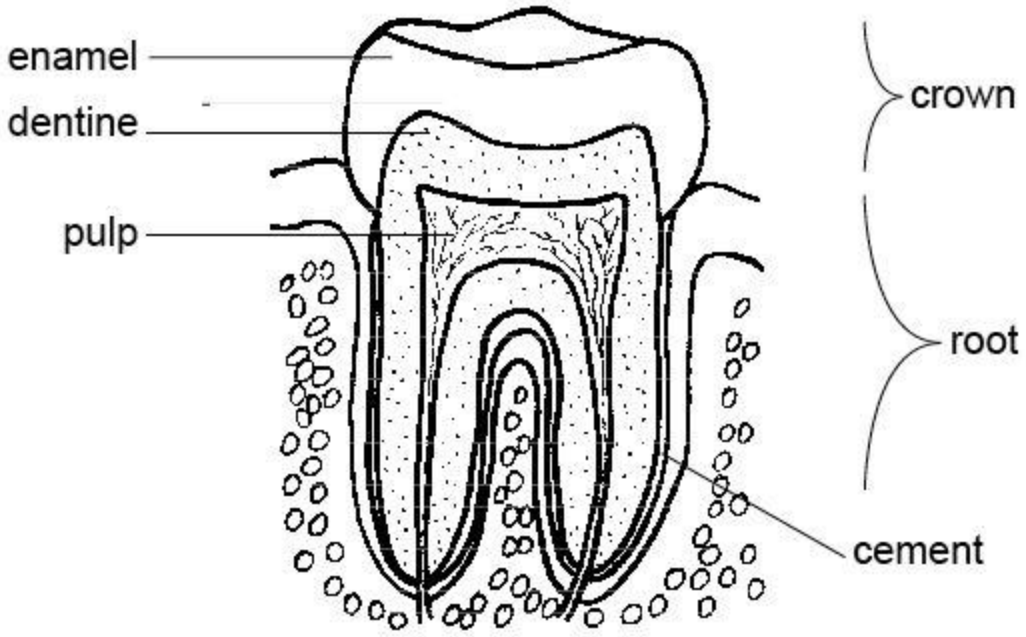

Figure 26. Tooth Structure

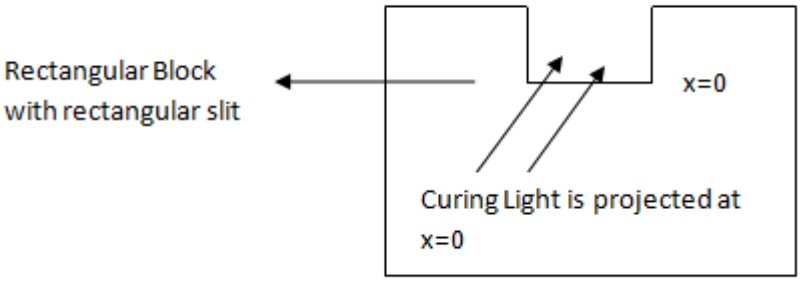

Figure 27. Physical model of the rectangular
domain with the rectangular channel (slice/slit).

The channel is thus long enough so that the slice can be considered a semi-infinite domain both mathematically and experimentally. Moreover as Teflon^{TM} has a very low conductivity (~0.25 W/mK), lateral heat loss is low, and the one-dimensional conduction problem is essentially replicated in the laboratory.

Let us now imagine that the tooth is sliced, and we take into consideration one rectangular slice of the tooth. This rectangular slice is the slice in which the analytical heat transfer analysis is performed. The physical model of the Teflon^{TM} block replicating

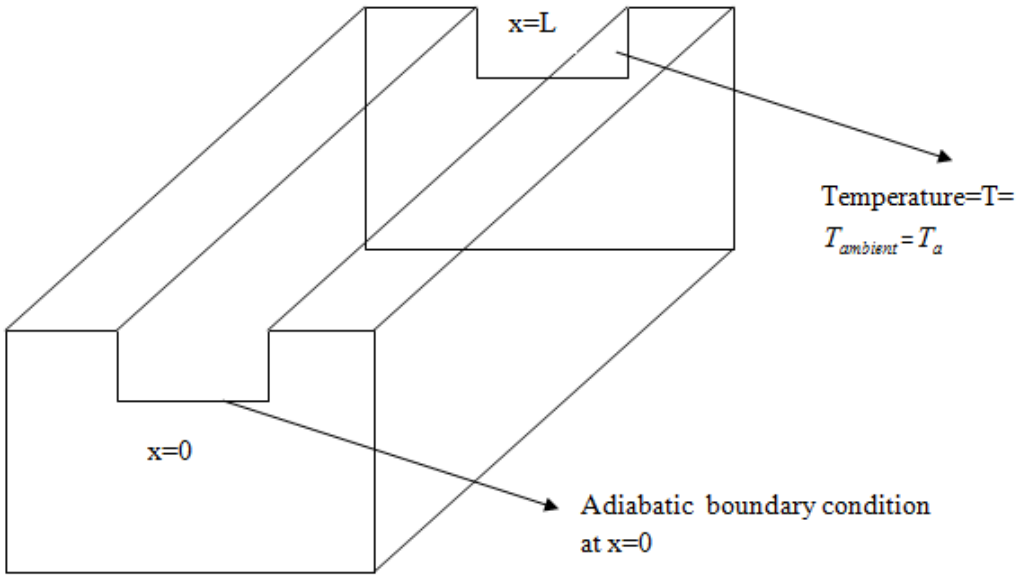

Figure 28. Solution domain and co-ordinates

the rectangular block with a rectangular cavity of 2 mm $\times$ 4 mm in area is shown in Figure 28. The rectangular sample is made up of Teflon^{TM}.

The transient heat conduction problem is solved under the assumption of constant thermophysical properties. The heat generation term in the differential energy balance is modeled with a variety of function, including a constant. A solution for a finite length domain is considered for the sake of completeness as well. Figure 28 shows the solution domain and coordinates.

3.3 Governing Equation, Boundary and Initial Conditions

Governing Equation. The governing equation with time- and space-dependent heat generation is,

$$\rho C \frac{\partial T(x,t)}{\partial t} = k \frac{\partial^2 T(x,t)}{\partial x^2} + q'''(x,t) \qquad t > 0 \qquad (3.4)$$

Boundary conditions at $x = L$ (finite length) and at $x \to \infty$ are,

$$T = T_b \text{ at } t > 0,\ x = L, \qquad (3.5)$$

$$T = T_{\infty} \qquad \text{at } t > 0,\ x \to \infty \tag{3.6}$$

where T_b is the temperature of the back-end of the rectangular sample and q''' is the heat generation term due to polymerization of light activated resin by the curing light. The boundary condition at $x = 0$ and, t > 0 is considered for constant heat flux, convection-conduction (mixed) and constant temperature conditions. A constant heat flux boundary condition refers to the case where the curing light is pressed directly onto the surface of the resin at $x = 0$. Thus this boundary condition that is most appropriate for the actual polymerization process. A mixed boundary condition is appropriate where there is heat loss to the ambient by convection while receiving the net radiant heat flux from a distance. A constant temperature boundary condition a limiting case and is considered for completeness. In summary, the boundary conditions are,

Adiabatic Case: $$\frac{\partial T}{\partial x} = 0 \tag{3.7}$$

Convection-Conduction Case: $$k\frac{\partial T}{\partial x} = h(T - T_{amb}) \tag{3.8}$$

Isothermal case: $$T = T_i \tag{3.9}$$

where T_{amb} and T_i are the ambient and initial temperature respectively.

The initial condition for the solution irrespective of the boundary condition at x = 0 is,

$$T = T_i \qquad at\ \ x,\ t = 0 \tag{3.10}$$

The above governing equations, initial and boundary conditions are changed into non-dimensional forms so as to simplify the solution of the problem. Equation (3.4) is written,

$$\frac{\partial \theta(\eta,\tau)}{\partial \tau} = \frac{\partial^2 \theta}{\partial \eta^2} + \frac{L^2}{k} q'''(\eta,\tau) \qquad \text{at } \tau > 0 \tag{3.11}$$

where η =0 for finite case and $\eta \to \infty$ for semi-infinite case.

The dimensionless variables are: τ =time constant= $\frac{\alpha t}{L^2}$; α = thermal diffusivity= $\frac{k}{\rho C}$; $\eta = \frac{x}{L}$; $Bi = \frac{hL}{k}$ =Biot number; and θ is the relative temperature difference.

The boundary conditions at η =1 (for finite cases) and at $\eta \to \infty$ are,

$\theta = 0$ at τ >0, η =1 (3.12)

$\theta = 0$ at τ >0, $\eta \to \infty$ (3.13)

The boundary conditions for the three conditions at η =0 and τ >0 are mentioned below:

Adiabatic Case: $\frac{\partial \theta}{\partial \eta} = 0$ (3.14)

Convection-Conduction Case: $\frac{\partial \theta}{\partial \eta} = Bi(\theta)$ (3.15)

Isothermal case: $\theta = 0$ (3.16)

The dimensionless initial condition for the one-dimensional problem is mentioned below:

$\theta = 0$ at η, τ =0 (3.17)

3.4 Solution

Six cases are considered ad are framed taking into consideration the several boundary conditions at $\eta = 0$ and the two different heat generation terms. The governing equation, the boundary conditions at the two ends, the initial condition and the solution are mentioned under each case in this section of the thesis. Detailed explanations of the solution for all cases are given in Appendix A. Generally, all the cases are solved using the general integral transform technique. The cases that are considered are:

a) Case 1. constant heat generation term at isothermal boundary condition at $\eta = 0$.

b) Case 2. constant heat generation term at adiabatic boundary condition at $\eta = 0$.

c) Case 3. constant heat generation term at conduction-convection boundary condition (mixed) at $\eta = 0$.

d) Case 4. varying heat generation term with space and time at isothermal boundary condition at $\eta = 0$.

e) Case5. varying heat generation term with space and time at adiabatic boundary condition at $\eta = 0$.

f) Case4. varying heat generation term with space and time at conduction-convection boundary condition at $\eta = 0$,

3.4.1 Finite domain

Case 1.

Governing Equation

$$\frac{\partial \theta(\eta,\tau)}{\partial \tau} = \frac{\partial^2 \theta}{\partial \eta^2} + \frac{L^2}{k} q''' \qquad \text{at } \tau > 0 \qquad (3.18)$$

Boundary Conditions

$$\theta = 0 \qquad \text{at } \eta = 0, \tau > 0 \qquad (3.19)$$

$$\theta = 0 \qquad \text{at } \tau > 0, \ \eta = 1 \qquad (3.20)$$

Initial Condition

$$\theta = 0 \qquad \text{at } \eta, \ \tau = 0 \qquad (3.21)$$

Solution

$$\theta(\eta,\tau)=\frac{q'''L^2(\eta-\eta^2)}{2k}-\frac{2q'''L^2}{k}\sum_{n=0}^{\infty}(1-(-1)^n)e^{-\lambda_n{}^2\tau}\frac{1}{\lambda_n{}^3}\sin(\lambda_n\eta) \tag{3.22}$$

Eigen values

$$\lambda_n=\sin^{-1}(0)=n\pi \qquad \text{n=0,1,2,3.....} \tag{3.23}$$

Case 2.

Governing Equation

$$\frac{\partial\theta(\eta,\tau)}{\partial\tau}=\frac{\partial^2\theta}{\partial\eta^2}+\frac{L^2}{k}q''' \qquad \text{at } \tau>0 \tag{3.24}$$

Boundary Conditions

$$\frac{\partial\theta}{\partial\eta}=0 \qquad \text{at } \eta=0,\ \tau>0 \tag{3.25}$$

$$\theta=0 \qquad \text{at } \tau>0,\ \eta=1 \tag{3.26}$$

Initial Condition

$$\theta=0 \qquad \text{at } \eta,\ \tau=0 \tag{3.27}$$

Solution

$$\theta(\eta,\tau)=\frac{q'''L^2(1-\eta^2)}{2k}-\frac{2q'''L^2}{k}\sum_{n=0}^{\infty}(-1)^n e^{-\lambda_n{}^2\tau}\frac{1}{\lambda_n{}^3}\cos(\lambda_n\eta) \tag{3.28}$$

Eigenvalues

$$\lambda_n=\cos^{-1}(0)=(2n+1)\pi/2 \qquad \text{n=0,1,2,3.....} \tag{3.29}$$

Case 3.

Governing Equation

$$\frac{\partial\theta(\eta,\tau)}{\partial\tau} = \frac{\partial^2\theta}{\partial\eta^2} + \frac{L^2}{k}q''' \qquad \text{at } \tau > 0 \tag{3.30}$$

Boundary Conditions

$$\frac{\partial\theta}{\partial\eta} = Bi(\theta) \qquad \text{at } \eta = 0, \tau > 0 \tag{3.31}$$

$$\theta = 0 \qquad \text{at } \tau > 0,\ \eta = 1 \tag{3.32}$$

Initial Condition

$$\theta = 0 \qquad \text{at } \eta,\ \tau = 0 \tag{3.33}$$

Solution

$$\theta = \frac{q''' L^2((1+\eta Bi) - \eta^2(1+Bi))}{2k(1+Bi)} - \frac{2q''' L^2}{2k(1+Bi)} \times$$
$$\sum_{n=0}^{\infty} e^{-\lambda_n{}^2\tau} \sin\lambda_n(1-\eta)\frac{2(\lambda_n{}^2 + Bi^2)}{(\lambda_n{}^2 + Bi^2 + Bi)}\int_0^1 \sin\lambda_n(1-\eta')((1+\eta' Bi) - \eta'^2(1+Bi))d\eta' \tag{3.34}$$

$$\lambda_n \cot\lambda_n = -Bi \tag{3.35}$$

Case 4.

Governing Equation

$$\frac{\partial\theta(\eta,\tau)}{\partial\tau} = \frac{\partial^2\theta}{\partial\eta^2} + \frac{L^2 q'''(\eta,\tau)}{k} \qquad \text{at } \tau > 0 \tag{3.36}$$

Boundary Conditions

$\theta = 0$ at $\eta = 0, \tau > 0$ (3.37)

$\theta = 0$ at $\tau > 0,\ \eta = 1$ (3.38)

Initial Condition

$\theta = 0$ at $\eta,\ \tau = 0$ (3.39)

Solution

$$\theta(\eta,\tau) = \frac{2L^2}{k}\sum_{n=1}^{\infty}\sin(\lambda_n\eta)e^{-\lambda_n{}^2\tau}\int_{\tau'=0}^{\tau}e^{\lambda_n{}^2\tau'}\int_{\eta'=0}^{1}\sin(\lambda_n\eta')q'''(\eta',\tau')d\eta' d\tau' \quad (3.40)$$

Eigenvalues

$\lambda_n = \sin^{-1}(0) = (n-1)\pi$ n=1,2,3... (3.41)

Case 5.

Governing Equation

$$\frac{\partial\theta(\eta,\tau)}{\partial\tau} = \frac{\partial^2\theta}{\partial\eta^2} + \frac{L^2}{k}q'''(\eta,\tau) \quad \text{at } \tau > 0 \quad (3.42)$$

Boundary Conditions

$\frac{\partial\theta}{\partial\eta} = 0$ at $\eta = 0, \tau > 0$ (3.43)

$\theta = 0$ at $\tau > 0,\ \eta = 1$ (3.44)

Initial Condition

$$\theta = 0 \qquad \text{at } \eta,\ \tau = 0 \tag{3.45}$$

Solution

$$\theta(\eta,\tau) = \frac{2L^2}{k}\sum_{n=1}^{\infty}\cos(\lambda_n\eta)e^{-\lambda_n{}^2\tau}\int_{\tau'=0}^{\tau}e^{\lambda_n{}^2\tau'}\int_{\eta'=0}^{1}\cos(\lambda_n\eta')q'''(\eta',\tau')d\eta' d\tau' \tag{3.46}$$

Eigenvalues

$$\lambda_n = (2n-1)\pi/2 \qquad \text{n=1,2,3...} \tag{3.47}$$

Case-6.

Governing Equation

$$\frac{\partial\theta(\eta,\tau)}{\partial\tau} = \frac{\partial^2\theta}{\partial\eta^2} + \frac{L^2}{k}q'''(\eta,\tau) \qquad \text{at } \tau > 0 \tag{3.48}$$

Boundary Conditions

$$\frac{\partial\theta}{\partial\eta} = Bi(\theta) \qquad \text{at } \eta = 0,\ \tau > 0 \tag{3.49}$$

$$\theta = 0 \qquad \text{at } \tau > 0,\ \eta = 1 \tag{3.50}$$

Initial Condition

$$\theta = 0 \qquad \text{at } \eta,\ \tau = 0 \tag{3.51}$$

Solution

$$\theta(\eta,\tau)=\frac{2L^2}{k}\sum_{n=1}^{\infty}\sin\lambda_n(1-\eta)\frac{(\lambda_n{}^2+Bi^2)}{(\lambda_n{}^2+Bi^2)+Bi}.e^{-\lambda_n{}^2\tau}\int_{\tau'=0}^{\tau}e^{\lambda_n{}^2\tau'}\int_{\eta'=0}^{1}\sin\lambda_n(1-\eta').q'''(\eta',\tau')d\eta'd\tau' \tag{3.52}$$

Eigenvalues

$$\lambda_n\cot\lambda_n=-Bi \tag{3.53}$$

3.4.2 Semi-infinite domain

For this domain, a constant heat generation term gives an unbounded solution, and thus the solution for the first three cases cannot be found out.

Case 4.

Governing Equation

$$\frac{\partial\theta(\eta,\tau)}{\partial\tau}=\frac{\partial^2\theta}{\partial\eta^2}+\frac{L^2}{k}q'''(\eta,\tau) \qquad \text{at } \tau>0 \tag{3.54}$$

Boundary Conditions

$$\theta=0 \qquad \text{at } \eta=0,\ \tau>0 \tag{3.55}$$

$$\theta\to 0 \qquad \text{at } \tau>0,\ \eta=\infty \tag{3.56}$$

Initial Condition

$$\theta=0 \qquad \text{at } \eta,\ \tau=0 \tag{3.57}$$

Solution

$$\theta(\eta,\tau)=\frac{L^2}{k}\int_{\tau'=0}^{\tau}\frac{d\tau'}{[4\pi(\tau-\tau')]^{1/2}}\int_{\eta'=0}^{\infty}q'''(\eta',\tau')[e^{\frac{-(\eta-\eta')^2}{4(\tau-\tau')}}-e^{\frac{-(\eta+\eta')^2}{4(\tau-\tau')}}]d\eta' \tag{3.58}$$

Case 5.

Governing Equation

$$\frac{\partial\theta(\eta,\tau)}{\partial\tau}=\frac{\partial^2\theta}{\partial\eta^2}+\frac{L^2}{k}q'''(\eta,\tau) \qquad \text{at } \tau>0 \qquad (3.59)$$

Boundary Conditions

$$\frac{\partial\theta}{\partial\eta}=0 \qquad \text{at } \eta=0,\ \tau>0 \qquad (3.60)$$

$$\theta\to 0 \qquad \text{at } \tau>0,\ \eta=\infty \qquad (3.61)$$

Initial Condition

$$\theta=0 \qquad \text{at } \eta,\ \tau=0 \qquad (3.62)$$

Solution

$$\theta(\eta,\tau)=\frac{L^2}{k}\int_{\tau'=0}^{\tau}\frac{d\tau'}{[4\pi(\tau-\tau')]^{1/2}}\int_{\eta'=0}^{\infty}q'''(\eta',\tau')[e^{\frac{-(\eta-\eta')^2}{4(\tau-\tau')}}+e^{\frac{-(\eta+\eta')^2}{4(\tau-\tau')}}]d\eta' \qquad (3.63)$$

Case 6.

Governing Equation

$$\frac{\partial\theta(\eta,\tau)}{\partial\tau}=\frac{\partial^2\theta}{\partial\eta^2}+\frac{L^2}{k}q'''(\eta,\tau) \qquad \text{at } \tau>0 \qquad (3.64)$$

Boundary Conditions

$$\frac{\partial \theta}{\partial \eta} = Bi(\theta) \qquad \text{at } \eta = 0, \tau > 0 \tag{3.65}$$

$$\theta \to 0 \qquad \text{at } \tau > 0,\ \eta = \infty \tag{3.66}$$

Initial Condition

$$\theta = 0 \qquad \text{at } \eta,\ \tau = 0 \tag{3.67}$$

Solution

$$\theta(\eta,\tau) = \int_{\lambda=0}^{\infty} \frac{2}{\pi(\lambda^2 + Bi^2)} (\lambda\cos\lambda\eta + Bi\sin\lambda\eta) e^{-\lambda^2\tau} \frac{L^2}{k} \times$$

$$\int_{\tau'=0}^{\tau} e^{\lambda^2\tau'} \int_{\eta'=0}^{\infty} q'''(\eta',\tau')(\lambda\cos(\lambda\eta') + Bi\sin(\lambda\eta'))d\eta' d\tau' d\lambda \tag{3.68}$$

3.5 Modeling the source term

The constant source term is not taken into consideration in our problem. The heat source term which depends on both the spatial coordinate and the time is modeled here taking the physics of the problem into consideration.

The source term is formulated with the in the framework established by references [2], [19], and [23]. The heat source is defined as the product of the heat of polymerization reaction, H_R, and the rate of the polymerization reaction, R_p,

$$q''' = H_R \times R_p \tag{3.69}$$

According to Rabek [19], under very simplified condition, if it is assumed that a steady state condition and the propagation and the termination rates are independent of the macro-radial size of the polymer, the rate of the polymerization can be written as

$$R_p = -d[M]/dt = (R_i / k_t)^{1/2} k_p M \quad (3.70)$$

where M is the concentration of the monomer present in the resin

As the initiation reaction of the photo-polymerization is driven by the light absorption. Thus the initial reaction rate, R_i, is given by the product of the absorbed light intensity into the resin with the amount of free radical production quantum yield, ϕ,

$$R_i = I_a \times \phi \quad (3.71)$$

Substituting Eqn. (3.73) into Eqn.(3.72) gives,

$$R_p = (I_a \times \phi / k_t)^{1/2} k_p M \quad (3.72)$$

The absorbed light intensity depends on the absorption coefficient, the temporal and the spatial dependence of the irradiance, the reflectivity, and the maximum incident radiation. Considering reflectivity as zero for the present, the absorbed light intensity could be written,

$$I_a = I \times f(\eta) \times g(\tau) \times \mu_a \times e^{-\mu_a \eta L} \quad (3.73)$$

where I is the maximum amount of light intensity incident on the resin surface at x/L = 0 and μ_a is the absorption coefficient and is defined by the product of ε, molar extinction coefficient and S, concentration of the photo-initiator.

As the intensity of light diminishes with the axial distance and so does the absorption coefficient, a exponential decay term could be marked in Eqn. (3.73). The functions $f(\eta)$ and $g(\tau)$ are defined as the spatial dependence of the azimuthally symmetric laser irradiance and the temporal dependence of the laser irradiance respectively.

$$f(\eta) = e^{-\eta^2} \tag{3.74}$$

and,

$$g(\tau) = e^{-\tau^2} \tag{3.75}$$

In this paper, the distribution of the light source on the surface of the resin of the considered domain is considered to be of Gaussian shape both for the azimuthally symmetric and the temporal dependence of the laser irradiance. On contrary, if the light exposed on the resin is varying with time then the temporal dependence of the laser irradiance, $g(\tau)$, can be considered to have a step function profile, Appendix D.

As the absorption coefficient, μ_a, is determined by the product of the molar extinction coefficient, ε (how strongly a chemical species absorbs light into it at a given wavelength) and the concentration of the photo-initiator that will absorb the light energy, S, i.e.,

$$\mu_a = \varepsilon \times S \tag{3.76}$$

So substituting Eqns.(3.73-3.76) into Eqn. (3.72) gives

$$R_p = (I \times e^{-\eta^2} \times e^{-\tau^2} \times \varepsilon S \times e^{-\varepsilon S \eta L} \times \phi / k_t)^{1/2}\, k_p M \tag{3.77}$$

or,

$$R_p = B \times \sqrt{e^{-(\tau^2+\eta^2+\varepsilon S \eta L)}}\ , \tag{3.78}$$

where $B = k_p M \sqrt{\dfrac{I \varepsilon S \phi}{k_t}}$ (3.79)

So the source term is expressed as

$$q''' = H_R B \exp(-(\tau^2 + \eta^2 + \varepsilon S \eta L)) \quad . \tag{3.80}$$

The source term in this thesis is somewhat similar to Jakubinek et al. [8] in matter of the idea behind the chemical kinetics for a photo-polymerization process. As the chemical kinetics of the photo-polymerization is same for all resins, so the basic mathematical formulation of the source term cannot be different. The source term of the current thesis is different from Jakubinek et al. [8] paper from the point of view that the spatial dependence of the azimuthally symmetric laser irradiance, $f(\eta)$, and the temporal dependence of the laser irradiance, $g(\tau)$, terms are different. The solution domain considered in this thesis is an one-dimensional rectangular heat transfer problem with a source term, while the paper by Jakubinek et al. [8] tells about a cylindrical two-dimensional domain. Except the paper by Jakubinek et al. [8], all other papers in the literature review has not solved the heat conduction equation for photo-polymerization problem. So the mathematical formulation suggested in their papers is quite different from that in this thesis.

3.6 Results

3.6.1 Temperature versus time and curing depth graphs for some assumed values

Figures 28-30 are plotted for the adiabatic boundary condition (Case-5) for the solution of Eq. (3.46).

The values of the thermo-physical quantities assumed to plot the graphs are shown in Table 1. The ambient temperature is taken to be $25^0 C$.

The dimensionless temperature i.e. θ / T_a is plotted against the dimensionless time, τ, for different values of dimensionless length, η. θ is the relative difference between two temperatures. Figure 29 shows the dimensionless temperature versus the dimensionless time curve. The unit of the intensity of the light has been changed from 1200 mW / cm^2 to the photons, so as to match the units ($1 W / m^2$ =4.57 $\mu mol / m^2 / s$).

The assumed values are provided by Minnesota Dental Research Center for Biomaterials and Biomechanics, University of Minnesota.

Table 1. Thermo-physical properties in the analytical solution.

Variables	Values
k_p	5.5 m^3/mol
k_t	1200 m^3/mol
ϕ	0.07
ε	4.6 m^2/mol
I	0.0548 $mol/m^2/s$
M	4.950 $kmol/m^3$
S	0.0247 $kmol/m^3$
ΔH_R	55.229 KJ/mol

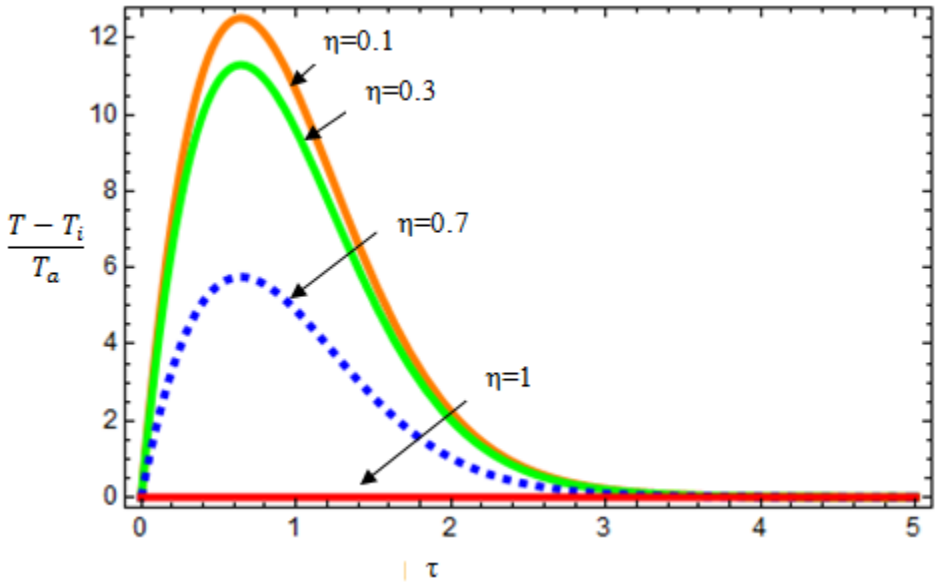

Figure 29. Dimensionless temperature versus dimensionless time (Case-5)

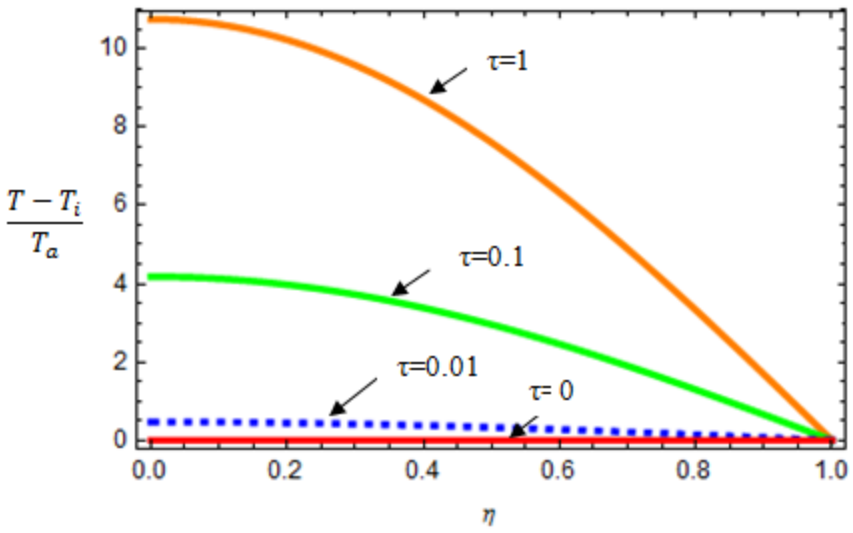

Figure 30. Dimensionless temperature and dimensionless specimen depth for different values of dimensionless time (Case-5).

Figure 29 is in good agreement with the measurement from the shape of the plot point of view, boundary and initial condition, as shown in Figure 49 of Chapter-5. The curve is seen to start at the point zero at η =0 and converge to zero when η= 1. As the boundary condition at η =1 is θ =0, thus the graph is expected to fall back to the point zero at η =1, which is exactly shown in Figure 29.

Next, the plot between the dimensionless temperature and the curing depth is shown in Figure 30. The shape of Figure 30 also shows good agreement with the experiment as shown in Figure 51 of Chapter 5. It shows that the temperature is the highest when the curing depth is zero and gradually decreases to a point zero with increasing curing depth.

The range of the curing depth values in dimensional form, x, remains within the range of 0 to 22 mm. If 30% of the curing depth value is taken into consideration then the curing depth of the resin is 6.6mm. The restoration depth in practical purpose is within the range of 5-6 mm. Thus the assumed value from the analytical curve nearly comes into co-ordination with the theoretical aspect.

A three-dimensional plot shown in Figure 31, shows the correlation between the dimensionless temperature, dimensionless time and the dimensionless curing depth for the composite resin material (properties mentioned in Table 1).

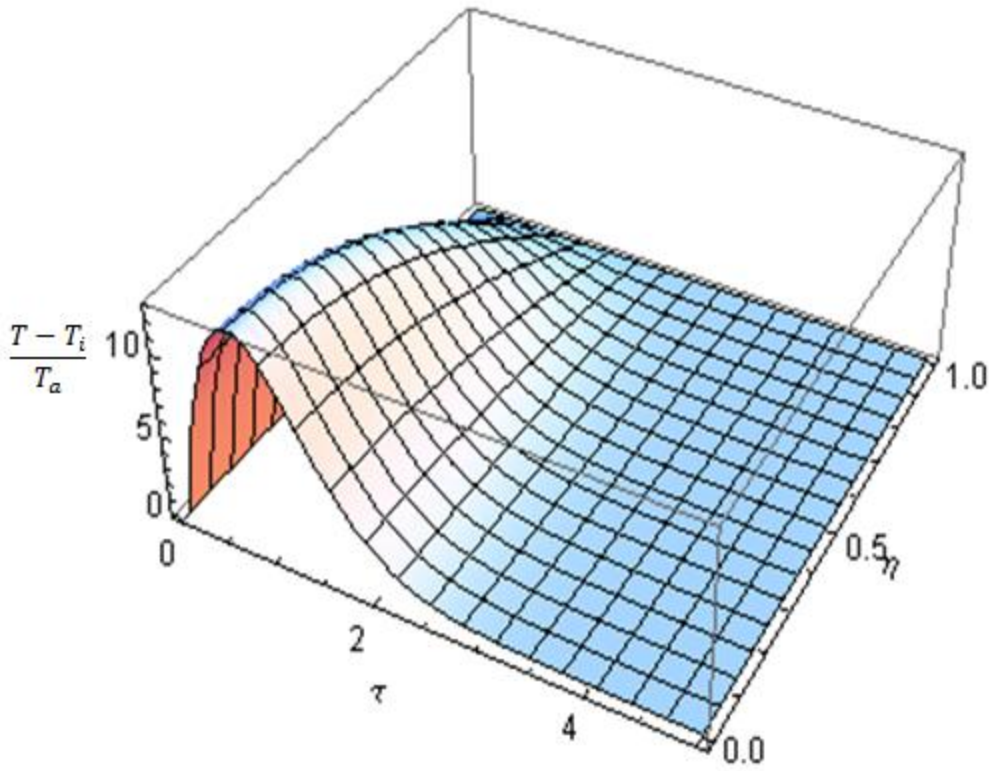

Figure 31. Contour of dimensionless temperature, time and specimen depth

The graphs of the temperature versus time graphs are plotted for some assumed values. If the individual thermo-physical constant properties like the propagation rate constant, termination rate constant, heat of reaction, molar extinction coefficient , concentration of monomer and photo-initiator are known for the three different resin, the temperature -time graph for different curing depth and the temperature-curing depth graph at different times can be easily plotted.

As the shape of the graph of Figure 29 and Figure 30 matches with the experimental result graphs in Figure 49 and Figure 51 of chapter 5, it proves the validity of the analytical solution.

3.6.2 Comparison of the source term, q''', for the three resins by substituting the values from the experiment results in Eq. (3.46) (Case-5)

The dimensional form of the Eq. (3.46) is,

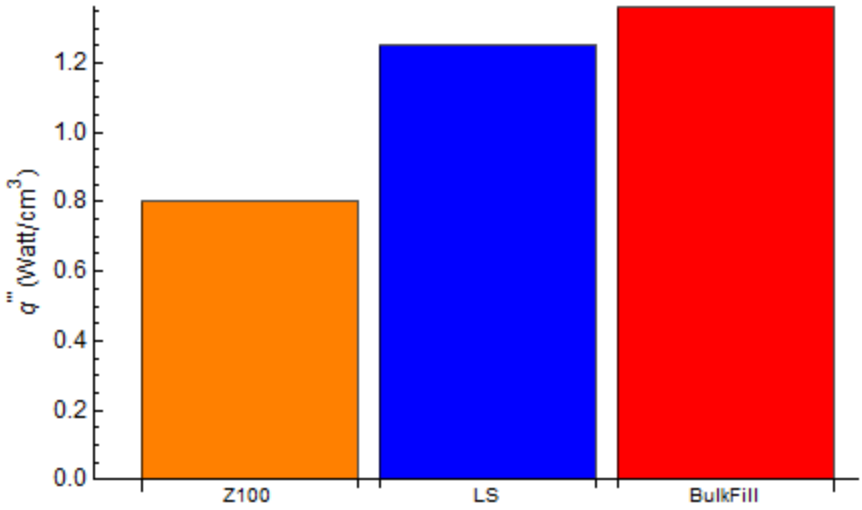

Figure 32. Source term for three different resins.

$$\Delta T(x,t) = \frac{2\alpha}{kL}\sum_{n=1}^{\infty}\cos(\lambda_n x)\exp(-\alpha\lambda_n{}^2 t)\int_{t'=0}^{t}\exp(\alpha\lambda_n{}^2 t')\int_{x'=0}^{L} q'''(x',t')\cos(\lambda_n x')dx'dt' \qquad (3.81)$$

The values of thermal diffusivity, α, and thermal conductivity , k, for three resins can be obtained from the Table B-2 of Appendix-B.

From Figure 49, values of temperature for the three resins for time = 20 seconds is taken into account while plotting Figure 32. According to Figure 32. the heat generation due to polymerization, q''', is lowest for Z100 , while it is nearly the same for the other two composite resins, LS and BulkFill.

Chapter 4

Experimental Design and Procedure

4.1 Design of the experiment

The overall design of the experiment is simple and replicates the assumptions made in the analytical problem of Chapter 3. Figure 33 shows a photograph of the total set-up. The Teflon channel which carries the resin composite is mounted over a square Teflon base (Figure 34) with the help of the removable double sided tape. Attaching the channel to the base minimizes heat losses and secures the position of the channel during an experiment from moving. The rectangular channel has a cross section of $2\ \text{mm} \times 4$ mm and length of 22 mm. The overall dimensions are 10 mm x 10 mm. (Figure 35). Instrumentation comprises an Elipar S10 LED Curing Light from 3M ESPE, a FLIR camera from FLIR, and air temperature and humidity sensor. The specifications of the curing light and the FLIR camera are shown in Table 2. Table 3. lists the properties of Teflon™.

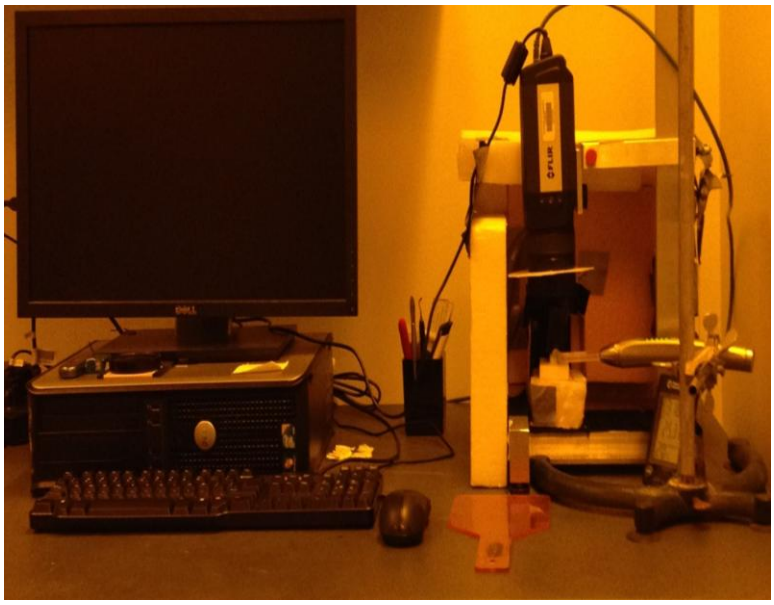

Figure 33. Experimental set-up

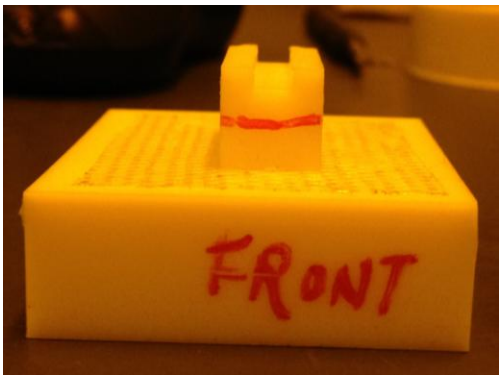

Figure 34. Front view of the channel and base.

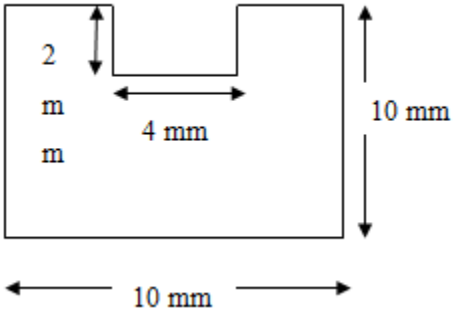

Figure 35. Front side of the teflon base.

Table 2. Specifications of the curing light and FLIR camera.

Light Types	Specifications
Elipar™ S10 LED Curing Light	Utilizable wavelength range 430–480 nm Light intensity 1200 mW/ cm^2 Optically active light emission area 60–65 mm^2 10 mm light guide
FLIR Camera	A655sc brand 640 × 480 LWIR resolution with 17 micron pixels Full frame 14-bit data at up to 50 fps

Table 3. Specifications of Teflon.

Material Property
Density= 2200 kg/ m^3 Melting point = 600 K, Thermal conductivity= 0.25 W/mK

Figure 36. Curing light

Figure 37. Cardboard walls.

To prevent any major heat loss due to convection, the left , right and back sides of the experimental set-up is covered with Styrofoam (Figure 33) Further convective loss is minimized with three cardboard walls covering the sides of a Styrofoam base on which the channel and its base rest, Figure 37. The IR camera is placed above the rectangular Teflon specimen at a height of about 5 cm.

The curing light is placed at the front end of the channel, i.e., at x = 0, with the tip of the curing light almost touching the channel. As the diameter of the curing light tip is 10 mm, it is partially (~5 mm) covered with a black velvet sheet to focus the light on the

Figure 38. Closer view of the experimental set-up.

resin sample only and also to minimize scattering/noise in the IR reading due to conduction and convection in directions other than the x-axis. The curing light tip covered with the black sticker is shown in Figure 36.

The red line shown in Figure 34 is the position where the bottom of the light curing tip is. Thus the 5-10 mm height of the rectangular channel is covered with the curing light tip, while the rest of the curing light tip is covered with the black sticker as mentioned above. This black sticker used is 15 mm high and thus prevents any convection from the front part of the specimen. A close view of the specimen with the curing light is shown in Figure 38.

4.2 Experimental Procedure

The temperature profiles of the channel before and after curing of the composite specimen are measured with the IR camera. In both cases, the curing light is turned on for 20s. An IR reading of the background temperature is also used to accurately position the channel under the camera. A simple ad hoc procedure is followed: (1) The rectangular Teflon block is pressed tightly with fingers for a few seconds so as to reveal the position of the channel in the IR field of view. As body heat raises the temperature of the channel, it could be easily seen in the IR field and is marked in the visual output of the camera using its embedded software (Figure 39). (2) The position of the channel is adjusted so as to see it properly in the camera field of view. (3) A line

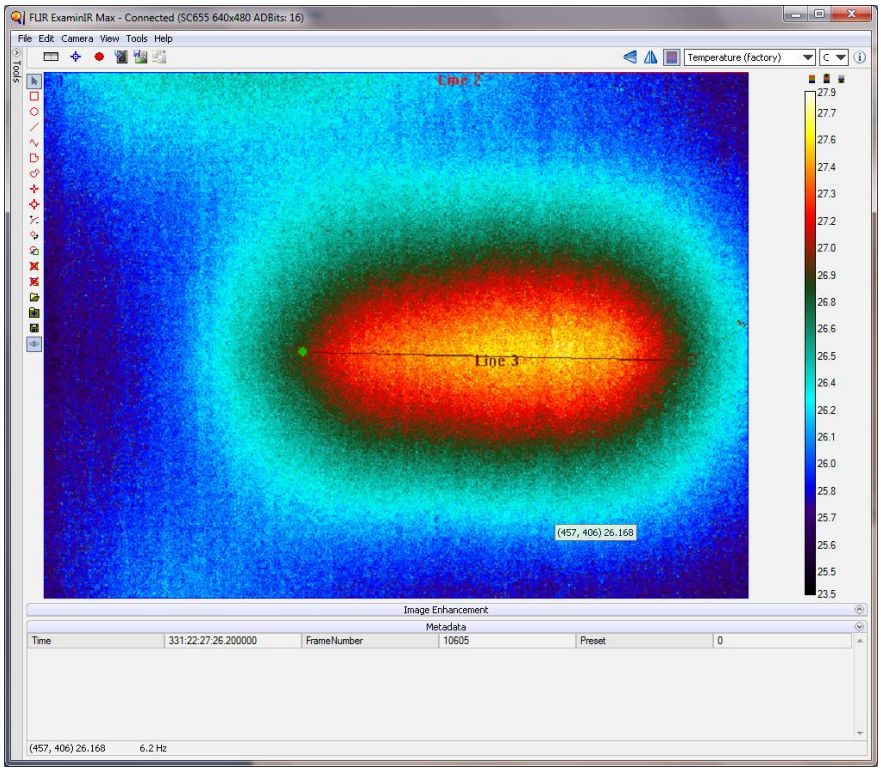

Figure 39. Marker Line 3 on the channel.

marker is then drawn in the screen from the front to the back end of the channel to outline the domain of the temperature measurements. By moving the cursor on the computer screen the temperature of the channel and resin at each position are seen. An ambient temperature sensor provided a validating measurement of the initial temperature as given by the IR camera.

In each experiment, the channel is first lined with a sheet of Teflon tape before filling it with resin composite. The tape assured easy removal of the specimen after curing and hardening has taken place. After the channel is filled with resin, it is placed in exactly the same position as determined in the initial positioning procedure. Guidelines drawn on the Styrofoam base guide this placement. When thermal equilibrium, calibration of the IR camera is performed, together with non-uniformity correction and bad pixel replacement using the software provided with the camera. Next, the temperature of the channel in the Teflon block (sidewalls of the top surface) measured by the camera is determined by moving the cursor nearly 2mm above and below the

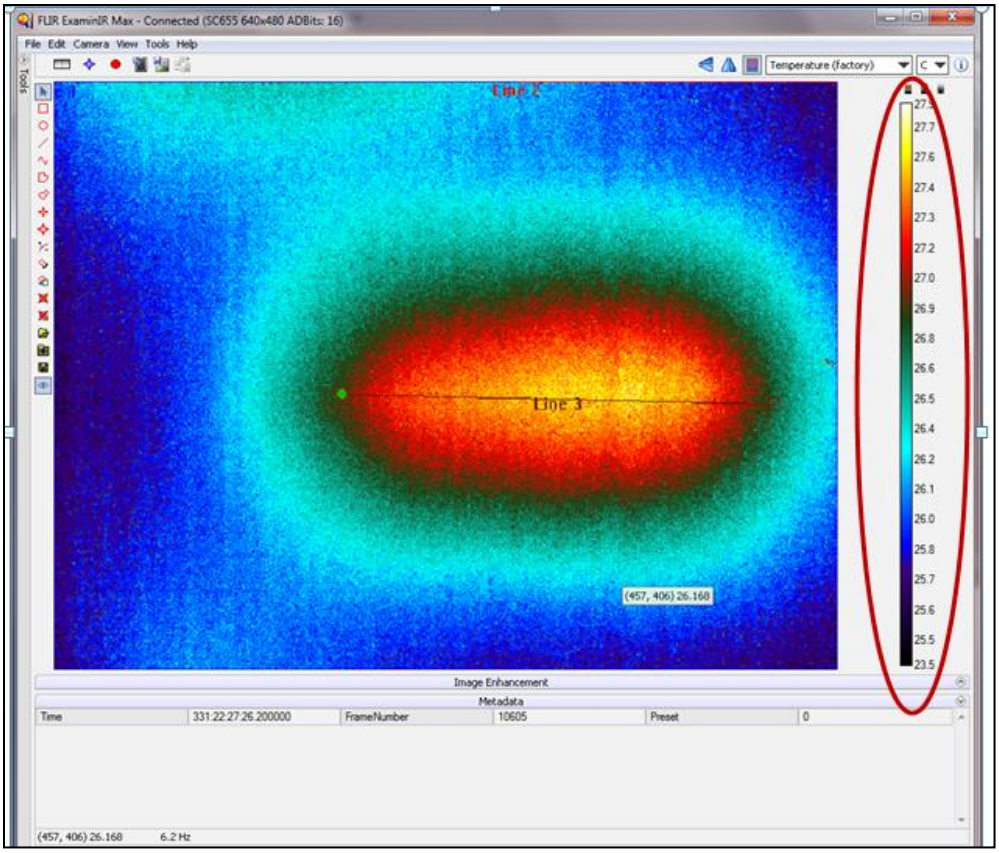

Figure 40. Temperature bar.

Line 3 in Figure 39. When the temperature at the sidewall becomes the same as the sensor temperature, the experiment can begin.

The IR camera and the curing light are switched on simultaneously. The curing light is switched off automatically after 20 s, but the temperature measurement is performed for a period of 2 min. The irradiance of the curing light at x = 0 and heat generated from the polymerization of the resin raised the temperature of both the resin and the Teflon block. The rise in temperature could be either marked from the temperature bar on the software screen , Figure 40, or by moving the cursor on or above the Line 3 of Figure 39. The rise in temperature in the resin is marked because of the conversion to heat of the light it absorbed and due to its polymerization.

The temperature measurement is repeated with the cured resin and the curing light turned on for the same duration, i.e., 20 s after the Teflon channel and cured resin reached the ambient temperature. The aim is to determine the rise in temperature due to

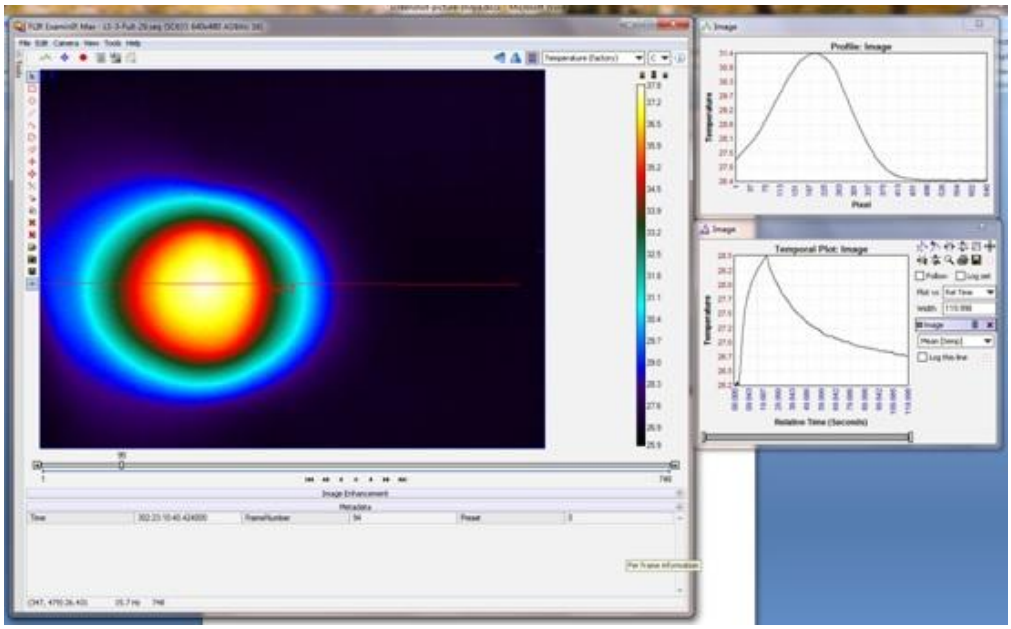

Figure 41. Visual output with the temporal and profile plots.

Table 4. Curing depth of each resin

Resin Compound	Curing depth (mm)
3M™ ESPE Z100™	13-14 ± 2
Filtek LS	8-9 ± 1
Filtek Bulk Fill	15-16 ± 1

the curing light only. By way of example, the spatial profile of the temperatures at one time point and the temporal changes of the maximum temperature for one reading of the IR camera are shown in Figure 41. The temperature versus time plot for the first reading gives us the temperature rise due to polymerization and curing light while the temperature rise for the second reading is due to the curing light only. So, the difference in temperature between the first and second measurements gives the contribution due to the polymerization reaction only. A closer look of the curing process of the resin from the prospective of the IR camera for time in the order of , t=14 s, 23 s, 38 s, 63 s, 79 s , 90 s, 102 s and 115 s is shown in Figure 42.

In order to determine the curing depth of the composite resin the uncured resin is scraped with the help of a spatula and the curing depth is measured with the help of a measuring scale. After taking the second reading, the specimen is removed from the view of the IR camera. The results of the scratch test are shown in Table 4. The table

(a) (b)

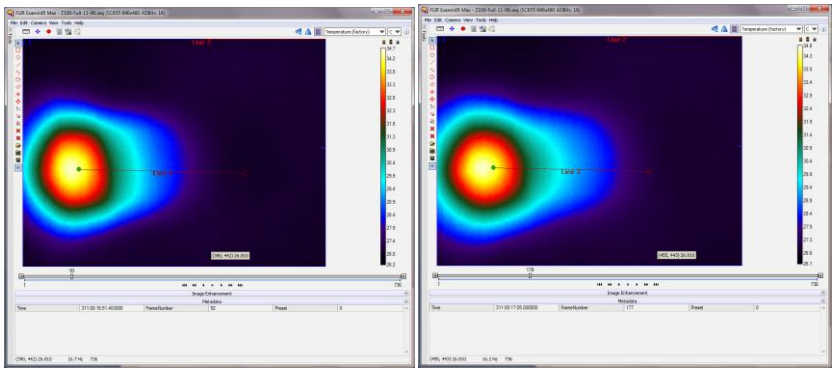

(c) (d)

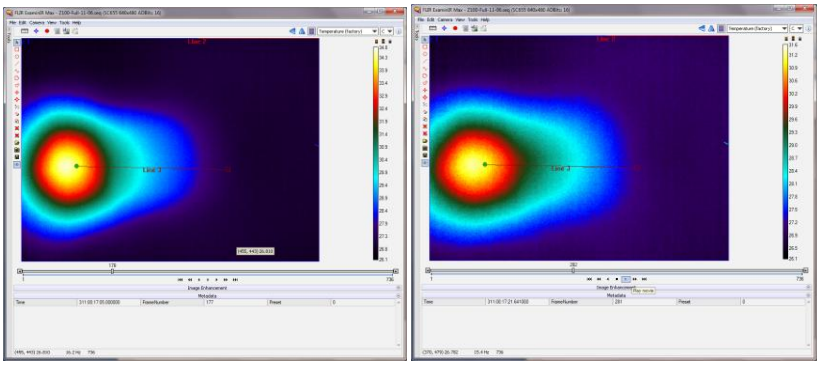

(e) (f)

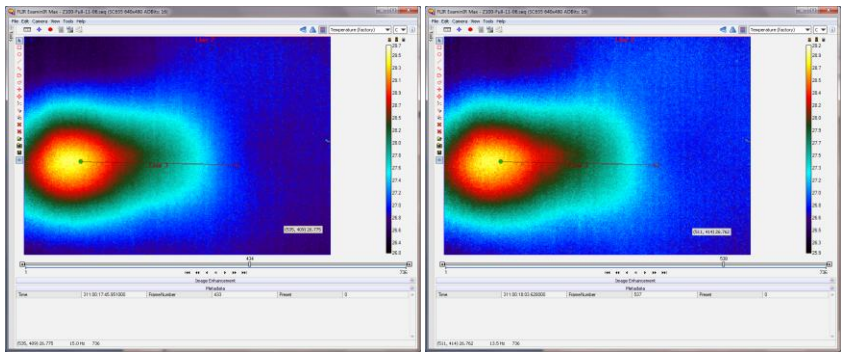

(g) (h)

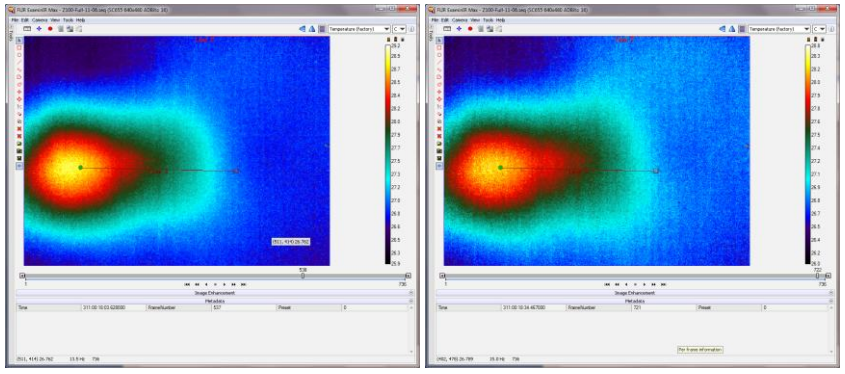

Figure 42. Thermographs showing the curing process (a) t = 14 s (b) t = 23 s (c) t = 38 s (d) t = 63 s (e) t = 79 s (f) t = 90 s (g) t = 102 s (h) t = 115 s.

Figure 43. Top surface covered with black sticky paper.

reveals that the resin compound Filtek Bulk Fill has the highest curing depth of 15 to 16 mm among the three composite resins. As the maximum depth of the cavity preparation for the restorative purpose is within 5 mm to 6 mm, all the above resins are fit for that purpose. As the curing depth of the resins obtained from the experiment exceeded the maximum cavity depth of restoration (5-6 mm) by a large scale, so further experiments are performed to check the validity of the curing depth results.

Some modifications in the experiment model is done. Those are: (1) the top surface of the Teflon™ channel is covered with the back sticky paper, so as to confirm that the curing depth is not increasing because of the top surface curing, Figures 43-44 (2) the black sticky paper is pasted on the front surface of the Teflon™ block with a 2mm by 4 mm for the curing light only, Figures 45-46. The design (2) is done so as to confirm that the curing light only focuses on the resin and nowhere else.

The entire experiment as mentioned earlier is repeated. The result for the curing depth still remains unchanged.

Figure 44. Closer look of the experimental set-up for design (1).

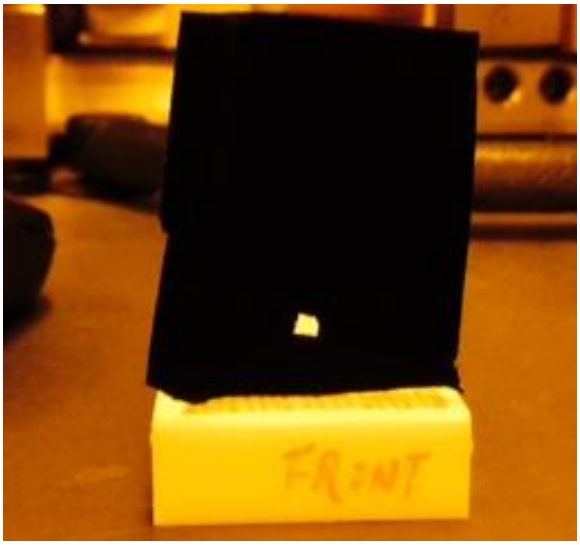

Figure 45. Front surface covered with a hole for the curing light.

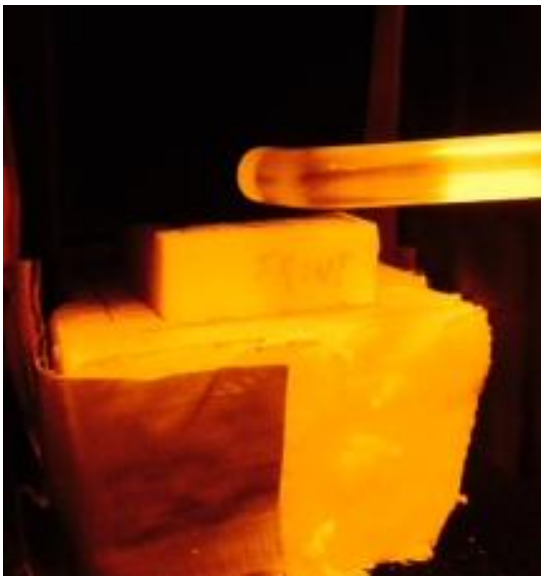

Figure 46. Closer look of the experimental set-up for design (2).

Chapter 5

Experimental Results

5.1 Experimental Graphs

As mentioned in the previous chapter, the first 20 s measures the temperature rise due to heat generation by both the curing light and the polymerization reaction. Figure 47 shows typical results for the three commercially available restorative resins for the first exposure. The results for the second experiment with cured resin samples are shown in Figure 48. Figure 47 shows the temperature rise due only to the heat generation by the curing light. In Figure 49, this temperature difference, showing the contribution from the polymerization reaction only, is plotted for each of the three commercial resins. Three to four runs are performed so as to reach to a valid conclusion.

The plots of the temperature in degree centigrade versus the number of pixel and of the temperature versus the curing depth in mm are shown in Figures 50 and 51, respectively. The profile plot option in the ExaminIR software produced plots of the temperature versus the number of pixel. The latter is converted to the depth within the specimen in mm. For example, the entire length of the Teflon specimen holder is 338 pixels, but it measured 22 mm. Thus, 1 pixel is equal to 0.065 mm in length.

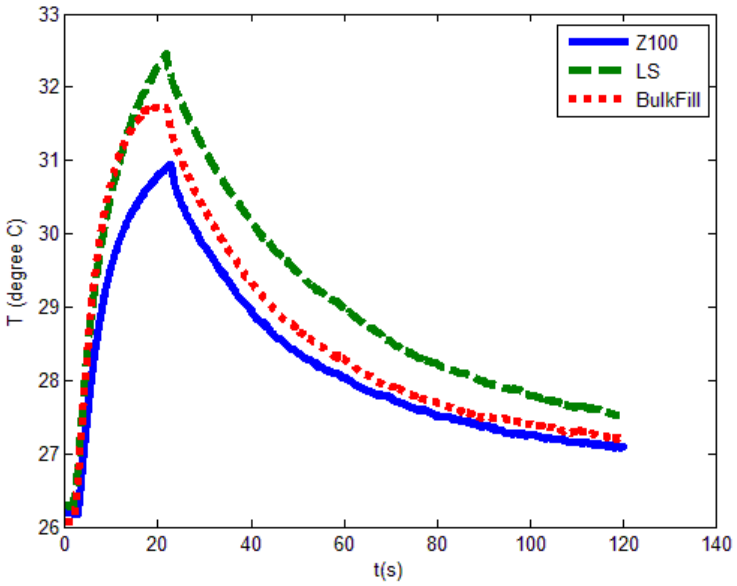

Figure 47. Results in first 20 s curing along the central position of the channel for $0 \le \eta \le 1$.

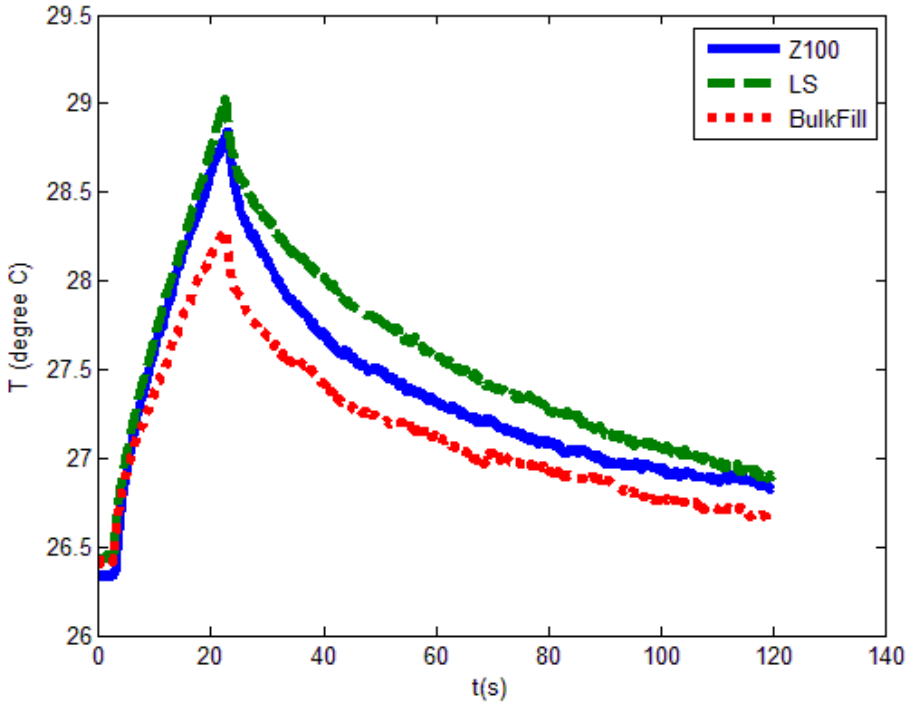

Figure 48. Results of the second 20 s curing along the central position of the channel for $0 \le \eta \le 1$.

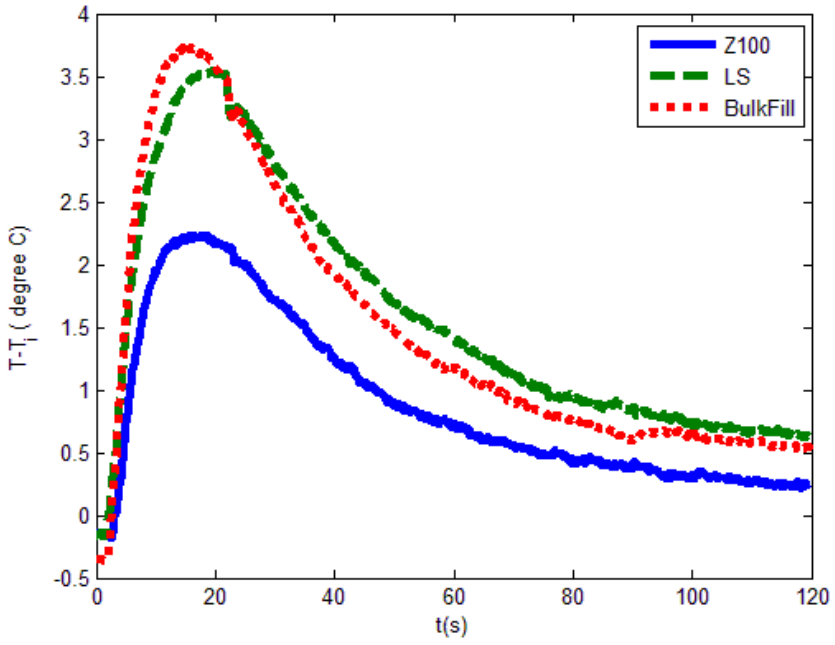

Figure 49. Temperature difference from the first and the second exposure along the central position of the channel for $0 \le \eta \le 1$.

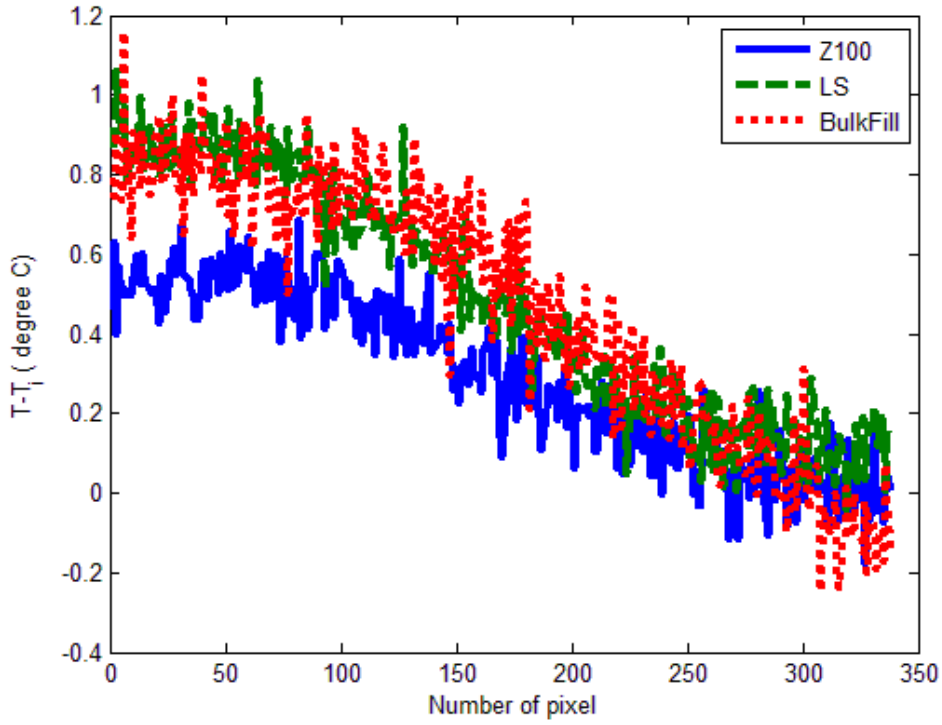

Figure 50. Temperature versus pixel number for t = 90 s and $0 \leq \eta \leq 1$.

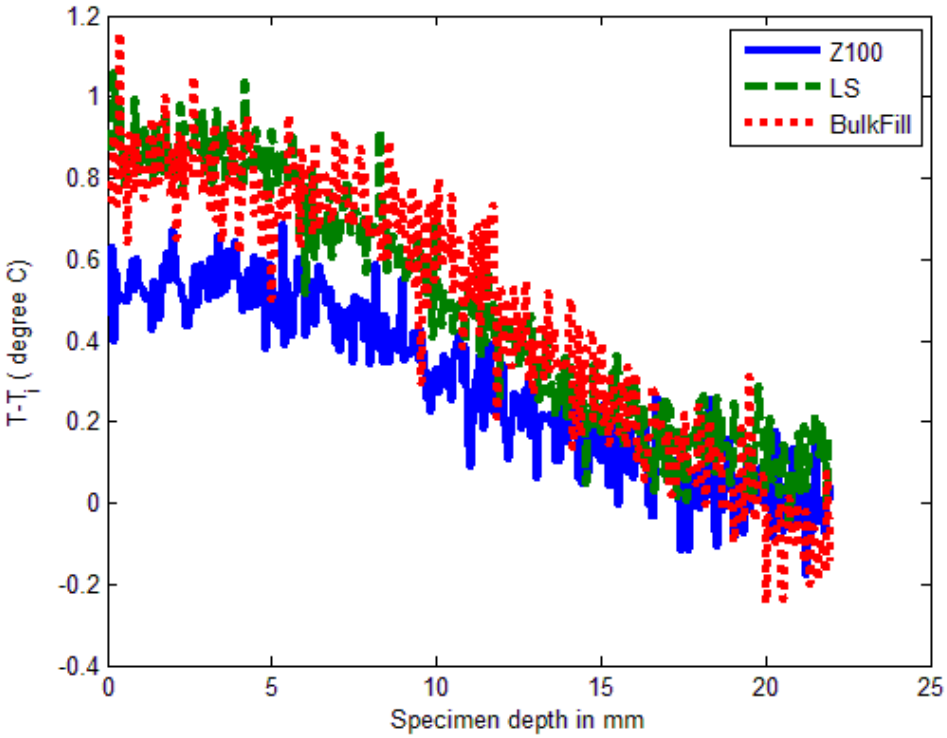

Figure 51. Temperature versus specimen depth for t = 90 s and $0 \leq \eta \leq 1$.

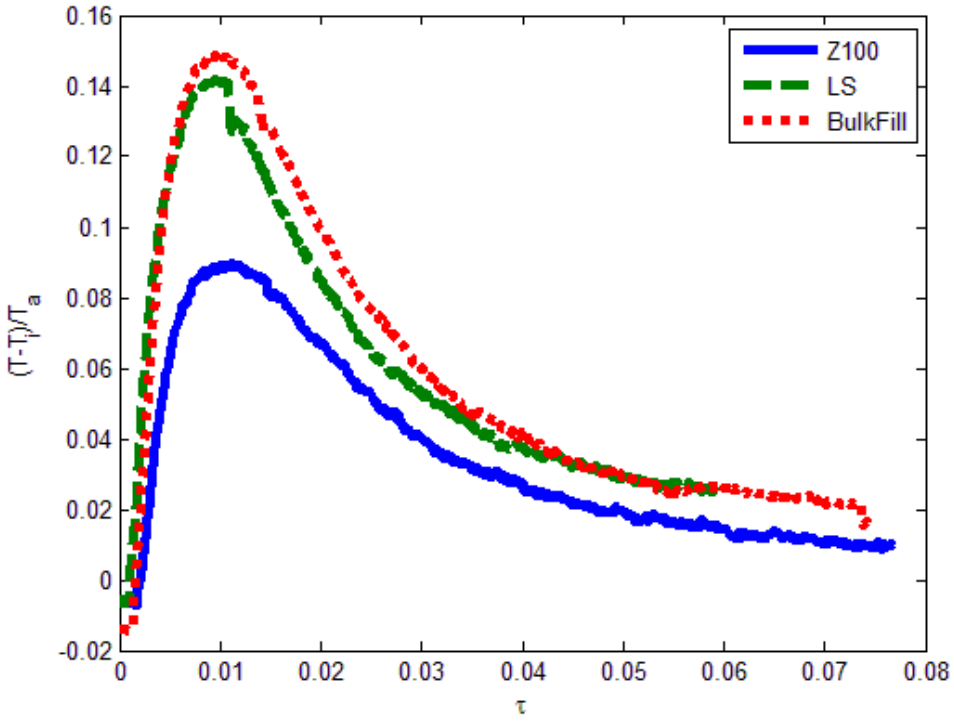

(a)

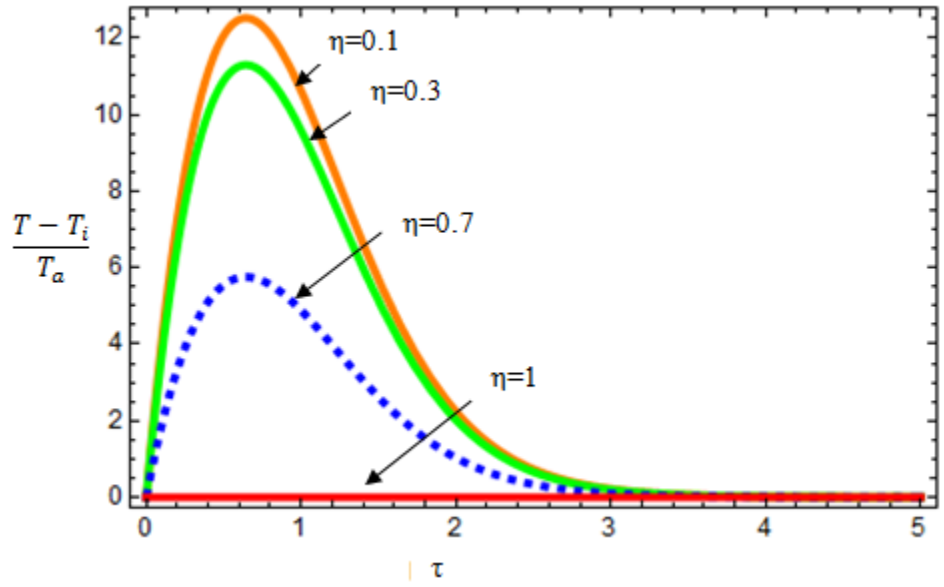

(b)

Figure 52.

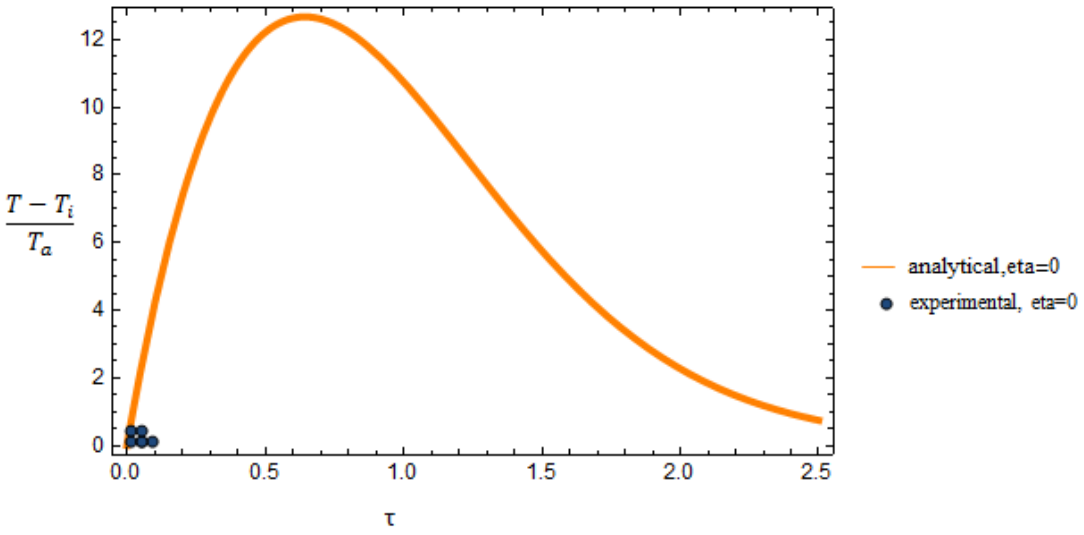

(c)

Figure 52. Temperature versus time. (a) Experiment; (b) analytical solution from assumed values (c) comparison of the analytical and experimental solution.

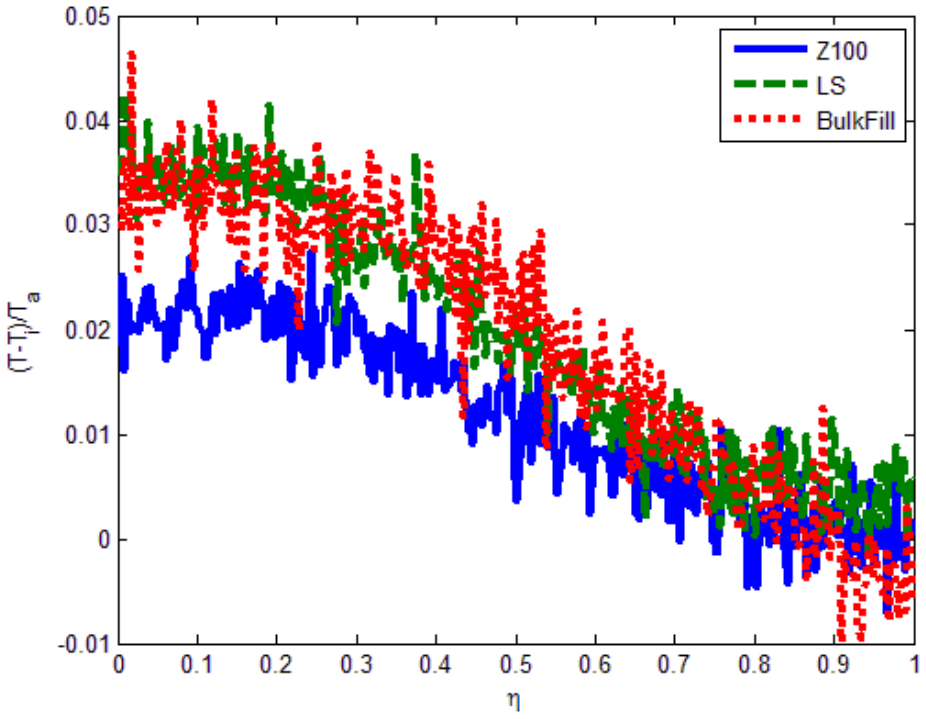

(a)

Figure 53.

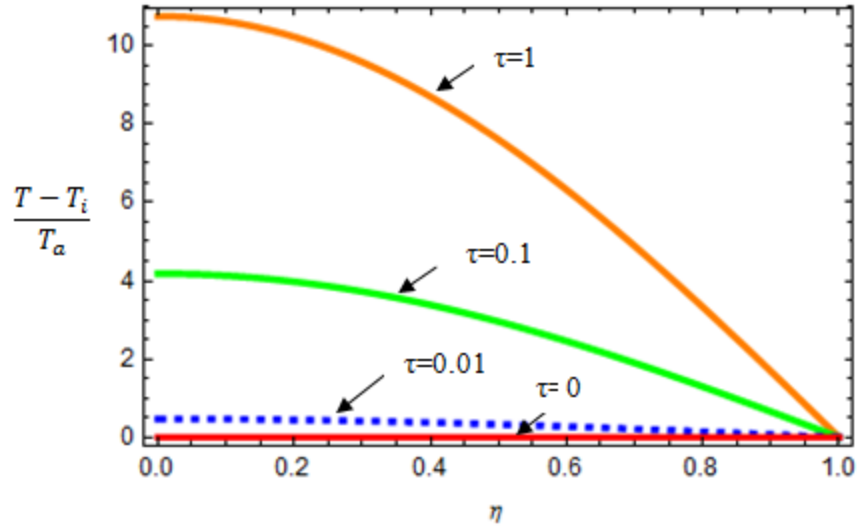

(b)

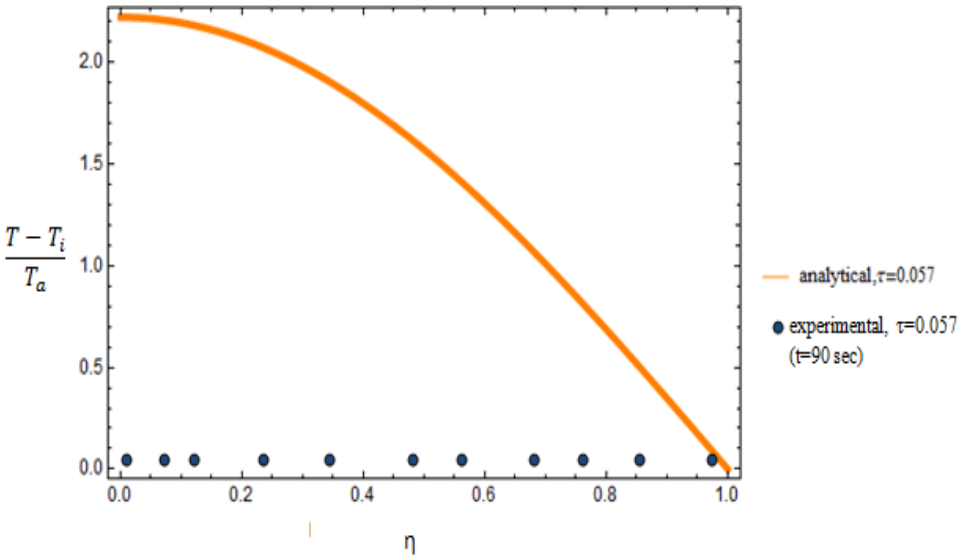

(c)

Figure 53. Temperature versus specimen depth. (a) Experiment; (b) analytical solution from assumed values (c) comparison of the analytical and experimental solution.

The nature of the experimental plots agreed with the analytical solution very well. The shapes of the graphs in both the cases, temperature versus time and temperature versus specimen depth, are very similar but there lies different between the assumed values of the analytical plot and the experimental results. Thus when plotted together, the experimental results does not match with the analytical results well.

5.2 Uncertainty Analysis

The dimensional form of the Eqn. (3.81) is taken into account while doing the error analysis. The percentage of error,

$$error\,\% = [(\frac{\Delta\alpha}{\alpha})^2 + (\frac{\Delta k}{k})^2 + (\frac{\Delta L}{L})^2 + (\frac{\Delta x}{x})^2 + (\frac{\Delta t}{t})^2 + (\frac{\Delta q'''}{q'''})^2]^{1/2} \quad . \qquad (5.1)$$

The percentage of the error in measurement of the three composite is found by this formula.

For Z100:

$\alpha = 3.098 \pm 0.01 \ m^2/s$

$k = 0.54 \pm 0.0027$ W/mK

$L = 0.022 \pm 0.00065$ m

$x = 0.022 \pm 0.00065$ m

$t = 20 \pm 0.1$ s

$q''' = 0.8 \pm 0.05$ W/m^2

By substituting the values in the Eqn. (5.1), the percentage of error is calculated to be 8%.

For LS:

$\alpha = 2.39 \pm 0.01 \ m^2/s$

$k = 0.54 \pm 0.0027$ W/mK

$L = 0.022 \pm 0.00065$ m

$x = 0.022 \pm 0.00065$ m

$t = 20 \pm 0.1$ s

$q''' = 1.28 \pm 0.15$ W/m^2

By substituting the values in the Eqn. (5.1), the percentage of error is calculated to be 10%.

For BulkFill:

$\alpha = 3.03 \pm 0.01 \ m^2/s$

$k = 0.54 \pm 0.0027$ W/mK

$L = 0.022 \pm 0.00065$ m

$x = 0.022 \pm 0.00065$ m

$t = 20 \pm 0.1\,\mathrm{s}$

$q''' = 1.36 \pm 0.2\,\mathrm{W}/m^2$

By substituting the values in the Eqn. (5.1), the percentage of error is calculated to be 15.3%.

Chapter 6

Conclusion

The analytical approach to the heat-conduction problem is modeled in Chapter 3 for light activated curing or dental restorative resins. The analytical model takes into account the heat that is generated inside the resin due to the process of heat conduction and polymerization. The one-dimensional heat conduction equation is solved for the adiabatic boundary condition at x = 0. The integral transform method is used to solve the above mentioned problem.

To validate the analytical model, an experiment is designed replicating the boundary condition (Case-5) of the analytical solution. The reading is recorded using an IR camera and the temporal and profile plots are plotted using the software of the IR camera.

The shape and the trend in the graph for both the analytical and the experimental solution agreed well with each other. But the values of the analytical results for individual axes are much greater than the experimental results, so the graphs do not match well when plotted on the same space.

As shown in Table 4 of Chapter 4, the curing depth for all the three resins are well beyond 5-6 mm. Thus all the resins are suitable from the curing depth point of view. Figure 54 shows the heat generation (in J/cm^3) from the polymerization process for all the three resins.

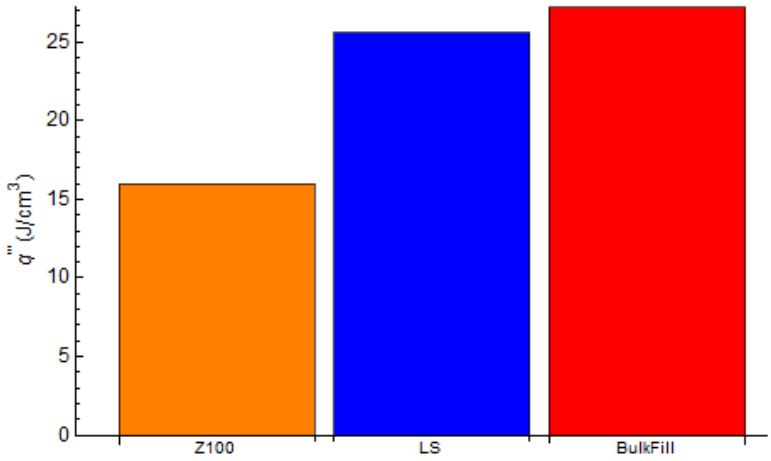

Figure 54. Source term for three different resins.

As it is clearly shown in Figure 54, the heat released from the polymerization process for the three light-activated dental resins is most for Filtek Bulk Fill and least for 3M™ ESPE Z100™. This makes 3M™ ESPE Z100™ the most suitable resin out of the three to be used for the dental restoration process.

A comparative study on these three resins is also carried out by Fok et al. [5] in his paper. Thus the comparison of the results of temperature rise due to polymerization and heat generation due to polymerization between the current and Fok et al. [5] paper will surely help in knowing the ranges in values. Table 5 and Table 6 compares Fok et al. [5] and the current thesis results for the temperature rise and heat generation for the three resins, Z100, BulkFill and LS.

Table 5. Comparison in temperature rise ($T - T_i$) in ^{o}C due to polymerization values.

Resin Compound	Fok et al. [5] values	Current thesis values
3M™ ESPE Z100™	4.5	2.2
Filtek LS	5.5	3.5
Filtek Bulk Fill	4.7	3.7

Table 6. comparison in heat generation term in J/cm^3 due to polymerization values.

Resin Compound	Fok et al. [5] values	Current thesis values
3M™ ESPE Z100™	11	16
Filtek LS	33	25.6
Filtek Bulk Fill	19	27.2

As Tables 5-6 clearly show, the values of Fok et al. [5] and the current paper both for the temperature rise and heat generation due to polymerization is nearly the same but the trend is different.

Future Research

(1) Though the base model both in the form of an axisymmetric model-orphan mesh (two-dimensional) and rectangular slab (three-dimensional) is simulated with the help of Abaqus 6.11 (Appendix C), further work is needed in this field. In this thesis, the composite resin is taken as a solid, homogeneous while specifying the section and the section assignment in Abaqus, but they should actually be treated as shell and composite and the properties like ply name, integration point, orientation angle etc. must be provided to Abaqus so as to get a proper contour plot.

(2) The values of the curing depth obtained from the experimental results for the three resins are large in comparison to the restoration depth used for practical purpose ($\approx$5 to 6 mm). Multiple approaches are tried but with data no closer to 5-6 mm. The reason for these high values may be the behavior of the Teflon block towards the reflected curing light that provokes curing of the resin from the top and sides (Figure 55). As the blue color curing light helps in the polymerization of the resins (considered in this thesis) , so this reflected rays help in increasing the curing depth.

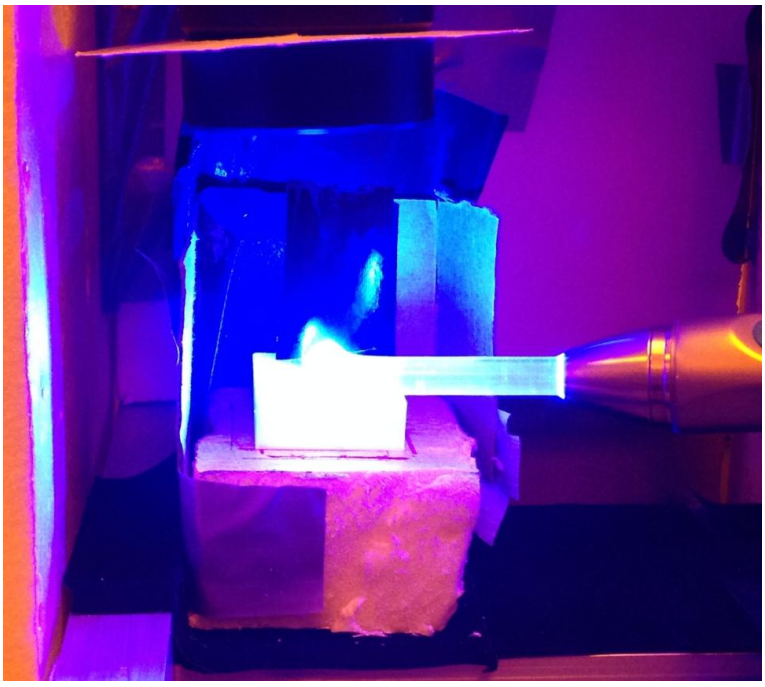

Figure 55. Reflection of the blue light by Teflon.

When the light is projected on the resin, some of it falls on the Teflon block. The Teflon block reflects the blue light as shown in Figure 55. To eliminate this reflection, the design shown in Figure 46 is tried, but the result still remain unchanged.

The white color of the teflon block may be the cause of this problem. Future work must be performed on some dull colored holder with same low thermal conductivity as Teflon, which would rather absorb light than reflecting it.

(3) Further work can be carried on in solving the same one-dimensional heat conduction rectangular domain problem with the temporal dependence of the laser irradiance, $g(\tau)$, as a Step function instead of a Gaussian distribution when the light exposed on the resin is varying with time. Some work in this reference is shown in Appendix D.

(4) Correct data's for the thermo-physical properties of the three resins must be collected from 3M or any chemical department , so as to get graphs with valid values corresponding the experimental results.

(5) Heat generated by the curing light must be mathematically formulated and solved, so as to determine the exact contribution from the heat generation solely due to curing light and due to polymerization, only.

References

[1] Balland, D., R. Guillard, and J. C. Andre., "Industrial Photochemistry VI. Light Distribution in Photopolymerizable Composite Materials and Heterogeneities Observed in Light Sources Used |or the Photoreaction." *Polymer Photochemistry*,4.2 (1984): 111-33.

[2] Bechtel, J. H. "Heating of Solid Targets with Laser Pulses," *Journal of Applied Physics*,46 (1975): 1585.

[3]Broyer, E., and C. W. Macosko, "Heat Transfer and Curing in Polymer Reaction Molding." *AIChE Journal*, 22.2 (1976): 268.

[4] Chen, Y., J. Ferracane, and S. Prahl, "A Pilot Study of a Simple Photon Migration Model for Predicting Depth of Cure in Dental Composite." *Dental Materials* ,21.11 (2005): 1075-086.

[5] Fok, A., C-H.Young , C. Carrera, and W. Douglas, "Comparing Heat Generated by Different Filling Techniques Using Thermal Imaging." (2013).

[6] Fried, D., R. E. Glena, J. D. B. Featherstone, and W. Seka, "Permanent and Transient Changes in the Reflectance of CO2 Laser-irradiated Dental Hard Tissues at Lambda = 9.3,9.6,10.3, and 10.6 Mu M and at Fluences of 1-20 J/cm2." Lasers in Surgery Medicine, 20 (1997): 22-31.

[7] Hannig, M., and B. Bott, "In-vitro Pulp Chamber Temperature Rise during Composite Resin Polymerization with Various Light-curing Sources." *Dental Materials*, 15 (1999): 275-81.

[8] Jakubinek, M. B., C. O' Neill, C. Felix, R. B. Price, and M. A. White, "Temperature Excursions at the Pulp-dentin Junction during the Curing of Light-activated Dental Restorations." *Dental Materials*, 24 (2008): 1468-476.

[9]Kleverlaan, C. J., and A. J. Gee, "Curing Efficiency and Heat Generation of Various Resin Composites Cured with High-intensity Halogen Lights." *European Journal of Oral Science*, 112 (2004): 84-88.

[10] Lee, LY James., and Christopher W. Macosko. "Heat Transfer in Polymer Reaction Molding."International Journal of Heat and Mass Transfer 23 (1980): 1479-492.

[11] Lin, Min., Feng Xu, Tian Jian Lu, and Bo Feng Bai. "A Review of Heat Transfer in Human Tooth—Experimental Characterization and Mathematical Modeling." Dental Materials 26.6 (2010): 501-13.

[12] Lloyd, C. H., A. Joshi, and E. McGlynn, "Temperature Rises Produced by Light Sources and Composites during Curing." *Dental Materials* 2 (1986): 170-74.

[13] Maffezzoli, A., A. Della Pietra, S. Rengo, L. Nicolais, and G. Valletta. "Photopolymerization of Dental Composite Matrices," Biomaterials 15 (1994): 1221-228.

[14]Masutani, S., J. C. Setcos, R. J. Schnell, and R. W. Phillips, "Temperature Rise during Polymerization of Visible Light-activated Composite Resins." *Dental Materials* 4 (1988): 174-78.

[15] Motawea, Inas., Amal Alshorbagy, Rabab Ibrahim, and HossamSallam, "3-D Finite Element Analysis of Transient Heat Transfer and Thermal Stress in a Crowned Mandibular First Molar Tooth." *Thermal Issues in Emerging Technologies, Theta* (2007) : 139-143.

[16]Olcer, N. Y. "On the Theory of Conductive Heat Transfer in Finite Regions with Boundary Conditions of the Second Kind." *International Journal of Heat and Mass Transfer* 8 (1965): 529-56.

[17] Ozisik, M. Necati. Heat Conduction. John Wiley, New York, 1980. pp. 536-543.

[18] Perry, M. F., and G. W. Young. "A Mathematical Model for Photopolymerization From a Stationary Laser Light Source." Macromolecular Theory and Simulations: 14.1 (2005): 26-39.

[19] Rabek, Jan F. Photochemistry and Photophysics. Vol. 4. Florida: CRC, 1991.

[20] Racz, L. M., and B. Abedian. "Cure Kinetics of Light-activated Polymers." *Journal of Polymer Science, Part B: Polymer Physics*,36 (1998): 2887-894.

[21] Shortall, A. C., and E. Harrington. "Temperature Rise during Polymerization of Light-activated Resin Composites." *Journal of Oral Rehabilitation*, 25 (1998): 908-13.

[22] Shultz, A. R., and M. G. Joshi. "Kinetics of Photoinitiated Free-radical Polymerization." *Journal of Polymer Science: Polymer Physics Edition*, 22.10 (1984): 1753-771.

[23] Siedlecki, J., and M. Ciesielski. "Mathematical Model for Thermal Processes in Photopolymerization." *Scientific Research of the Institute of Mathematics and Computer Science*,4.11 (2012): 113-19.

[24] Stansbury, J. W. "Curing Dental Resins and Composites by Photopolymerization."Journal of Esthetic and Restorative Dentistry 12.6 (2007): 300-08.

[25] Zach, Leo., and Gerson Cohen. "Pulp Response to Externally Applied Heat." Oral Surgery, Oral Medicine, Oral Pathology, Oral Radiology and Endodontology (1965): 515-30.

[26] Zuerlin, Michael J., Daniel Fried, Charles Q. Le, and John D.B Featherstone. "Thermal and Chemical Modification of Dentin by 9–11-μm CO2 Laser Pulses of 5–100-μs Duration." Lasers in Surgery and Medicine 31.4 (2002): 275-82.
[27] Zuerlein M.J., F. D., Seka W., and J. D. B.Featherstone . "Modeling thermal emission in dental enamel induced by 9-11 [mu] m laser light." *Applied Surface Science* ,(1998): 127-129, 863-8.

Websites:

[28]http://solutions.3m.com/wps/portal/3M/en_US/3M-ESPE-NA/dental-professionals/products/espe-catalog/?N=5144829+3294735975&rt=rud

[29]http://solutions.3m.com/wps/portal/3M/en_US/3M-ESPE-NA/dental-professionals/products/espe-catalog/?N=5145652+3294735719&rt=rud

[30]http://solutions.3m.com/wps/portal/3M/en_US/3M-ESPE-NA/dental-professionals/products/espe-catalog/?N=5144829+3294736416&rt=rud

Appendix A

Derivation of equations from the analytical section

Finite Domain

A.1 Derivation of Eqn.(3.24)

In this appendix, the symbol l is used for length in this Appendix instead of L. The mathematical formulation of this problem is given as

$$\frac{\partial\theta(\eta,\tau)}{\partial\tau}=\frac{\partial^2\theta(\eta,\tau)}{\partial\eta^2}+\frac{l^2}{k}q''' \qquad \text{in } 0<\eta<1,\ \tau>0 \qquad (A.1)$$

$$\theta=0 \qquad \text{at } \eta=0,\tau>0 \qquad (A.2)$$

$$\theta=0 \qquad \text{at } \eta=1,\tau>0 \qquad (A.3)$$

$$\theta=0 \qquad \text{for } \tau=0 \text{ in } 0\le\eta\le1 \qquad (A.4)$$

This problem is split up into a steady state problem for $\theta_s(\eta)$.

$$\frac{\partial^2\theta_s}{\partial\eta^2}+\frac{l^2}{k}q'''=0 \qquad \text{in } 0<\eta<1 \qquad (A.5)$$

$$\theta_s=0 \quad \text{at } \eta=0 \quad \text{and} \quad \theta_s=0 \quad \text{at } \eta=1 \qquad (A.6)$$

The homogeneous problem for $\theta_h(\eta,\tau)$ is,

$$\frac{\partial^2\theta_h}{\partial\eta^2}=\frac{\partial\theta_h}{\partial\tau} \qquad \text{in } 0<\eta<1,\ \tau>0 \qquad (A.7)$$

$$\theta_h=0 \text{ at } \eta=0 \quad \text{and} \quad \theta_h=0 \text{ at } \eta=1 \qquad (A.8)$$

The solution of the original problem (A.1) is determined from,

$$\theta(\eta,\tau)=\theta_s(\eta)+\theta_h(\eta,\tau) \qquad (A.9)$$

The solution of the steady state problem, Eqn. (A.5) is,

$$\theta_s = \frac{q'''l^2}{2k}(\eta - \eta^2) \qquad \text{(A.10)}$$

The solution of the homogeneous problem, Eqn. (A.7) is,

$$\theta_h(\eta,\tau) = -2\sum_{n=0}^{\infty} e^{-\lambda_n{}^2\tau}\sin(\lambda_n\eta)\int_0^1 \theta_s(\eta')\sin(\lambda_n\eta')d\eta' \qquad \text{(A.11)}$$

and λ_n's are the positive roots of

$$\sin(\lambda_n) = 0 \qquad \text{or} \qquad \lambda_n = n\pi, \qquad \text{n=0,1,2....} \qquad \text{(A.12)}$$

Introducing Eqn. (A.10) and (A.11) into Eqn. (A.9) and performing the integrations,

$$\theta(\eta,\tau) = \frac{q'''l^2(\eta-\eta^2)}{2k} - \frac{2q'''l^2}{k}\sum_{n=0}^{\infty}(1-(-1)^n)e^{-\lambda_n{}^2\tau}\frac{1}{\lambda_n{}^3}\sin(\lambda_n\eta) \qquad \text{(A.13)}$$

A.2 Derivation of Eqn.(3.30)

The mathematical formulation of this problem is,

$$\frac{\partial\theta(\eta,\tau)}{\partial\tau} = \frac{\partial^2\theta(\eta,\tau)}{\partial\eta^2} + \frac{l^2}{k}q''' \qquad \text{in } 0<\eta<1,\ \tau>0 \qquad \text{(A.14)}$$

$$\frac{\partial\theta}{\partial\eta} = 0 \qquad \text{at } \eta = 0, \tau > 0 \qquad \text{(A.15)}$$

$$\theta = 0 \qquad \text{at } \eta = 1, \tau > 0 \qquad \text{(A.16)}$$

$$\theta = 0 \qquad \text{for } \tau = 0 \text{ in } 0 \le \eta \le 1 \qquad \text{(A.17)}$$

This problem is split up into a steady-state problem for $\theta_s(\eta)$,

$$\frac{\partial^2 \theta_s}{\partial \eta^2} + \frac{l^2}{k} q''' = 0 \qquad \text{in } 0 < \eta < 1 \qquad (A.18)$$

$$\frac{\partial \theta_s}{\partial \eta} = 0 \quad \text{at } \eta = 0 \quad \text{and} \quad \theta_s = 0 \quad \text{at } \eta = 1 \qquad (A.19)$$

and a homogeneous problem for $\theta_h(\eta, \tau)$ is,

$$\frac{\partial^2 \theta_h}{\partial \eta^2} = \frac{\partial \theta_h}{\partial \tau} \qquad \text{in } 0 < \eta < 1,\ \tau > 0 \qquad (A.20)$$

$$\frac{\partial \theta_h}{\partial \eta} = 0 \quad \text{at } \eta = 0 \quad \text{and} \quad \theta_h = 0 \quad \text{at } \eta = 1 \qquad (A.21)$$

The solution of the original problem, Eqn. (A.14), is determined from,

$$\theta(\eta, \tau) = \theta_s(\eta) + \theta_h(\eta, \tau) \qquad (A.22)$$

The solution of the steady state problem, Eqn. (A.18), is,

$$\theta_s = \frac{q''' l^2}{2k}(1 - \eta^2) \qquad (A.23)$$

The solution of the homogeneous problem, Eqn. (A.20), is,

$$\theta_h(\eta, \tau) = -2\sum_{n=0}^{\infty} e^{-\lambda_n^2 \tau} \cos(\lambda_n \eta) \int_0^1 \theta_s(\eta') \cos(\lambda_n \eta') d\eta' \qquad (A.24)$$

and λ_n's are the positive roots of

$$\cos(\lambda_n) = 0 \qquad \text{or} \qquad \lambda_n = \frac{(2n+1)\pi}{2}, \qquad \text{n=0,1,2....} \qquad (A.25)$$

Introducing Eqns. (A.23) and (A.24) into Eqn. (A.22) and performing the integrations,

$$\theta(\eta,\tau) = \frac{q'''l^2}{2k}(1-\eta^2) - \frac{2q'''l^2}{k}\sum_{n=0}^{\infty}(-1)^n e^{-\lambda_n^2\tau}\frac{1}{\lambda_n^3}\cos(\lambda_n\eta) \qquad (A.26)$$

A.3 Derivation of Eqn.(3.36)

The mathematical formulation of this problem is,

$$\frac{\partial\theta(\eta,\tau)}{\partial\tau} = \frac{\partial^2\theta(\eta,\tau)}{\partial\eta^2} + \frac{l^2}{k}q''' \qquad \text{in } 0<\eta<1,\ \tau>0 \qquad (A.27)$$

$$\frac{\partial\theta}{\partial\eta} = Bi(\theta) \qquad \text{at } \eta=0, \tau>0 \qquad (A.28)$$

$$\theta = 0 \qquad \text{at } \eta=1, \tau>0 \qquad (A.29)$$

$$\theta = 0 \qquad \text{for } \tau=0 \text{ in } 0\le\eta\le1 \qquad (A.30)$$

This problem is split up into a steady-state problem for $\theta_s(\eta)$,

$$\frac{\partial^2\theta_s}{\partial\eta^2} + \frac{l^2}{k}q''' = 0 \qquad \text{in } 0<\eta<1 \qquad (A.31)$$

$$\frac{\partial\theta_s}{\partial\eta} = Bi(\theta_s) \qquad \text{at } \eta=0 \qquad \text{and} \qquad \theta_s = 0 \qquad \text{at } \eta=1 \qquad (A.32)$$

and a homogeneous problem for $\theta_h(\eta,\tau)$,

$$\frac{\partial^2\theta_h}{\partial\eta^2} = \frac{\partial\theta_h}{\partial\tau} \qquad \text{in } 0<\eta<1,\ \tau>0 \qquad (A.33)$$

$$\frac{\partial \theta_h}{\partial \eta} = Bi\theta_h \quad \text{at} \quad \eta = 0 \qquad \text{and} \qquad \theta_h = 0 \qquad \text{at } \eta = 1 \qquad (A.34)$$

The solution of the original problem, Eqn. (A.27), is,

$$\theta(\eta, \tau) = \theta_s(\eta) + \theta_h(\eta, \tau) \qquad (A.35)$$

The solution of the steady-state problem, Eqn. (A.31), is,

$$\theta_s = \frac{q''' l^2((1+\eta Bi) - \eta^2(1+Bi))}{2k(1+Bi)} \qquad (A.36)$$

The solution of the homogeneous problem, Eqn. (A.33), is,

$$\theta_h = \frac{-2q''' l^2}{2k(1+Bi)} \sum_{n=0}^{\infty} e^{-\lambda_n{}^2 \tau} \sin\lambda_n(1-\eta) \frac{2(\lambda_n{}^2 + Bi^2)}{(\lambda_n{}^2 + Bi^2 + Bi)} \int_0^1 \sin\lambda_n(1-\eta')((1+\eta' Bi) - \eta'^2(1+Bi))d\eta'$$

(A.37)

and λ_n's are the positive roots of,

$$\lambda_n \cot\lambda_n = -Bi \qquad \text{n=0,1,2...} \qquad (A.38)$$

Eqn. (A.38) is a transcendental equation, and its roots are found in from [17]..

Introducing Eqns. (A.36) and (A.37) into Eqn. (A.35) and performing the integrations,

$$\theta = \frac{q'''l^2((1+\eta Bi)-\eta^2(1+Bi))}{2k(1+Bi)} - \frac{2q'''l^2}{2k(1+Bi)} \times$$

$$\sum_{n=0}^{\infty} e^{-\lambda_n{}^2\tau} \sin\lambda_n(1-\eta)\frac{2(\lambda_n{}^2+Bi^2)}{(\lambda_n{}^2+Bi^2+Bi)}\int_0^1 \sin\lambda_n(1-\eta')((1+\eta' Bi)-\eta'^2(1+Bi))d\eta' \qquad (A.39)$$

A.4 Derivation of Eqn.(3.42)

The mathematical formulation of this problem is,

$$\frac{\partial\theta(\eta,\tau)}{\partial\tau} = \frac{\partial^2\theta(\eta,\tau)}{\partial\eta^2} + \frac{l^2}{k}q''' \qquad \text{in } 0<\eta<1,\ \tau>0 \qquad (A.40)$$

$$\theta = 0 \qquad \text{at } \eta = 0, \tau > 0 \qquad (A.41)$$

$$\theta = 0 \qquad \text{at } \eta = 1, \tau > 0 \qquad (A.42)$$

$$\theta = 0 \qquad \text{for } \tau = 0 \text{ in } 0 \le \eta \le 1 \qquad (A.43)$$

The Eqn. (A.40) can be solved by using the inversion formula and integral transform.

Inversion Formula: $\theta(\eta,\tau) = \sum_{n=1}^{\infty} \frac{X(\lambda_n,\eta)}{N(\lambda_n)} \bar{\theta}(\lambda_n,\tau)$ (A.44)

Integral transform: $\bar{\theta}(\lambda_n,\tau) = \int_{\eta'=0}^{1} X(\lambda_n,\eta')\theta(\eta',\tau)d\eta'$ (A.45)

where

$$N(\lambda_n) \equiv \int_0^1 [X(\lambda_n,\eta)]^2 d\eta \qquad (A.46)$$

and the functions $X(\lambda_n,\eta), N(\lambda_n)$, and eigenvalues λ_n are obtainable from the Table B.1 of Appendix B for different combinations of boundary conditions at $\eta = 0$ and

$\eta = 1$. Using the inversion formula, the integral transform and boundary conditions, the heat conduction problem, Eqn. (A.40), becomes,

$$\theta(\eta,\tau) = \sum_{n=1}^{\infty} \frac{X(\lambda_n,\eta)}{N(\lambda_n)} e^{-\lambda_n{}^2\tau} \frac{l^2}{k} \int_{\tau'=0}^{\tau} e^{\lambda_n{}^2\tau'} \bar{q}^{'''}(\lambda_n,\tau')d\tau' \qquad (A.47)$$

where

$$\bar{q}^{'''}(\lambda_n,\tau') = \int_{\eta'=0}^{1} \sin(\lambda_n\eta') q'''(\eta',\tau')d\eta' \qquad (A.48)$$

and

$$q''' = H_p \times (I \times e^{-\eta^2} \times e^{-\tau^2} \times \varepsilon S \times e^{-\varepsilon S \eta L} \times \phi / k_t)^{1/2}\, k_p M \qquad (A.49)$$

The eigenfunctions $X(\lambda_n,\eta)$, the normalization integral $N(\lambda_n)$ and the expression defining the eigenvalues λ_n for this problem are obtained from Table B1 of Appendix B,

$$X(\lambda_n,\eta) = \sin(\lambda_n\eta) \qquad (A.50)$$

$$1/N(\lambda_n) = 2 \qquad (A.51)$$

$$\sin\lambda_n = 0 \quad \text{and} \quad \lambda_n = (n-1)\pi \quad n=1,2,3.... \qquad (A.52)$$

Introducing Eqn. (A.50) to Eqn.(A.52) in Eqn. (A.47), the solution is,

$$\theta(\eta,\tau) = \frac{2L^2}{k} \sum_{n=1}^{\infty} \sin(\lambda_n\eta) e^{-\lambda_n{}^2\tau} \int_{\tau'=0}^{\tau} e^{\lambda_n{}^2\tau'} \int_{\eta'=0}^{1} \sin(\lambda_n\eta') q'''(\eta',\tau')d\eta' d\tau' \qquad (A.53)$$

A.5 Derivation of Eqn. (3.48)

The mathematical formulation of this problem is,

$$\frac{\partial\theta(\eta,\tau)}{\partial\tau}=\frac{\partial^2\theta(\eta,\tau)}{\partial\eta^2}+\frac{l^2}{k}q''' \qquad \text{in } 0<\eta<1,\ \tau>0 \qquad (A.54)$$

$$\frac{\partial\theta}{\partial\eta}=0 \qquad \text{at } \eta=0,\tau>0 \qquad (A.55)$$

$$\theta=0 \qquad \text{at } \eta=1,\tau>0 \qquad (A.56)$$

$$\theta=0 \qquad \text{for } \tau=0 \text{ in } 0\le\eta\le1 \qquad (A.57)$$

Eqn. (A.54) can be solved by using the inversion formula and integral transform.

Inversion Formula: $$\theta(\eta,\tau)=\sum_{n=1}^{\infty}\frac{X(\lambda_n,\eta)}{N(\lambda_n)}\bar{\theta}(\lambda_n,\tau) \qquad (A.58)$$

Integral transform: $$\bar{\theta}(\lambda_n,\tau)=\int_{\eta'=0}^{1}X(\lambda_n,\eta')\theta(\eta',\tau)d\eta' \qquad (A.59)$$

where

$$N(\lambda_n)\equiv\int_0^1[X(\lambda_n,\eta)]^2d\eta \qquad (A.60)$$

and the functions $X(\lambda_n,\eta), N(\lambda_n)$, the eigenvalues λ_n are obtainable from the Table B.1 of Appendix B for different combination of boundary conditions at $\eta=0$ and $\eta=1$. Using the inversion formula, the integral transform and boundary conditions, the heat conduction problem, Eqn. (A.54), becomes,

$$\theta(\eta,\tau)=\sum_{n=1}^{\infty}\frac{X(\lambda_n,\eta)}{N(\lambda_n)}e^{-\lambda_n^2\tau}\frac{l^2}{k}\int_{\tau'=0}^{\tau}e^{\lambda_n^2\tau'}\bar{q}'''(\lambda_n,\tau')d\tau' \qquad (A.61)$$

where

$$\bar{q}'''(\lambda_n,\tau') = \int_{\eta'=0}^{1} \cos(\lambda_n \eta') q'''(\eta',\tau') d\eta' \qquad (A.62)$$

and

$$q''' = H_p \times (I \times e^{-\eta^2} \times e^{-\tau^2} \times \varepsilon S \times e^{-\varepsilon S \eta L} \times \phi / k_t)^{1/2}\, k_p M \qquad (A.63)$$

The eigenfunctions $X(\lambda_n,\eta)$, the normalization integral $N(\lambda_n)$ and the expression defining the eigenvalues λ_n are obtained from Table B1 of Appendix B,

$$X(\lambda_n,\eta) = \cos(\lambda_n \eta) \qquad (A.64)$$

$$1/N(\lambda_n) = 2 \qquad (A.65)$$

$$\cos\lambda_n = 0 \qquad \text{and} \qquad \lambda_n = \frac{(2n-1)\pi}{2} \qquad \text{n=1,2,3....} \qquad (A.66)$$

Introducing Eqn. (A.64) to Eqn.(A.66) in Eqn. (A.61), the solution is,

$$\theta(\eta,\tau) = \frac{2L^2}{k} \sum_{n=1}^{\infty} \cos(\lambda_n \eta) e^{-\lambda_n^2 \tau} \int_{\tau'=0}^{\tau} e^{\lambda_n^2 \tau'} \int_{\eta'=0}^{1} \cos(\lambda_n \eta') q'''(\eta',\tau') d\eta' d\tau' \qquad (A.67)$$

A.6 Derivation of Eqn. (3.54)

The mathematical formulation of this problem is,

$$\frac{\partial\theta(\eta,\tau)}{\partial\tau} = \frac{\partial^2\theta(\eta,\tau)}{\partial\eta^2} + \frac{l^2}{k} q''' \qquad \text{in } 0<\eta<1,\ \tau>0 \qquad (A.68)$$

$$\frac{\partial\theta}{\partial\eta} = Bi\theta \qquad \text{at } \eta = 0, \tau > 0 \qquad (A.69)$$

$$\theta = 0 \qquad \text{at } \eta = 1, \tau > 0 \qquad (A.70)$$

$$\theta = 0 \qquad \text{for } \tau = 0 \text{ in } 0 \le \eta \le 1 \qquad (A.71)$$

The Eqn. (A.68) can be solved by using the inversion formula and integral transform,

Inversion Formula: $\theta(\eta,\tau)=\sum_{n=1}^{\infty}\frac{X(\lambda_n,\eta)}{N(\lambda_n)}\bar{\theta}(\lambda_n,\tau)$ (A.72)

Integral transform: $\bar{\theta}(\lambda_n,\tau)=\int_{\eta'=0}^{1}X(\lambda_n,\eta')\theta(\eta',\tau)d\eta'$ (A.73)

where

$$N(\lambda_n)\equiv\int_0^1[X(\lambda_n,\eta)]^2\,d\eta \qquad (A.74)$$

and the functions $X(\lambda_n,\eta), N(\lambda_n)$, and the eigenvalues λ_n are obtainable from the Table B1 of Appendix B for different combination of boundary conditions at $\eta=0$ and $\eta=1$. Using the inversion formula, the integral transform and boundary conditions , the heat conduction problem, Eqn. (A.68), becomes

$$\theta(\eta,\tau)=\sum_{n=1}^{\infty}\frac{X(\lambda_n,\eta)}{N(\lambda_n)}e^{-\lambda_n^2\tau}\frac{l^2}{k}\int_{\tau'=0}^{\tau}e^{\lambda_n^2\tau'}\bar{q}'''(\lambda_n,\tau')d\tau' \qquad (A.75)$$

where

$$\bar{q}'''(\lambda_n,\tau')=\int_{\eta'=0}^{1}\sin(\lambda_n(1-\eta'))q'''(\eta',\tau')d\eta' \qquad (A.76)$$

and

$$q'''=H_p\times(I\times e^{-\eta^2}\times e^{-\tau^2}\times\varepsilon S\times e^{-\varepsilon S\eta L}\times\phi/k_t)^{1/2}\,k_pM \qquad (A.77)$$

The eigenfunctions $X(\lambda_n,\eta)$, the normalization integral $N(\lambda_n)$ and the expression defining the eigenvalues λ_n are obtained from Table B1 of Appendix B,

$$X(\lambda_n,\eta)=\sin(\lambda_n(1-\eta)) \qquad (A.78)$$

$$\frac{1}{N(\lambda_n)}=2\frac{\lambda_n{}^2+Bi^2}{\lambda_n{}^2+Bi^2+Bi} \qquad (A.79)$$

$$\lambda_n\cot\lambda_n=-Bi \qquad \text{(transcendental equation, [17], pg. 654} \qquad (A.80)$$

Introducing Eqn. (A.78) to Eqn.(A.80) in Eq. (A.75), the solution is,

$$\theta(\eta,\tau)=\frac{2L^2}{k}\sum_{n=1}^{\infty}\sin\lambda_n(1-\eta)\frac{(\lambda_n{}^2+Bi^2)}{(\lambda_n{}^2+Bi^2)+Bi}.e^{-\lambda_n{}^2\tau}\int_{\tau'=0}^{\tau}e^{\lambda_n{}^2\tau'}\int_{\eta'=0}^{1}\sin\lambda_n(1-\eta').q'''(\eta',\tau')d\eta'd\tau' \qquad (A.81)$$

Semi-Infinite Domain

A.7 Derivation of Eqn. (3.60)

The mathematical formulation of this problem is,

$$\frac{\partial\theta(\eta,\tau)}{\partial\tau}=\frac{\partial^2\theta(\eta,\tau)}{\partial\eta^2}+\frac{l^2}{k}q''' \qquad \text{in } 0<\eta<1,\ \tau>0 \qquad (A.82)$$

$$\theta=0 \qquad \text{at } \eta=0,\tau>0 \qquad (A.83)$$

$$\theta\to 0 \qquad \text{at } \eta\to\infty,\tau>0 \qquad (A.84)$$

$$\theta=0 \qquad \text{for } \tau=0 \text{ in } 0\le\eta\le 1 \qquad (A.85)$$

The Eqn. (A.82) can be solved by using the inversion formula and integral transform,

Inversion Formula: $\theta(\eta,\tau)=\sum_{n=1}^{\infty}\frac{X(\lambda_n,\eta)}{N(\lambda_n)}\bar{\theta}(\lambda_n,\tau)$ (A.86)

Integral transform: $\bar{\theta}(\lambda_n,\tau)=\int_{\eta'=0}^{\infty} X(\lambda_n,\eta')\theta(\eta',\tau)d\eta'$ (A.87)

where

$$N(\lambda_n)\equiv\int_0^{\infty}[X(\lambda_n,\eta)]^2 d\eta \quad (A.88)$$

and the functions $X(\lambda_n,\eta), N(\lambda_n)$ are obtainable from the Table B2 for different combination of boundary conditions at $\eta=0$ and $\eta\to\infty$. Using the inversion formula, the integral transform and boundary conditions, the heat conduction problem, Eqn. (A.82) becomes,

$$\theta(\eta,\tau)=\int_{\lambda=0}^{\infty}\frac{2}{\pi}\sin(\lambda\eta)e^{-\lambda_n^2\tau}\frac{l^2}{k}\int_{\tau'=0}^{\tau}e^{\lambda_n^2\tau'}\bar{q}'''(\lambda,\tau')d\tau' d\beta \quad (A.89)$$

where

$$\bar{q}'''(\lambda,\tau')=\int_{\eta'=0}^{\infty}\sin(\lambda\eta')q'''(\eta',\tau')d\eta' \quad (A.90)$$

and

$$q'''=H_p\times(I\times e^{-\eta^2}\times e^{-\tau^2}\times\varepsilon S\times e^{-\varepsilon S\eta L}\times\phi/k_t)^{1/2}\,k_p M \quad (A.91)$$

The eigenfunctions $X(\lambda_n,\eta)$, the normalization integral $N(\lambda_n)$ for this problem are obtained from Table B2 of Appendix B,

$$X(\lambda_n,\eta)=\sin(\lambda\eta) \quad (A.92)$$

$$\frac{1}{N(\beta)} = \frac{2}{\pi} \qquad (A.93)$$

$$\frac{2}{\pi}\int_{\lambda=0}^{\infty} e^{-\lambda^2(\tau-\tau')}\sin(\lambda\eta)\sin(\lambda\eta')d\lambda = \frac{1}{(4\pi(\tau-\tau'))^{(1/2)}}[e^{-\frac{(\eta-\eta')^2}{4(\tau-\tau')}} - e^{-\frac{(\eta+\eta')^2}{4(\tau-\tau')}}] \qquad (A.94)$$

Introducing Eqn. (A.92) to Eqn.(A.94) in Eqn. (A.89), the solution is found as

$$\theta(\eta,\tau) = \frac{l^2}{k}\int_{\tau'=0}^{\tau}\frac{d\tau'}{(4\pi(\tau-\tau'))^{(1/2)}}\int_{\eta'=0}^{\infty} q'''(\eta',\tau').[e^{-\frac{(\eta-\eta')^2}{4(\tau-\tau')}} - e^{-\frac{(\eta+\eta')^2}{4(\tau-\tau')}}]d\eta' \qquad (A.95)$$

A.8 Derivation of Eqn. (3.65)

The mathematical formulation of this problem is,

$$\frac{\partial\theta(\eta,\tau)}{\partial\tau} = \frac{\partial^2\theta(\eta,\tau)}{\partial\eta^2} + \frac{l^2}{k}q''' \qquad \text{in } 0<\eta<1,\ \tau>0 \qquad (A.96)$$

$$\frac{\partial\theta}{\partial\eta} = 0 \qquad \text{at } \eta = 0, \tau > 0 \qquad (A.97)$$

$$\theta \to 0 \qquad \text{at } \eta \to \infty, \tau > 0 \qquad (A.98)$$

$$\theta = 0 \qquad \text{for } \tau = 0 \text{ in } 0 \le \eta \le 1 \qquad (A.99)$$

Eqn. (A.96) can be solved by using the inversion formula and integral transform.

Inversion Formula: $$\theta(\eta,\tau) = \sum_{n=1}^{\infty}\frac{X(\lambda_n,\eta)}{N(\lambda_n)}\bar{\theta}(\lambda_n,\tau) \qquad (A.100)$$

Integral transform: $$\bar{\theta}(\lambda_n,\tau) = \int_{\eta'=0}^{\infty} X(\lambda_n,\eta')\theta(\eta',\tau)d\eta' \qquad (A.101)$$

where

$$N(\lambda_n) \equiv \int_0^{\infty} [X(\lambda_n, \eta)]^2 \, d\eta \qquad (A.102)$$

and the functions $X(\lambda_n, \eta), N(\lambda_n)$ are obtainable from the Table B2 for different combination of boundary conditions at $\eta = 0$ and $\eta \to \infty$. Using the inversion formula, the integral transform and boundary conditions, the heat conduction problem (A.96) becomes

$$\theta(\eta, \tau) = \int_{\lambda=0}^{\infty} \frac{2}{\pi} \cos(\lambda \eta) e^{-\lambda_n^2 \tau} \frac{l^2}{k} \int_{\tau'=0}^{\tau} e^{\lambda_n^2 \tau'} \bar{q}^{'''}(\lambda, \tau') d\tau' d\beta \qquad (A.103)$$

where

$$\bar{q}^{'''}(\lambda, \tau') = \int_{\eta'=0}^{\infty} \cos(\lambda \eta') q'''(\eta', \tau') d\eta' \qquad (A.104)$$

and

$$q''' = H_p \times (I \times e^{-\eta^2} \times e^{-\tau^2} \times \varepsilon S \times e^{-\varepsilon S \eta L} \times \phi / k_t)^{1/2} \, k_p M \qquad (A.105)$$

The eigenfunctions $X(\lambda_n, \eta)$, the normalization integral $N(\lambda_n)$ for this problem are obtained from Table B2 of Appendix-B ,

$$X(\lambda, \eta) = \cos(\lambda \eta) \qquad (A.106)$$

$$1/N(\lambda) = 2/\pi \qquad (A.107)$$

$$\frac{2}{\pi} \int_{\lambda=0}^{\infty} e^{-\lambda^2(\tau - \tau')} \cos(\lambda \eta) \cos(\lambda \eta') d\lambda = \frac{1}{(4\pi(\tau - \tau'))^{(1/2)}} [e^{-\frac{(\eta - \eta')^2}{4(\tau - \tau')}} + e^{-\frac{(\eta + \eta')^2}{4(\tau - \tau')}}] \qquad (A.108)$$

Introducing Eqn. (A.106) to Eqn.(A.108) in Eqn. (A.103), the solution is found as

$$\theta(\eta,\tau)=\frac{l^2}{k}\int_{\tau'=0}^{\tau}\frac{d\tau'}{(4\pi(\tau-\tau'))^{(1/2)}}\int_{\eta'=0}^{\infty}q'''(\eta',\tau').[e^{-\frac{(\eta-\eta')^2}{4(\tau-\tau')}}+e^{-\frac{(\eta+\eta')^2}{4(\tau-\tau')}}]d\eta' \qquad (A.109)$$

A.9 Derivation of Eqn. (3.70)

The mathematical formulation of this problem is,

$$\frac{\partial\theta(\eta,\tau)}{\partial\tau}=\frac{\partial^2\theta(\eta,\tau)}{\partial\eta^2}+\frac{l^2}{k}q''' \qquad \text{in } 0<\eta<1,\ \tau>0 \qquad (A.110)$$

$$\frac{\partial\theta}{\partial\eta}=Bi\theta \qquad \text{at } \eta=0,\tau>0 \qquad (A.111)$$

$$\theta\to 0 \qquad \text{at } \eta\to\infty,\tau>0 \qquad (A.112)$$

$$\theta=0 \qquad \text{for } \tau=0 \text{ in } 0\le\eta\le 1 \qquad (A.113)$$

Eqn. (A.110) can be solved by using the inversion formula and integral transform.

Inversion Formula: $\theta(\eta,\tau)=\sum_{n=1}^{\infty}\frac{X(\lambda_n,\eta)}{N(\lambda_n)}\bar{\theta}(\lambda_n,\tau)$ (A.114)

Integral transform: $\bar{\theta}(\lambda_n,\tau)=\int_{\eta'=0}^{\infty}X(\lambda_n,\eta')\theta(\eta',\tau)d\eta'$ (A.115)

where

$$N(\lambda_n)\equiv\int_0^{\infty}[X(\lambda_n,\eta)]^2\,d\eta \qquad (A.116)$$

and the functions $X(\lambda_n,\eta), N(\lambda_n)$ are obtainable from the Table B2 of Appendix B for different combination of boundary conditions at $\eta=0$ and $\eta=1$. Using the inversion formula, the integral transform and boundary conditions, the heat conduction problem, Eqn. (A.110), becomes,

$$\theta(\eta,\tau)=\int_{\lambda=0}^{\infty}(\lambda\cos\lambda\eta+Bi\sin\lambda\eta)\frac{2}{\pi(\lambda^2+Bi^2)}e^{-\lambda^2\tau}\frac{l^2}{k}\int_{\tau'=0}^{\tau}e^{\lambda^2\tau'}\bar{q}^{'''}(\lambda,\tau')d\tau' d\beta \tag{A.117}$$

where

$$\bar{q}^{'''}(\lambda,\tau')=\int_{0}^{\infty}X(\lambda,\eta')q'''(\eta',\tau')d\eta' \tag{A.118}$$

and

$$q'''=H_p\times(I\times e^{-\eta^2}\times e^{-\tau^2}\times\varepsilon S\times e^{-\varepsilon S\eta L}\times\phi/k_t)^{1/2}\,k_pM \tag{A.119}$$

The eigenfunctions $X(\lambda_n,\eta)$, the normalization integral $N(\lambda_n)$ for this problem are obtained from Table B2 ,

$$X(\lambda,\eta)=\lambda\cos\lambda\eta+Bi\sin\lambda\eta \tag{A.120}$$

$$\frac{1}{N(\beta)}=\frac{2}{\pi}\frac{1}{\lambda^2+Bi^2} \tag{A.121}$$

Introducing Eqn. (A.120) to Eqn.(A.121) in Eqn. (A.117), the solution is,

$$\theta(\eta,\tau)=\int_{\lambda=0}^{\infty}\frac{2}{\pi(\lambda^2+Bi^2)}(\lambda\cos\lambda\eta+Bi\sin\lambda\eta)e^{-\lambda^2\tau}\frac{l^2}{k}\int_{\tau'=0}^{\tau}e^{\lambda^2\tau'}\,.$$

$$\int_{\eta'=0}^{\infty}q'''(\eta',\tau')\,(\lambda\cos\lambda\eta'+Bi\sin\lambda\eta')\,\mathrm{d}\eta'\,\mathrm{d}\tau'\,\mathrm{d}\lambda \tag{A.122}$$

Appendix-B

The tables for the; physical properties of resins and the eigenfunctions, normalization functions

Table B1. Eigenfunctions and the normalization functions for finite domain problem.

No	**Boundary Condition at** $\eta = 0$	**Boundary Condition at** $\eta = 1$	$X(\lambda_n, \eta)$	$\frac{1}{N(\lambda_n)}$	**Eigen-values**
1	$\theta = 0$	$\theta = 0$	$\sin(\lambda_n \eta)$	2	$\sin \lambda_n = 0$
2	$\frac{\partial \theta}{\partial \eta} = 0$	$\theta = 0$	$\cos(\lambda_n \eta)$	2	$\cos(\lambda_n) = 0$
3	$\frac{\partial \theta}{\partial \eta} + Bi\theta = 0$	$\theta = 0$	$\sin \lambda_n (1-\eta)$	$\frac{2(\lambda_n^2 + Bi^2)}{(\lambda_n^2 + Bi^2 + Bi)}$	$\lambda_n \cot \lambda_n = -Bi$

Table B2. Eigenfunctions and the normalization functions for semi-infinite domain problem.

No	**Boundary Condition at** $\eta = 0$	$X(\lambda, \eta)$	$\frac{1}{N(\lambda)}$
1	$\theta = 0$	$\sin(\lambda \eta)$	$\frac{2}{\pi}$
2	$\frac{\partial \theta}{\partial \eta} = 0$	$\cos(\lambda \eta)$	$\frac{2}{\pi}$
3	$\frac{\partial \theta}{\partial \eta} + Bi\theta = 0$	$\lambda \cos \lambda \eta + Bi \sin \lambda \eta$	$\frac{2}{\pi} \frac{1}{\lambda^2 + Bi^2}$

Table B.3. Physical Properties of resins.

	description	Z100	LS	bulk
k1	hA/ρCV (m^2K/J)	0.048±0.008	0.046±0.004	0.063±0.01
k2	1/ρC (m^3K/J)	0.000000574	0.000000443	0.000000561
k3	(1/s)	0.55±0.10	0.31±0.05	0.57±0.06
t	Time at maximum temp. from composite only (s)	4.97	7.33	4.40
θc	Maximum temp heat from composite only (K)	5.04	10.71	8.27
qc	Heating rate per unit volume (J/scm^3)	6.06±0.86	10.37±0.79	10.98±0.81
q_l	Heating rate per unit volume from curing light (J/scm^3)	0.84±0.14	1.03±0.95	0.45±0.08
h	surface heat loss coefficient	92.21±16.49	112.13±14.71	118.07±20.21
qc/k3	Total heat produced per unit volume (J/cm^3)	11.09	19.40	33.62
K	Thermal Conductivity (W/mK)	0.54		0.54
ρ	Density (Kg/m^3)	2100	2278	1800
C	Heat capacity (J/Kg K)	830	990.8	990
A	Surface area (m^2)	3.51867E-05	3.47333E-05	3.50133E-05
V	Volume (m^3)	3.86687E-08	3.76863E-08	3.70391E-08

Appendix-C

Numerical Simulation of the basic model of axisymmetric tooth and rectangular block using Abaqus-6.11

C.1 For Z100 -Axisymmetric tooth model- Orphan Mesh Imported

NT11 in the legend box represents the nodal temperature in the transverse direction.

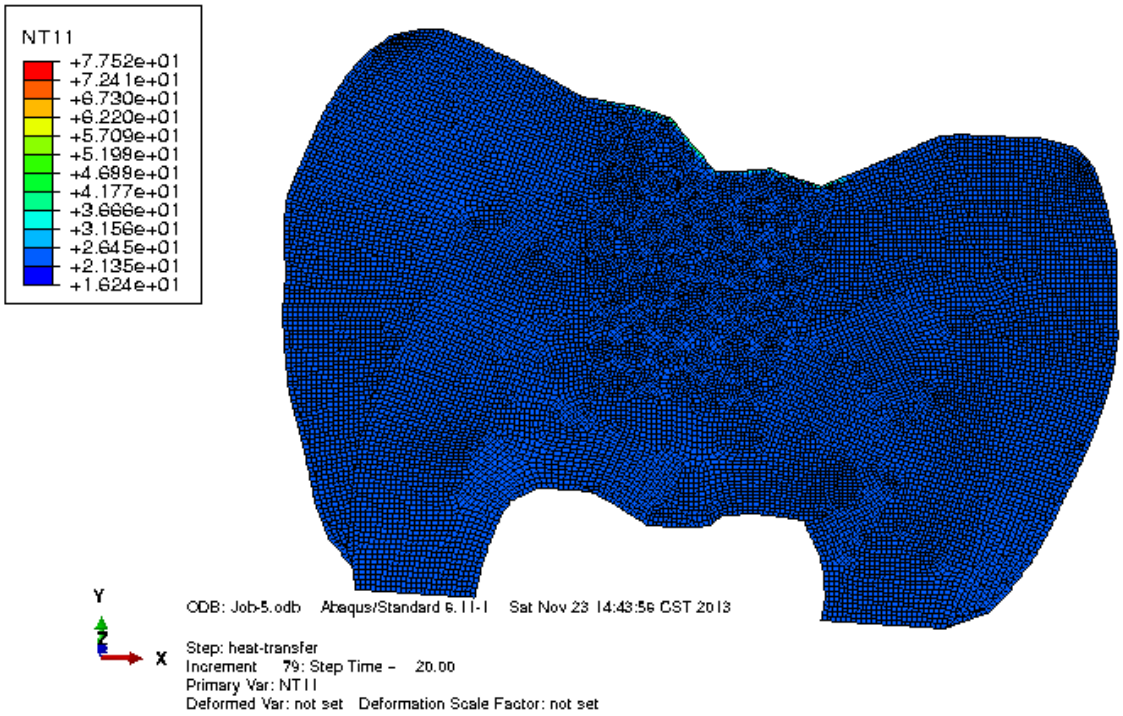


```
*Heading
** Job name: Job-5 Model name: HTA_RealTooth
** Generated by: Abaqus/CAE 6.11-1
*Preprint, echo=NO, model=NO, history=NO, contact=NO
**
** PARTS
**
*Part, name=PART-1
*Elset, elset=__PickedSurf21_S1, internal, instance=PART-1-1
 22117, 22126, 22156, 22882, 22909, 23002, 23044, 23045, 23046, 23047, 23377, 23380, 23381, 23382,
23384, 23386
 23390, 23394, 23398, 23473
*Elset, elset=__PickedSurf21_S2, internal, instance=PART-1-1
 22115, 22116, 22118, 22128, 22139, 22140, 22881, 22927, 22928, 22929, 22935, 22936, 22937, 22938,
22939, 23048
 23049, 23280, 23281, 23282, 23283, 23387, 23388, 23391, 23395, 23396, 23397, 23479, 23483
*Elset, elset=__PickedSurf21_S3, internal, instance=PART-1-1
 22141, 22930, 23050, 23471, 23472, 23476, 23477, 23480, 23481, 23482
*Surface, type=ELEMENT, name=_PickedSurf21, internal
```

```
__PickedSurf21_S1, S1
__PickedSurf21_S2, S2
__PickedSurf21_S3, S3
*End Assembly
**
** MATERIALS
**
*Material, name=COMPOSITE
*Conductivity
 0.54,
*Density
2100.,
*Specific Heat
830.,
*Material, name=HDPE
*Conductivity
 0.48,
*Density
950.,
*Specific Heat
1820.,
**
** PREDEFINED FIELDS
**
** Name: Predefined Field-1   Type: Temperature
*Initial Conditions, type=TEMPERATURE
_PickedSet10, 25.
** ----------------------------------------------------------------
**
** STEP: heat-transfer
**

*Step, name=heat-transfer
*Heat Transfer, end=PERIOD, deltmx=1.
1., 20., 0.0002, 20.,
**
** LOADS
**
** Name: Load-1   Type: Surface heat flux
*Dsflux
_PickedSurf21, S, 12000.
**
** OUTPUT REQUESTS
**
*Restart, write, frequency=0
**
** FIELD OUTPUT: F-Output-1
**
*Output, field, variable=PRESELECT
**
** HISTORY OUTPUT: H-Output-1
**
*Output, history, variable=ALL
*End Step
```

C.2 For Z100 -Rectangular model

Using the exactly same model as above but with mesh element type= DC3D20- A 20 node quadratic heat transfer brick and global element size = 1

Surface heat flux is applied at x = 0, and the predefined temperature is used at the boundary condition at 25 ^{o}C.

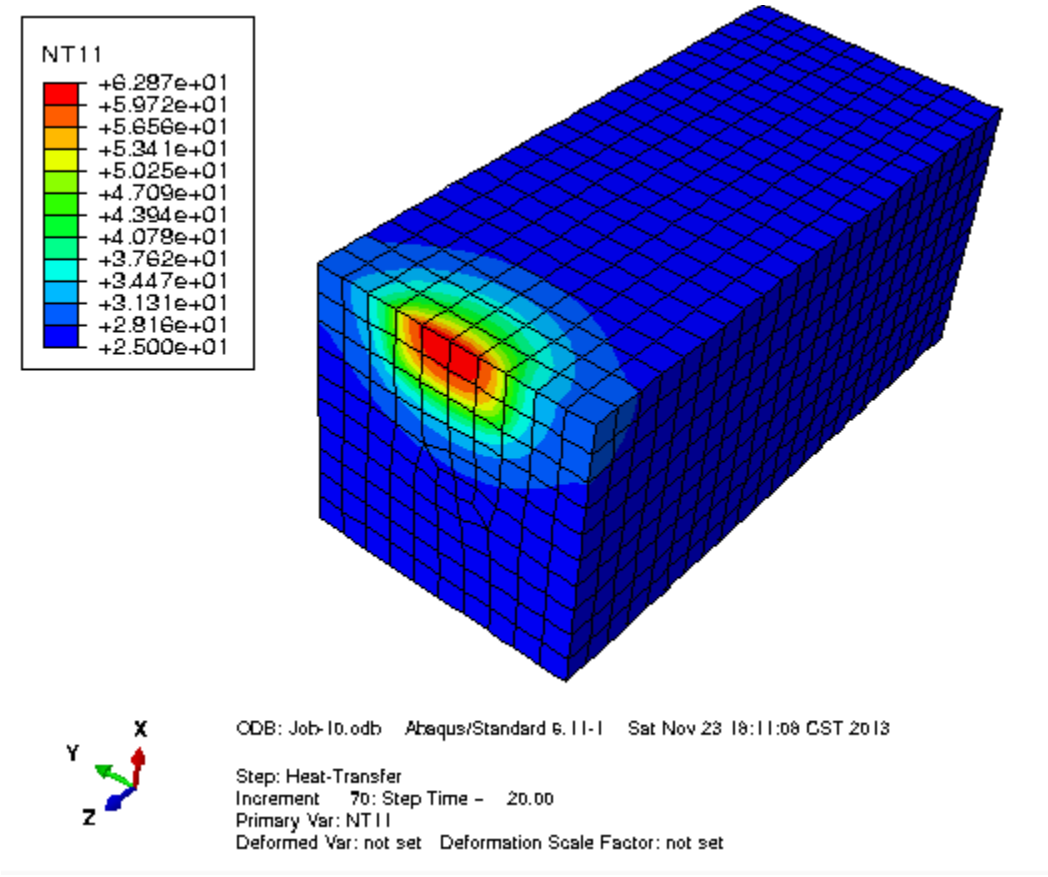

C.3 For LS -Axisymmetric tooth model- Orphan Mesh Imported

Exactly similar method as previous section C.1 is followed but with different material property and section assignment.

*Material, name=composite-LS
*Conductivity
0.54,
*Density
2278.,
*Specific Heat
991.,
**

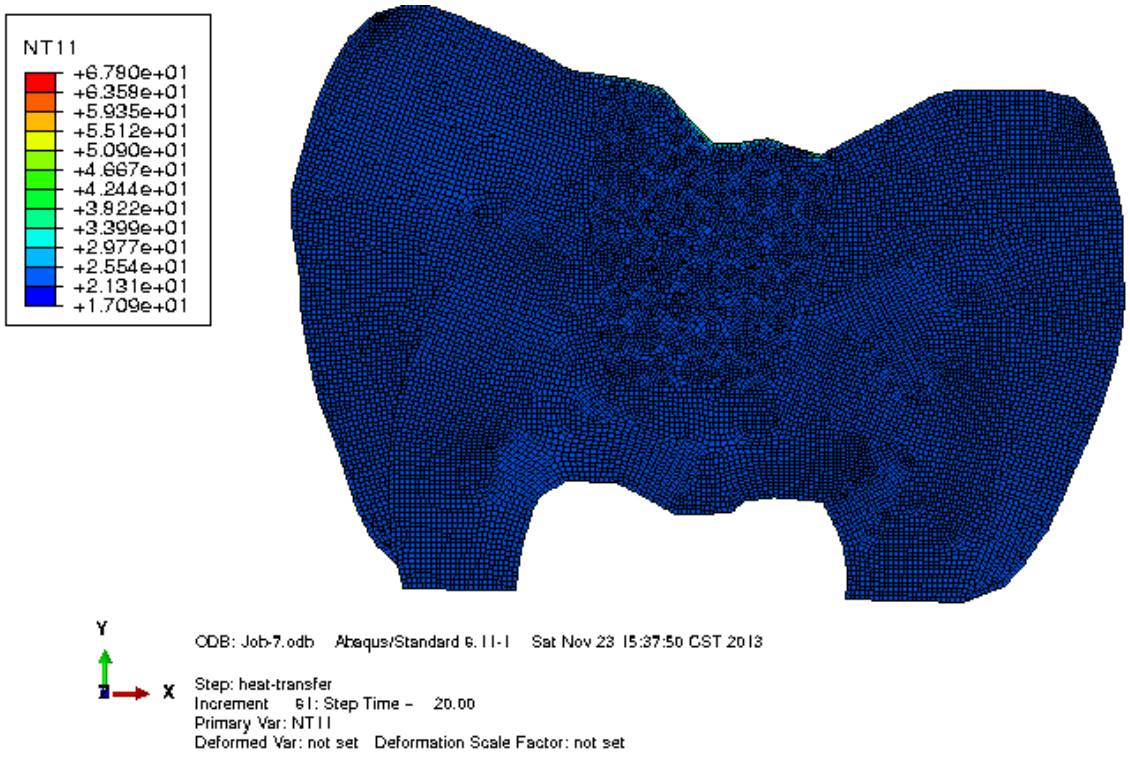

C.4 For LS -Rectangular model

A similar procedure is followed as in section C.2 but with the different material properties.

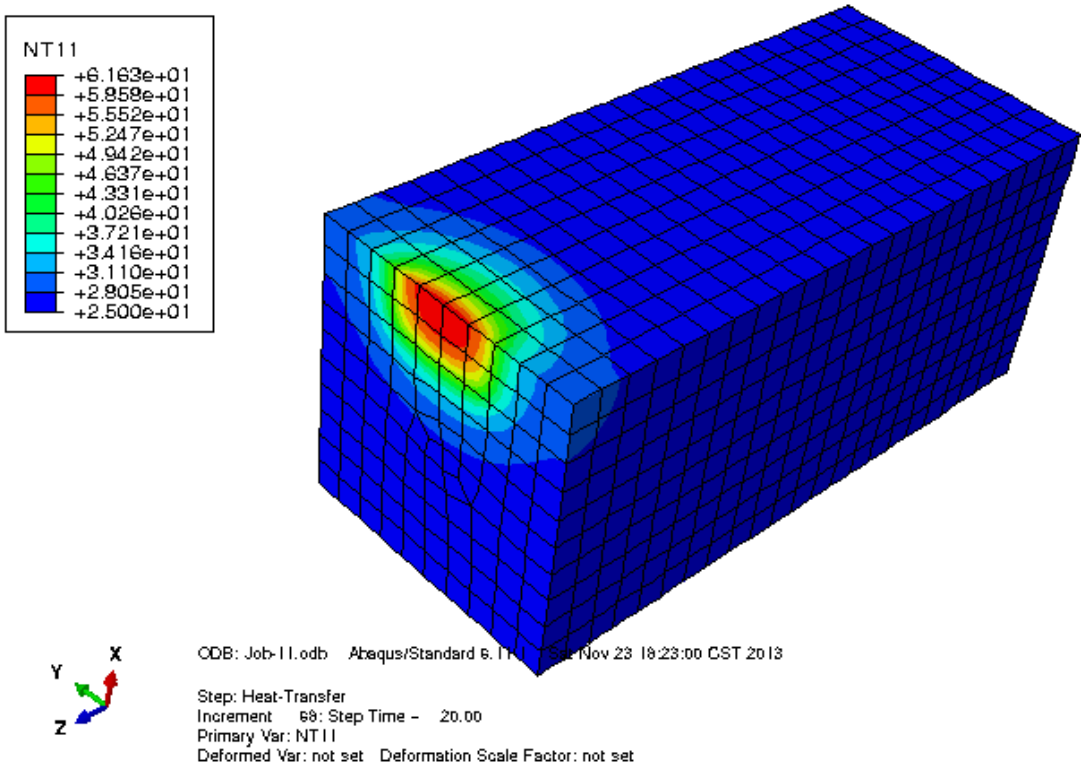

C.5 For BulkFill -Axisymmetric tooth model- Orphan Mesh Imported

** MATERIALS
**
*Material, name=Composite-BulkFill
*Conductivity
0.54,
*Density
1800.,
*Specific Heat
990.,

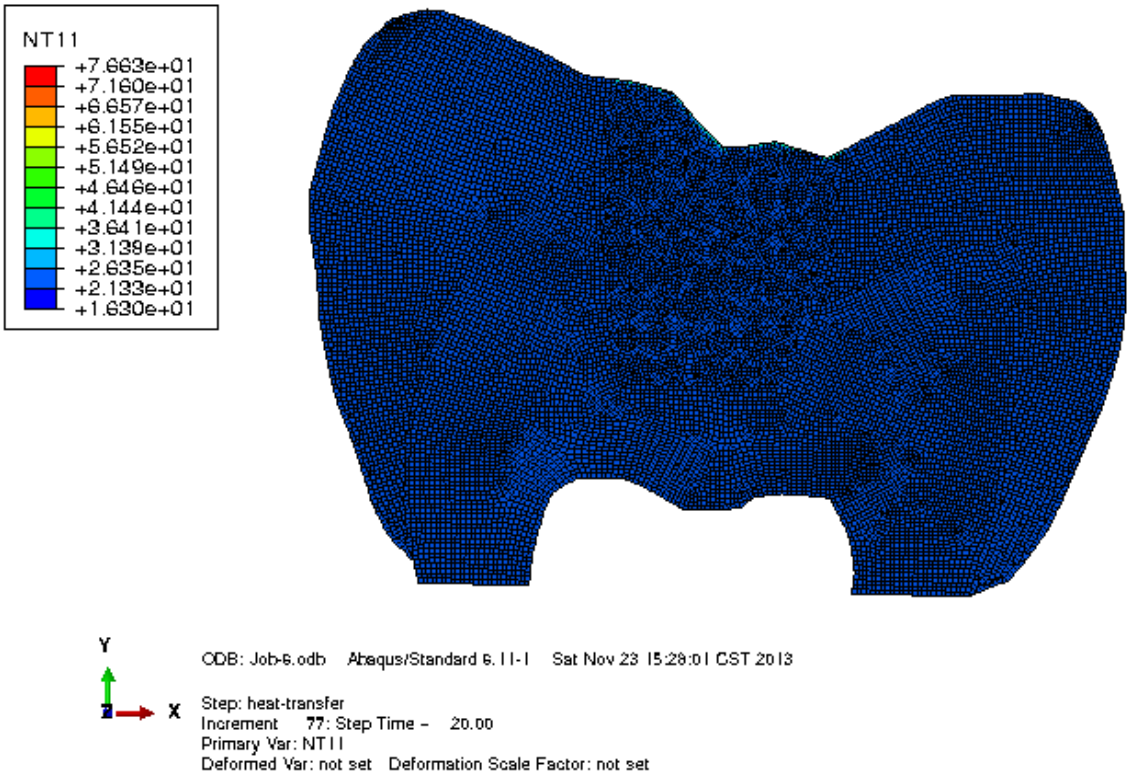

C.6 For LS -Rectangular model

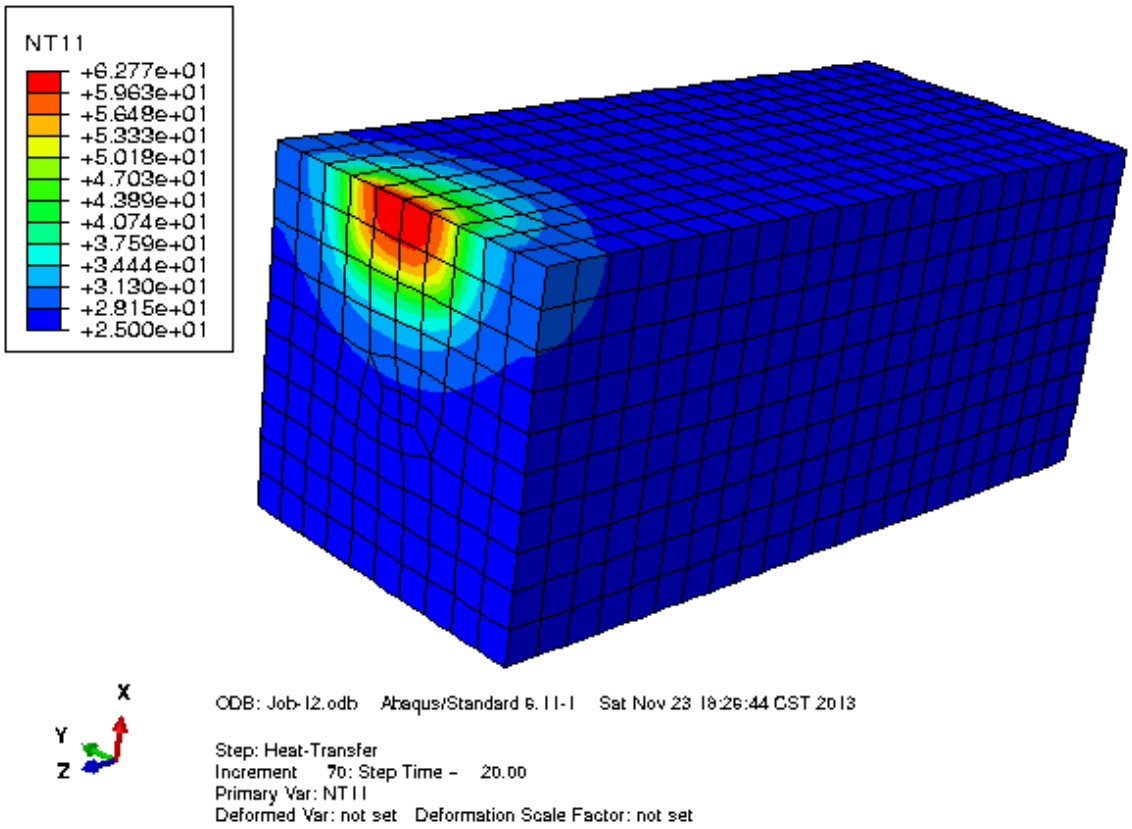

Appendix-D

Unit step function/ Heaviside function

The Heaviside function can be defined as,

$$u_c(t) = \begin{cases} 0, & \text{if } t < c \\ 1, & \text{if } t \geq c \end{cases} \tag{D.1}$$

where $u_c(t) = u(t-c) = H(t-c)$ (D.2)

The graph for the Heaviside function is given by,

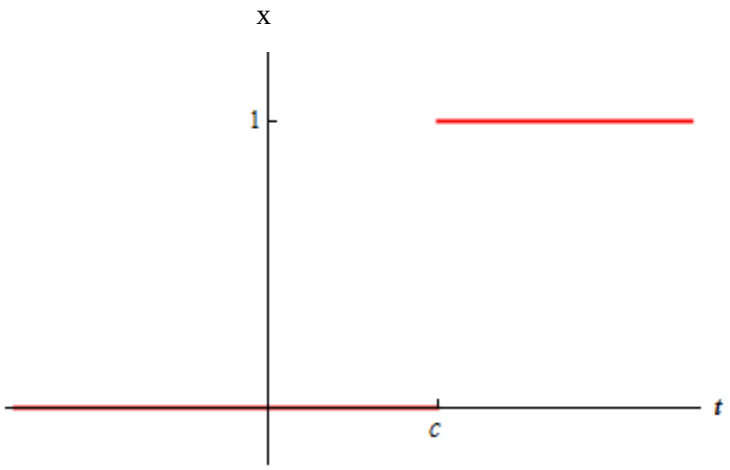

Figure 56. Graph for Heaviside Function.

Thus if the curing light is subjected for time duration $[0, t = 20s]$, then the Heaviside function can be expressed as,

$$u_c(t) = H(20-c) \tag{D.3}$$

Thus substituting the values of $g(\tau)$ as,

$$g(\tau) = H(20 - \tau) \tag{D.4}$$

in Eqn. (3.77) and Eqn. (3.80) of Chapter 3 gives,

$$R_p = (I \times e^{-\eta^2} \times \varepsilon \times S \times e^{-\varepsilon S \eta L} \times (\phi / k_t) \times H(20 - \tau))^{1/2} k_p M \tag{D.5}$$

$$q''' = H_R B \exp(-(\eta^2 + \varepsilon S \eta L)) \times H(20 - \tau) \tag{D.6}$$

where $B = k_p M \sqrt{\dfrac{I \varepsilon S \phi}{k_t}}$

Thus substituting the value of q''' in Eqn. (3.46) of Case-5 gives the plot between dimensionless temperature versus dimensionless time (shown for only one value of dimensionless specimen depth= 0) in Figure 57.

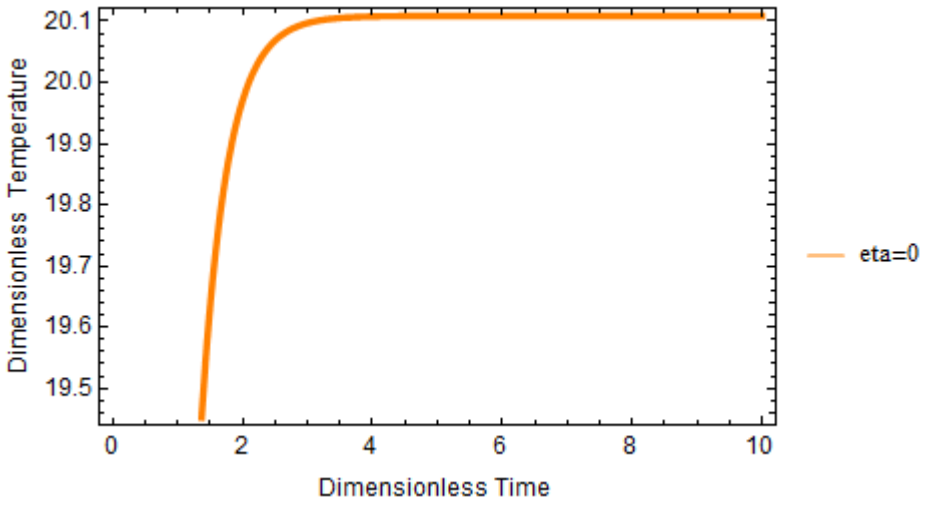

Figure 57. Dimensionless Temperature versus dimensionless time graph at η = 0 for the Heaviside $g(\tau)$ function.